UNIVERSITY OF SOUTHAMPTON

FACULTY OF SCIENCE

School of Physics and Astronomy

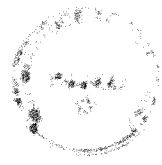

Calculation of Some Phenomenologically Relevant Quantities in Lattice QCD

Abdullah Shams Bin Tariq

Thesis for the degree of Doctor of Philosophy

August 2004

UNIVERSITY OF SOUTHAMPTON

ABSTRACT

FACULTY OF SCIENCE

SCHOOL OF PHYSICS AND ASTRONOMY

Doctor of Philosophy

CALCULATION OF SOME PHENOMENOLOGICALLY RELEVANT QUANTITIES IN LATTICE QCD

Abdullah Shams Bin Tariq

Somewhat mutually independent studies in lattice phenomenology, one on doublecharm baryon spectroscopy and one on an unquenched calculation of B_K are reported alongwith a study of possible solutions to the problem of extracting a signal for static quarks with reference to the Λ_b lifetime problem. All simulations are performed with non-perturbatively $\mathcal{O}(a)$-improved Wilson fermions. Double- and single-charm baryon masses and splittings are found in agreement with experiment where data is available and further predictions are provided. Sea quark effects are found to be significant in B_K, and seem to lower the value. For, the Λ_b-lifetime, a calculation using maximal variance reduced all-to-all propagators with novel fat static quarks is judged to be quite promising, while the extended propagator approach is found to be inefficient.

Contents

List of Tables

List of Figures

To my father

Acknowledgments

All gratitude is due to Allah for giving me this opportunity and for blessing my time and work here in Southampton.

Then I would like to acknowledge my father, who though far away back home, was always with me in spirit. It was his upbringing that has given me the strength and character to proceed this far. I really missed showing him my work every evening. My mother, sister Tultul, brothers Qamarullah and Nazmullah were also always there with their love and affection. Separation makes me appreciate them all the more, and having our first baby has made me understand what parents, especially mothers, go through for children. And Qamarullah's news of getting double first class in Economics has made me proud.

I must thank Rosy for her extremely patient support for my work that often had to go into odd and long hours. Not a single time did she complain. And, dear Sabah! I look forward to making up for the many times I had to leave her in tears, when I said goodbye to come to university.

I would like to express my deepest gratitude to my most respected Uncle and Aunts. They have been pillars of support in my life. The affection and prayers of my cousins, Rosy's family and other relatives is also very gratefully acknowledged. In particular, I would like to thank my father-in-law for his prayers and my mother-in-law for coming to see Sabah. I also remember the innumerable well-wishers whose messages I kept recieving all through the three years here.

I have thoroughly enjoyed working with my supervisor Jonathan Flynn, who, I am sure, knew of my weaknesses very well, but never uttered a word of discourage-

ment. His constant support, guidance and understanding, and all the sessions on his blackboard or elsewhere have been a wonderful experience. Most of my time was spent together with Federico Mescia. I probably learnt more from him than anywhere else. He has been a true friend and collaborator doing more than his share of work in every stage and I have indeed benefitted a great deal from his abilities and spirit of hard work.

I will also miss the friendly and relaxed, yet academic, atmosphere here at SHEP. Among the staff, the support and encouragement of Chris Sachrajda and the affectionate interest of Douglas Ross, Steve King, Tim Morris, Ken Barnes, Nick Evans, Stefano Moretti and Tomáš Blazek, and the postdocs and postgrads particularly Sandhya Choubey and David Rayner have made my time here all the merrier. Martin Hasenbusch has been a great help in the concluding period going through much of my thesis and suggesting improvements. I have indeed learnt a good deal from him. I also must specially thank Olly Rosten his interest and for his help with the binding for the initial submission while I was away, Jon Shock for going through my thesis proof-reading, and Iain Peddie and Martin Wiebusch for computing advice, and Martin Nolten and other group members for their friendship. I will never forget the fact that this group decided to shift the weekly seminar time, at least partly, to allow me to pray in peace.

Massimo di Pierro deserves my special gratitude, for his wonderful code, and unwavering support. I cannot deny that, in a sense, I learnt my bit of lattice QCD through his code. The Iridis computing support team of Ivan Wolton, Ian Hardy and Oz Parchment and the school computing team of Mike Hill and Simon Harris, as well as school staff, particularly, Christine Searle and Ceris French have been ever-helpful.

I would also like to specially thank Craig McNeile and Chris Michael and then (in alphabetical order of surnames) Damir Becirevic, Ken Bowler, Poul Damgaard, Christine Davies, Michele della Morte, Gregorio Herdoiza, Alan Irving, Andreas Kronfeld, Laurent Lellouch, David Lin, Vittorio Lubicz, Chris Maynard, Amarjit

Soni, Cecilia Tarantino, Giovanni Villadoro and Urs Wenger for their comments on and assistance with the work reported here.

My teacher Arun Basak has always been in touch and full of encouragement. He has allowed me to get on with my lattice work, but still given me more than due credit for any work that I left unfinished in work with him. The affection of Alfaz Uddin, Susanta Das, Hironmoy Sen Gupta, Fazle Bary Malik and Shamsher Ali has also been a blessing for me. I am also grateful to my teacher Gazi Sirajul Islam for opening a window to particle physics for me by taking me to the Abdus Salam ICTP in 1999, Ahsanul Habib for his early introduction to computing and encouragement, Abdul Wadud for his constant interest and to all to my teachers who have been a source of inspiration. I should also thank Sadequl Islam, without whose affectionate interest, I may have missed this opportunity.

We have also been specially blessed with such affection from people here that we will leave with a heart deeply saddened at this separation. We are grateful to Feroz Alam for being there for us when we arrived and all through our stay. The families of Mubarak Ahmad, Akram Ahmedi, Arif Nasser, Humayon Salim, Asim Malik, Toseef Anwar, Mohammad Salim, Mohammad Haroon, Mubarak Basra and Salim Malik have been most affectionate and forthcoming with support. I must also make a separate mention of Saeeda Ahmad, Hamida Begum, Nazhat Ahmedi and Rubina Nasser for their support, affection and prayers. The families of Nazmul Haq, Shaif-Ul-Alam and Mehdi Jafaripanah and others are worthy of special mention.

Last but not least, I must acknowledge the funding from the Commonwealth Scholarship Commission which made all this possible. The ACU and the British Council not only provided/administered the funding, but have done so in a manner that made us feel most honoured and welcome.

I have not been able to keep this brief, but I still feel I have missed some. It is indeed a great blessing that I have so many who have been at my side.

Oh! What distinctive wonders have Thou kept hidden in every particle.
Who can comprehend all the glorious detail of these mysteries?

– Hazrat Mirza Ghulam Ahmad

Chapter 1

Introduction

Amongst the couplings in the standard model the strong coupling has the odd characteristic of asymptotic freedom. Quarks are loosely bound at short distances but the force grows sharply as they are pulled apart, so much so, that an isolated quark has never been observed. Whereas for the other interactions in the standard model, one uses perturbation theory and neglects higher order processes; QCD at long distances or low energies becomes non-perturbative and a first principles calculation of the path integrals is required. This leads us to a discrete formulation of QCD on a 4-dimensional space time lattice, hence the name, lattice QCD.

There is a great deal of interesting phenomenology requiring lattice techniques. This thesis is formed of three such, somewhat mutually independent, projects in different areas of flavour physics phenomenology. The first one is a spectroscopy calculation on double charmed baryons. The first observation of these baryons at the SELEX experiment in Fermilab a couple of years back prompted this study. Results for double- and single-charmed baryon masses and spin splittings are reported some of which may be tested in future experiments.

The second project is on an unquenched calculation of B_K. The theoretical input of B_K with its large uncertainty remains one of the biggest obstacles in constraining the CKM unitarity triangle. The next major step required in reducing the errors is the incorporation of dynamical sea quarks. Exploratory results from an $N_f = 2$ calculation with clover fermions are presented providing some insight into what

effects to expect from the incorporation of sea quarks.

The third and unfinished project is on the unsolved problem of the Λ_b-lifetime. In terms of the heavy quark expansion, corrections from spectator effects at $\mathcal{O}(m_b^3)$ are required to be large to explain why Λ_b particles, on average, live about 20% shorter than B-mesons. On the lattice calculation side, there are difficult technical problems in extracting a signal from correlators with static b-quarks. Prospects of different approaches are studied and this has led to some useful understanding on what is required to extract a signal in such a case. Chapter 5 describes the understanding achieved so far and outlines future directions for the calculation.

In this manner the three problems in this thesis being related to charm, strange and beauty (heavy) quarks touch different areas of flavour physics. There is however very little focus on any of the issues concerning light quarks.

There are in a sense two aims in typical lattice phenomenology simulations: i) to test our understanding of QCD and ability to calculate quantities relevant to it, and ii) to perform calculations within QCD in order to check the consistency of the standard model or some other theoretical framework. The doublecharm spectroscopy calculation belongs to the first category, whereas the B_K and Λ_b belong to the second category exploring the limits of the standard model and the heavy quark expansion techniques respectively.

Again, in another way, lattice phenomenology calculations are either calculations in spectroscopy or of matrix elements. The projects in this thesis include both of these types, with the first one being an example of spectroscopy while the other two belong to the category of evaluation of matrix elements.

It should be emphasised that precision lattice QCD requires much greater computational and human resources as well as time than what was available for the work presented in this thesis. Hence, most of the results are somewhat exploratory, with certain recognised limitations. These studies also form the first bunch of simulations done locally on the University of Southampton cluster Iridis using the code FermiQCD. Nevertheless, attempts are made to extract some non-trivial information

that is of interest for phenomenology.

There is a brief, and by no means comprehensive, introduction to some basic ideas relevant to lattice phenomenology simulations in the next chapter. This is followed by the three chapters mentioned above on doublecharm baryons, B_K and Λ_b-lifetime. These chapters are reasonably self-contained and may be read independent of each other. The conclusions are summarised together in a final chapter at the end of the thesis.

Chapter 2

Basics of Lattice QCD Simulations

In this chapter, a basic overview of the background and practical issues involved in lattice simulations are described. Rather than taking the textbook approach, where everything is derived from continuum QCD, in this basic introduction an attempt will be made to provide a bottom-up view from the perspective of a lattice phenomenology practitioner. For a more conventional approach one may consult the available textbooks, *e.g.* [1–5] and/or the good number of review/overview articles available. Therefore in some cases the discretised elements are introduced directly as they occur in lattice simulations without a comprehensive discussion of the continuum formulation. Similarly, I always work in Euclidean space-time without showing the Minkowski counterparts of the expressions as they are never required in simulations.

2.1 QCD calculations on a lattice

Let us first introduce a hypercubic space-time lattice of $L^3 \times T$ points where L and T are the spatial and temporal dimensions respectively. The fermion-fields, ψ live on the discrete lattice sites and are $n_c \times n_{spin}$ complex matrices, whereas the gauge fields, $U \in SU(n_c)$ living on the links are $n_c \times n_c$ complex colour matrices.

We are interested in calculating Green's functions by evaluating path integrals

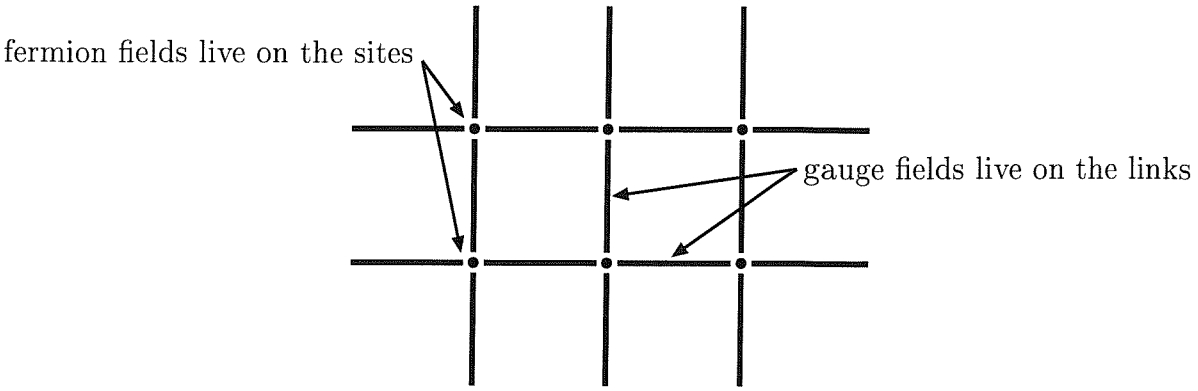

Figure 2.1: A schematic representation of the lattice in two dimensions with the fermion fields living on the sites and and the gauge fields on the links.

of the form:

$$\langle \mathcal{O} \rangle = \frac{1}{Z} \int \mathcal{D}U \mathcal{D}\psi \mathcal{D}\bar{\psi} \mathcal{O} e^{-\mathcal{S}_g[U] - \mathcal{S}_f[U,\psi,\bar{\psi}]}. \tag{2.1}$$

Here U is the gauge field, ψ's are the fermion fields and $\mathcal{S}_g$ and $\mathcal{S}_f$ are the gauge and fermionic parts of the action. $\mathcal{O}$ is a collection of operators describing the process we intend to investigate. The basic idea is to evaluate this integral using Monte Carlo methods, *i.e.* by averaging over a suitably weighted sample. Since we want the exponential in the integral to have a probabilistic interpretation, it has to be positive definite. Therefore we always work in Euclidian space-time. The action is discretised and put on the lattice and the following sections will introduce how this is implemented in practice.

2.2 Gauge configurations

Now, let us consider the fermionic integral . For $\mathcal{S}_f = \bar{\psi} Q \psi$

$$\int \mathcal{D}\bar{\psi} \mathcal{D}\psi e^{-\mathcal{S}_f} = \det Q[U]. \tag{2.2}$$

This is factorised into the weight, $\det Q[U]$ being the fermion determinant, and a set of gauge configurations is generated with the an effective action

$$\mathcal{S}_{\text{eff}} = \mathcal{S}_g - \log\det Q[U] = \mathcal{S}_g - \text{Tr}\log Q[U]. \tag{2.3}$$

Now we have only the gluonic degrees of freedom left in the integral. The first step is to generate, in Monte Carlo, a set of gauge configurations with suitable weights. In quenched QCD, $\det Q$ is constant (usually set to 1), leading to

$$\langle \mathcal{O} \rangle = \frac{1}{Z} \int \mathcal{D}U f(\text{propagators}[U])\, e^{-\mathcal{S}_g}, \tag{2.4}$$

where the operator $\mathcal{O}$ after integrating over fermionic degrees of freedom, has become some function of fermionic propagators.

On a lattice the gauge fields reside on the links between the lattice points. In our notation $U_\mu(x)$ is the link *ending* at x and originating from the lattice site one step away in the $\hat{\mu}$ direction. It may be noted that many authors use the opposite direction as their convention. This variable U corresponds to the Schwinger line or the phase picked up by a matter field while traversing this path

$$U_\mu(x) = e^{agA^c_\mu T_c} \simeq 1 + agA^c_\mu T_c + \cdots \tag{2.5}$$

From now on, for simplicity, $x + a\hat{\mu}$ will be written just as $x + \hat{\mu}$ with the a implied. Each of these links is a complex $n_c \times n_c$ colour matrix of $SU(n_c)$ and a set of these links spanning the volume of the lattice makes a gauge configuration. $n_c = 3$ for QCD simulations but the formulation does not change if one wants to use a different n_c, say, for large-n_c studies.

The construction of a discretised version of the continuum QCD gauge action is not unique. The simplest of these, the Wilson plaquette action is the one used in our simulation and is introduced below.

2.2.1 Wilson plaquette (gauge) action

The continuum gauge action expressed in terms of the bare coupling g_0 and the field strength tensor $F^{\mu\nu}$ is given by

$$S_g = -\frac{1}{2g_0^2}\int d^4x \mathrm{Tr}\,(F_{\mu\nu}F^{\mu\nu}) \tag{2.6}$$

Recalling the analogy with electromagnetism, where the curl of the vector potential gives the electromagnetic flux, one can define $F^{\mu\nu}$ in terms of path-ordered products of the gauge links around elementary plaquettes, which are the simplest gauge invariant quantity that can be constructed from these links.

$$P_{\mu\nu}(x) = U_\mu(x)U_\nu(x+a\hat{\mu})U_\mu^\dagger(x+a\hat{\nu})U_\nu^\dagger(x) \tag{2.7}$$

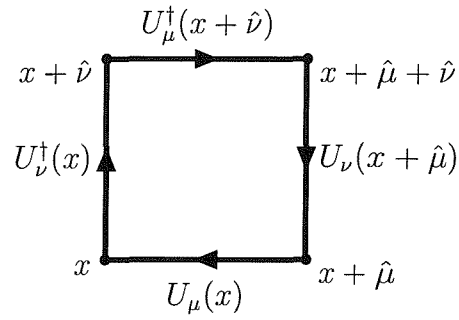

In Wilson's implementation of the gauge action [6], this is used to write the action in the form

$$\mathcal{S}_g^W = -\beta\sum_{x,\mu<\nu}\left[1-\frac{1}{N}\mathrm{Re}\,\mathrm{Tr}\,P_{\mu\nu}(x)\right], \tag{2.8}$$

where $\beta = 2N/g_0^2$ is the lattice coupling and directly relates to the lattice spacing. It may be noted here that the Wilson gauge action has no discretisation errors of $\mathcal{O}(a)$, *i.e.*

$$\mathcal{S}_g^W = \mathcal{S}_g^{\mathrm{cont}} + \mathcal{O}(a^2). \tag{2.9}$$

2.2.2 Quenching

As mentioned earlier, the configurations, in general, are generated with the weight $\exp(-S_g[U] + \mathrm{Tr}\log Q[U]) = \det Q[U]\exp(-S_g[U])$. The quark determinant is expensive to calculate and make the simulations a few orders more costly. Quenching

refers to setting this to a constant, typically unity. This has the effect of removing internal quark loops [7–9]. Rigorous derivations of this can be found in textbooks such as [3]. The propagating quarks are called valence quarks, while the virtual ones that occur only in the loops are called *sea* quarks. Removing the loops is equivalent to saying that the sea quarks are infinitely massive. Therefore, a *dynamical* simulation refers to one with sea quarks of finite-mass, that propagate within closed quark loops.

In a truly unquenched simulation one would have the sea and valence quarks at the same mass as one has in the real world. However, since it is expensive to generate data sets for many sets of sea quarks, there is another class of simulations where there are several values of valence quark mass on for a given sea quark. Such simulations are termed *partially quenched*, because these are like quenched, but with a non-infinite mass for the sea quark.

Though physically quenching has more to do with quarks, in practice it is the gauge configurations that are generated with a difference, the difference being in the weight with which they are generated. The remaining simulation remains exactly the same but just uses the *quenched* or *unquenched* configurations as input.

2.2.3 Monte Carlo generation of the gauge configurations

Our aim is to evaluate correlation functions of the form eq. (2.4) which is of the form

$$\int dU f(...[U])\mathcal{P}[U] \rightarrow \frac{1}{N}\sum_i f(U_i) \tag{2.10}$$

with $\mathcal{P}[U_i]$ being $1/Z$ times the Boltzmann weight with our action in the exponential. The U_i's are already distributed with the appropriate weights and the f's on the rhs can be simply averaged for our answer. Since the number of degrees of freedom in the integration is very large, one has to use a Monte Carlo method for the integration. For this we need to generate configurations, U_i with the distribution $\mathcal{P}[U_i]$ through a *Markov process*, which is one where U_i is generated stochastically

from its predecesssor U_{i-1} in a manner that satisfies

$$\mathcal{T}(U_{i-1} \to U_i)\mathcal{P}(U_{i-1}) = \mathcal{T}(U_i \to U_{i-1})\mathcal{P}(U_i), \tag{2.11}$$

where $\mathcal{T}$ is the relevant transition probability to reach one configuration from the other. However, using all these is not efficient, since successive configurations will be correlated, with the Markov chain being characterised by a *correlation time.* Moreover, the configurations need to be allowed to equilibrate before they can be used. Sketched below are the typical steps in the full process, as observed in practice:

- **Choosing the volume:** The first step is to decide on the volume. Practical considerations such as limitations on computing power are more important than anything else here. One would like to the choose the volume large enough that finite volume effects (changes in the result when you change the volume) are small. This should be the case as long as the Compton wavelengths of the simulated quarks are reasonably small compared to the spatial dimensions of the lattice. It should be noted that the lattice spacing in physical units(fm) is not known beforehand and one usually relies on previous simulations in similar regions of parameter space.

- **Choice of β and κ:** For β one ideally tries to go as high as possible as that refers to a finer lattice. For the κ_{sea} again one would like to simulate lighter (more realistic) quarks and therefore choose one or more values of κ_{sea} as large as possible without slowing down the process too much. Another input that goes in for improved Wilson fermions is the values of c_{SW} which is simply determined for the β as given in sec. 2.3.2.

- **Hot or cold start:** The first configuration to start off the subsequent update steps can be chosen to be made up of either unit or random $SU(3)$ matrices along the links. If unit matrices are used, it is termed a cold start, whereas a hot start implies random $SU(3)$ links. However, the final configurations should be independent of this choice. A cold start option is useful for simple tests on

code components on a unit gauge configuration, which is exactly what a cold start sets up. For completeness, it should also be mentioned that one may use a previously generated configuration as the starting point.

- **Algorithms to generate the Markov chain:** There is more than one method of generating the Markov chain of configurations. A popular choice for general Monte Carlo calculations is the Metropolis algorithm [10]. For quenched configurations, a more efficient algorithm is the Cabibbo-Marinari heatbath method [11]. This is the one we use to generate the configurations for our doublecharm study. It is usually efficient to supplement the heatbath steps with some overrelaxation ones. There are other methods such as hybrid Monte Carlo or multiboson algorithms that are used for dynamical configurations.

- **Thermalisation or equilibration:** The plaquette variable has been introduced in eq. (2.7). The average value of the possible plaquettes is a simple and widely used measurable quantity of a configuration. In fig. 2.2, these values are plotted for the first 1000 update steps. When the values reach a stage that they are fiuctuating around some stable value, we say that the configurations are equilibrated or thermalised. It is important not to start using configurations before equilibration is achieved. It should be noted that equilibration also has some observable dependence and in an ideal world, one should check with the observable being calculated, however, in practice we get our real observable (the correlators) much later in the simulation and a decision on the configurations have to be made without that knowledge.

- **Decorrelation:** Even after equilibration, the configurations have some short-range autocorrelation (correlation with the past or future values). Therefore it is important that one measures this correlation length and uses configurations spaced by a separation that decorrelates them sufficiently. For this, one can use any standard statistical measures of autocorrelation. Just to give an example,

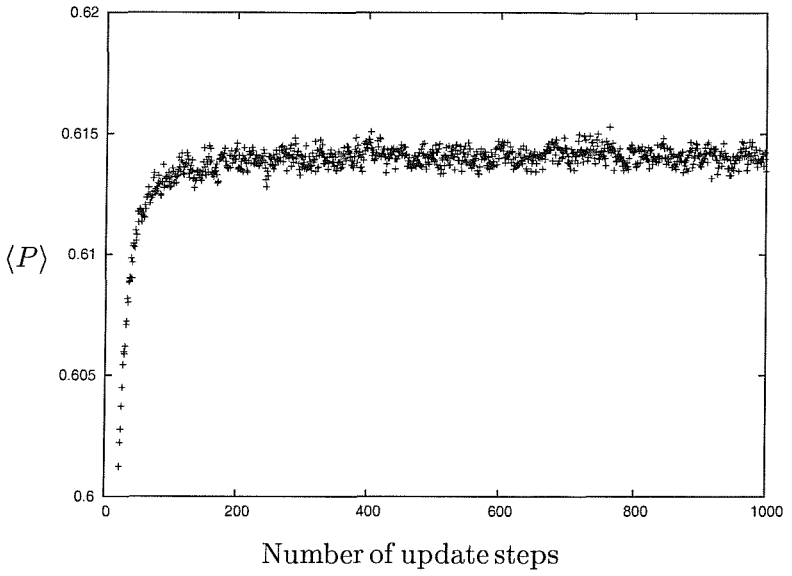

Figure 2.2: Average plaquette values for configurations from the first 1000 heatbath steps for a test case.

for the study on doublecharm baryons, where the configurations were generated here, we used 1000 heatbath steps to equilibrate and then 200 steps between each saved configuration to ensure decorrelation. It may be mentioned here that in principle, one could get correct results even using a correlated set of configurations if one could calculate enough of them. However, since the subsequent calculation of observables is much more expensive, particularly for quenched configurations, it is sensible to decorrelate the configurations first.

- **Technicalities for unquenched configurations:** Since the effective action

$$S_{\text{eff}} = \det Q[U] \exp(-S_g[U]) \tag{2.12}$$

is to be associated with a probabilistic interpretation, it has to be positive definite. But, $\det Q$ is not so. Therefore typically one uses

$$S_{\text{eff}} = \det(Q^\dagger[U]Q[U]) \exp(-S_g[U]) \tag{2.13}$$

corresponding to two degenerate quarks ($N_f = 2$). Fortunately, in nature the two lightest quarks are indeed nearly degenerate and significantly lighter than

the other flavours, hence it is physically justifiable to have two light quarks in the loops. It remains difficult to add an odd number of light quarks for Wilson fermions, but a third heavy quarks can be added without much trouble. This problem does not arise for overlap fermions.

Once we have our ensemble of decorrelated gauge configurations we may turn our attention to the fermionic part of our calculation.

2.3 Fermion propagators

Let us take the very simple example of the propagation of a pion. Then our operator of eq. (2.1) would consist of a pion creation operator at some point and an annihilation at some other point.

$$\begin{aligned} \mathcal{O} &= J_\pi(y)\bar{J}_\pi(x) \\ &= \left(u(y)\gamma_5\bar{d}(y)\right)\left(\bar{u}(x)\gamma_5 d(x)\right) \end{aligned} \tag{2.14}$$

Inside a correlation function, the quark fields can then be contracted to write the expression in terms of quark propagators of the form $S_q(x,y)^{ab}_{\alpha\beta}$, where a, b and α, β are colour and Dirac indices respectively. Generation of these propagators forms an important intermediate step in the simulation.

Looking at the QCD Lagrangian, the propagator is obtained by inverting the Dirac operator, Q

$$S_u(y,x)^{ad}_{\alpha\delta} = \langle u^a_\alpha(y)\bar{u}^d_\delta(x)\rangle = (Q^{-1})^{x,a,\alpha}_{y,d,\delta} \tag{2.15}$$

Computationally, this is usually the most expensive part of the simulation. The two most common algorithms for this inversion are the Minimum Residue (MR) method [12] and the Stabilised Biconjugate Gradient (BiCGStab) method [13, 14]. For our simulations we use the latter which, though slightly more expensive, is numerically more stable particularly for lighter masses.

Moreover, whereas the discretisation of the gauge action is conceptually straightforward, the discretisation of the fermion action leads to complications that are

amongst the major issues still being addressed.

A naively discretised lattice Dirac operator

$$Q_{\text{naive}} = \frac{1}{2}(\nabla_\mu + \nabla^*_\mu)\gamma_\mu + m_0, \tag{2.16}$$

∇ being the discretised derivative operator defined in sec. 2.3.1, gives a propagator of the form

$$S(p) = \frac{a}{\gamma_\mu \sin(ap_\mu) + ma}. \tag{2.17}$$

Apart from the pole at $ap = 0$ this has additional zeros at $ap = \pi$, *i.e.* there is a doubling in each dimension. This is known as the doubling problem and for four dimensions we have 16 copies of our fermion field.

This has led to different formulations (essentially discretisations) of the fermionic action. In this work we use Wilson fermions, which is introduced below. Details of the others are available in standard texts and are not repeated here.

2.3.1 Wilson fermions

One way out of the doubling problem is to add the Wilson term leading to the Wilson-Dirac operator [15]

$$Q_W = Q_{\text{naive}} - \frac{ar}{2}\nabla_\mu\nabla^*_\mu. \tag{2.18}$$

This explicitly breaks chiral symmetry but it is recovered in the continuum. Meanwhile the *doublers* acquire mass of the order of the cutoff, a^{-1}, thus removing the degeneracy. r can be an arbitrary non-zero number and is usually set to unity. The factor of $1/2$ is conventional.

Now for the discretised fermion action in terms of our fermion (ψ) and gauge-link (U) fields, one can define the covariant derivatives

$$\begin{aligned} \nabla_\mu\psi(x) &= \frac{1}{a}\left(U_\mu(x)\psi(x+\hat{\mu}) - \psi(x)\right) \\ \nabla^*_\mu\psi(x) &= \frac{1}{a}\left(\psi(x) - U^\dagger_\mu(x-\hat{\mu})\psi(x-\hat{\mu})\right). \end{aligned} \tag{2.19}$$

This leads to

$$\begin{aligned} \mathcal{S}_f[U,\bar{\psi},\psi] \;=\; \sum_x \Big\{ &-\frac{1}{2}\sum_{\mu=0}^{3} \big[\bar{\psi}(x)(1-\gamma_\mu)U_\mu(x)\psi(x+\hat{\mu}) \\ &\qquad + \bar{\psi}(x)(1+\gamma_\mu)U_\mu^\dagger(x-\hat{\mu})\psi(x-\hat{\mu})\big] \\ &+ \bar{\psi}(x)\big(m_0+4\big)\psi(x)\Big\}. \end{aligned} \tag{2.20}$$

It is further a matter of convention to rescale ψ and $\bar{\psi}$ by

$$\psi(x) \to \sqrt{2\kappa}\,\psi(x), \qquad \bar{\psi}(x) \to \bar{\psi}(x)\sqrt{2\kappa} \tag{2.21}$$

and fix κ by requiring $2\kappa(m_0+4)=1$. Thus κ determines the quark masses.

2.3.2 Clover improvement

While the gauge part of the Wilson action is free from $\mathcal{O}(a)$ errors, the fermionic part indeed suffers from discretisation errors of this order. Attempts to remove these errors are termed *improvement* and have received considerable attention. The Wilson fermion action is improved by adding a compensating $\mathcal{O}(a)$ term of the form [16]

$$-\frac{ac_{\mathrm{SW}}}{2}\sum_{x,\mu<\nu}\bar{\psi}(x)\sigma^{\mu\nu}G_{\mu\nu}(x)\psi(x) \tag{2.22}$$

where $G_{\mu\nu}(x)$ is given by

$$\begin{aligned} G_{\mu\nu}(x) \;=\; \frac{1}{4}\big[&U_\mu(x)U_\nu(x+a\hat{\mu})U_\mu^\dagger(x+a\hat{\nu})U_\nu^\dagger(x) \\ &+U_\nu(x)U_\mu^\dagger(x-a\hat{\mu}+a\hat{\nu})U_\nu^\dagger(x-a\hat{\mu})U_\mu(x-a\hat{\mu}) \\ &+U_\mu^\dagger(x-a\hat{\mu})U_\nu^\dagger(x-a\hat{\mu}-a\hat{\nu})U_\mu(x-a\hat{\mu}-a\hat{\nu})U_\nu(x-a\hat{\nu}) \\ &+U_\nu^\dagger(x-a\hat{\nu})U_\mu(x-a\hat{\nu})U_\nu(x)U_\mu^\dagger(x+a\hat{\mu}-a\hat{\nu})\big] \end{aligned} \tag{2.23}$$

and resembles a clover in shape [fig. 2.3], hence the name *clover*.

Like the Wilson r-term, this term, being of $\mathcal{O}(a)$, vanishes in the continuum limit and thus leaves the continuum action unchanged. c_{SW} is known as the Sheikholeslami-Wohlert coefficient and its value is determined perturbatively [17] or non-perturbatively [18] to achieve a cancellation of the $\mathcal{O}(a)$ discretisation artefacts.

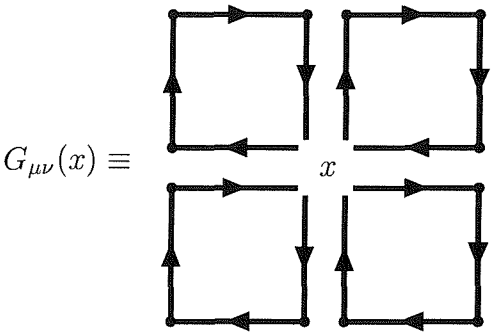

Figure 2.3: $G_{\mu\nu}$ in the clover term for $\mathcal{O}(a)$-improvement. The extra term is called a clover term due to the resemblance of this $G_{\mu\nu}$ with a clover.

For the quenched case, the non-perturbative value of $c_{\rm SW}$ is determined from the empirical formula [18] obtained after studying a series of couplings

$$c_{\rm SW} = \frac{1 - 0.656g_0^2 - 0.152g_0^4 - 0.054g_0^6}{1 - 0.922g_0^2}, \qquad 0 \leq g_0 \leq 1. \tag{2.24}$$

For two flavours of dynamical fermions, this gets modified to [19]

$$c_{\rm SW} = \frac{1 - 0.454g_0^2 - 0.175g_0^4 - 0.012g_0^6 - 0.045g_0^8}{1 - 0.720g_0^2}, \qquad 0 \leq g_0 \leq 1. \tag{2.25}$$

A similar expression for $N_f = 3$ is now available in [20].

Coming back to the point-of-view of the lattice simulation practitioner, when one refers to *non-perturbatively $\mathcal{O}(a)$-improved Wilson fermions*, it simply means, the value of $c_{\rm SW}$ used is from eq. (2.24) or eq. (2.25) as applicable.

2.4 The complete Wilson lattice action

We now have Wilson's lattice action for QCD

$$\begin{aligned} S_{\rm QCD}[U,\bar{\psi},\psi] &= \beta\sum\left(1-\frac{1}{3}{\rm ReTr}P\right) \\ &+\sum_x\Bigg\{-\kappa\sum_{\mu=0}^{3}\left[\bar{\psi}(x)(1-\gamma_\mu)U_\mu(x)\psi(x+\hat{\mu})\right. \\ &\qquad\left.+\bar{\psi}(x)(1+\gamma_\mu)U_\mu^\dagger(x-\hat{\mu})\psi(x-\hat{\mu})\right] \\ &+\bar{\psi}(x)\psi(x)\Bigg\}. \end{aligned} \tag{2.26}$$

We have traded parameters: $(g_0, m_0) \rightarrow (\beta, \kappa)$, with:

$$\beta = \frac{6}{g_0^2}, \qquad \kappa = \frac{1}{2m_0+8}. \tag{2.27}$$

In practice, β and κ are the parameters quoted and a higher value of β points to a finer lattice spacing while a larger κ points to a lighter quark in the simulation.

2.5 Correlation functions

So, for a given β (and $\kappa_{\rm sea}$ for a dynamical case) we will have one set of configurations and on each configuration we can generate several quark propagators at varying κ (quark mass). The typical propagator would have one end in the origin with the other one running over all points of the lattice. Next they need to be tied up according to the intended calculation. Effectively all the steps before this are generic and it is sometimes possible to find gauge configurations and occasionally propagators archived from previous work that can be reused. Configurations or propagators that are expensive to generate are usually archived anyway and intended to be used in multiple studies. But, the correlation function(s) or correlator(s) are specific to the study.

Essentially, all phenomenology calculations are either one of spectroscopy or of some matrix element. Basic elements of the correlation functions for such calculations are described below.

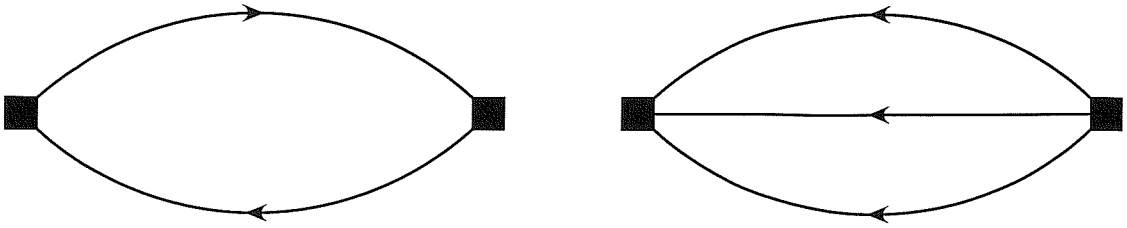

Figure 2.4: Meson and baryon 2-pt functions. The black boxes are meson/baryon creation/annihilation operators, while the arrows correspond to quarks propagators.

2.5.1 For a spectroscopy calculation

For spectroscopy, *i.e.* a calculation of mass, one looks at the propagation of the intended state. Therefore a creation operator with the right quantum numbers for the state is used to create the state at the origin and then it is annihilated after propagating for a while. This is typically called a two-point correlation function.

$$C_2(t) = \sum_{\vec{x}} \langle 0|\mathcal{O}(\vec{x},t)\mathcal{O}^\dagger(0)|0\rangle \tag{2.28}$$

where the subscript 2 denotes that it is a two-pt function. The sum over spatial sites projects on to zero momentum and then we can relate the correlators to the mass. Inserting a complete set of energy eigenstates and using

$$\mathcal{O}(t) = e^{Ht}\mathcal{O}e^{-Ht} \tag{2.29}$$

we get,

$$C_2(t) = \sum_n \frac{1}{2E_n}|\langle 0|\mathcal{O}|n\rangle|^2 e^{-E_n t}. \tag{2.30}$$

Here the normalisation is conventional. At large times only the lowest energy state survives giving

$$C_2(t) \overset{t\to\infty}{\longrightarrow} \frac{1}{2m_1}|\langle 0|\mathcal{O}|1\rangle|^2 e^{-m_1 t} \tag{2.31}$$

For visualisation, one often uses an effective mass plot [fig. (2.5)]. In this plot $\ln[C(t)/C(t+1)]$ asymptotically approaches the mass. The flat region is called the

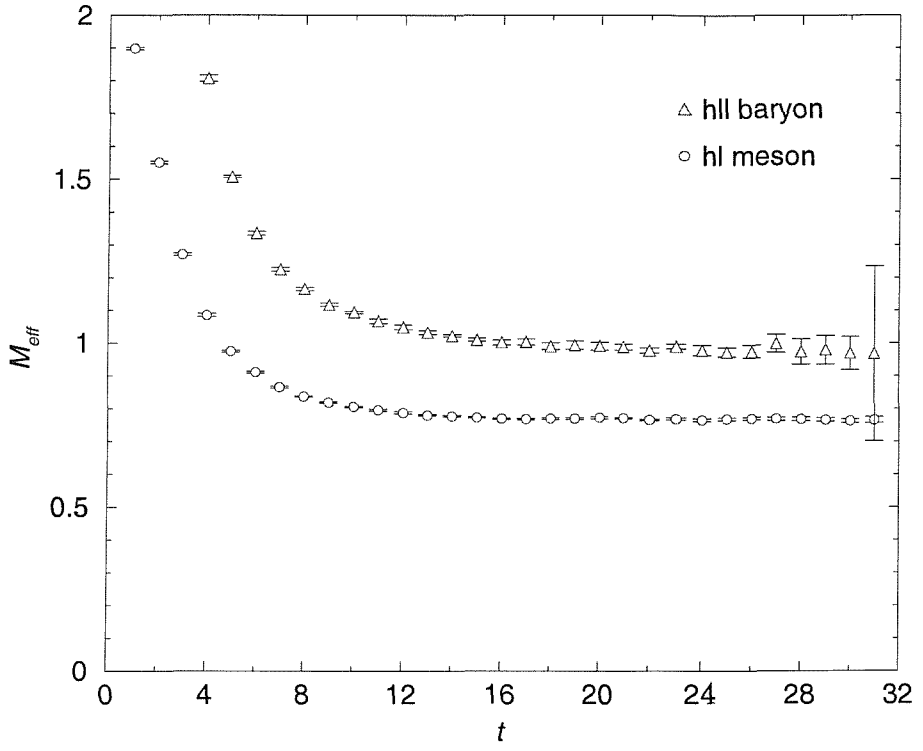

Figure 2.5: Example of an effective mass plot showing *hl* (heavy-light) and *hll* (heavy-light-light) hadron 2-pt functions on the first half of the lattice [heavy quarks are relativistic]. The plateaux are the regions where the plots are to be fitted.

plateau and this is where the correlator is supposed to contain purely the ground state. A fit-window is chosen as large as possible in this range and the correlator is then fitted by a suitable function to obtain the mass. It is also possible to start earlier and use a double exponential fit to obtain the first excited state as well, but identifying that state may not always be straightforward.

2.5.2 For a calculation of matrix elements

Determination of QCD matrix elements is one area where lattice methods are the only ways of obtaining rigorous quantitative estimates. Examples of B_K and the Λ_b lifetime calculations will be discussed in more detail in chapters 4 and 5 respectively. Typically, one has to evaluate 3-pt correlation functions with the physical states

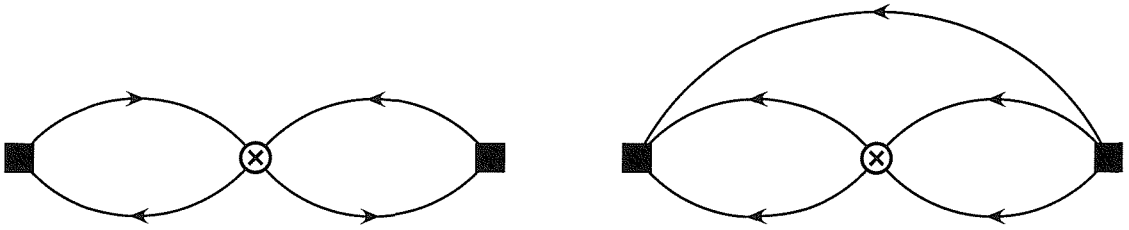

Figure 2.6: Example 3-pt functions. Here the circled crosses are four-quark operators. The above two diagrams, sometimes referred to as the *figure of eight* and *crab* diagrams respectively will occur in our B_K and Λ_b problems.

involved being created or annihilated at two of the three points, the operator sits at the third point and effects the required transition.

The sources for the physical states lead to extra factors of normalisation constants and exponentials that are removed by taking ratios with suitable two-point functions. After necessarily manipulation, the matrix element extracted from the simulation are for the lattice regularisation scheme and at the scale a^{-1}. For purpose of phenomenology, one uses renormalisation group running to convert this number, usually to some continuum scheme like $\overline{\text{MS}}$ and a convenient scale, μ (for example, μ will taken to be 2 GeV for B_K and m_b for the Λ_b-lifetime),

$$O_i^{\overline{\text{MS}},\mu} = Z_{ij}(\mu, a^{-1}) O_j^{\text{latt},a^{-1}}. \tag{2.32}$$

The matching can be done in two steps:

$$\text{latt}, a^{-1} \longrightarrow \overline{\text{MS}}, a^{-1} \longrightarrow \overline{\text{MS}}, \mu. \tag{2.33}$$

This process is explained in further detail in the relevant chapters.

2.6 Analysis of the simulated data

By analysis, here we refer to the manipulation of data after generating the correlation functions. It may be mentioned here that this stage of a lattice calculation, can be and usually is done on PCs with the components prior to this usually done on larger computers.

2.6.1 Statistical error: clustering + jackknife/bootstrap

When a correlator is calculated on a single gauge field configuration, it does not have the continuum properties, like the exponential long-time behaviour, required for the extraction of physically relevant information. These properties only re-emerge when one averages over a suitable number of gauge configurations, the statistical error being proportional to $1/\sqrt{N_{\rm conf}}$. There is more than one way to do to estimate the statistical error. In our case, we usually bunch one-tenth of our configurations into a cluster and average over them individually. Then the statistical error is obtained by a jackknife procedure [21, 22] over the ten clusters. Ideally, though, one should try different cluster or bin sizes and make sure the statistical error is stable. For a cluster size that is too small, the error is underestimated. Some prefer to use the bootstrap method [23]. Though there are different ways of estimating the error, for a simulation practitioner, for most practical purposes it is usually alright to use any of the alternatives.

2.6.2 Fitting the data

Once the averages and statistical errors for the data points are determined, the data has to be fitted to a suitable function. In case of 2-pt functions for spectroscopy it is usually an exponential function or some modification of it, whereas for ratios of 3-pt to 2-pt functions for matrix elements it may be fitting to a constant. There are other occasions as well in the analysis when one needs to fit some data. This is done in the typical χ^2-minimisation procedure, with

$$\chi^2(\text{fit parameters}) = \sum_i \frac{[f_{\rm sim}(x_i) - f_{\rm fit}(x_i; \text{fit parameters})]^2}{[\delta f_{\rm sim}(x_i)]^2}. \qquad (2.34)$$

For non-linear fits, probably the most widely used method is the Levenberg-Marquardt [24, 25]. In cases where there is correlation within the data, one may need to use a correlated fit.

2.6.3 Lattice to continuum matching

As mentioned in the previous section, the next step that comes up, only for matrix elements, is the matching from lattice regularisation to some continuum scheme as well as shifting the scale from the inverse lattice spacing to some more conveniently understood scale. The renormalisation coefficients required for this matching are usually calculated in a separate programme and end up as numbers that can be plugged into the analysis. There is also the choice between a perturbative and non-perturbative determination of the matching coefficients.

2.6.4 Determination of the lattice spacing

In the simulations masses come out as dimensionless quantities of the form $a \times$ mass. To remove the spacing, one has to choose a known physical quantity and set the scale using the experimental value. We usually use a ratio of the values of m_K^* and m_K. It should be noted there is always a systematic error associated to the choice of the quantity used to set the scale. It may be noted that for dynamical simulations in the continuum limit there should be no ambiguity. But, in the quenched case, even if one goes to the continuum limit quenching artefacts lead to a variation of the spacing.

2.6.5 Extra(inter)polation to the intended masses

In the simulation, it is not possible to use realistically light quarks as the cost of propagator inversion blows up as we go lighter, simulated quarks are around the strange-charm region. Even for strange or charm masses which can be simulated, we actually don't know where it exactly will be and therefore one needs to simulate at a range of quark masses (κ values) and then in the analysis stage one has to extrapolate or interpolate to realistic masses. Since the pseudoscalar mass squared is proportional to the quark mass, one can take a quantity and plot it against $(am_P)^2$. For the light (u, d) quarks, one often simply goes to $(am_P)^2 = 0$, or can try to be

precise by going to $(am_P)^2 = (am_\pi^{\rm phys})^2$. Similarly, the strange and charm scales can be set by using kaon and D mesons, or any other strange/charm quantity.

A probably less agreed upon issue is the form of fit-function for the extrapolation or interpolation. It is usual to look for any curvature in the data, however, unless there is convincing evidence of non-linearity, particularly unless one is convinced that one is seeing true chiral logs, it is probably sensible to simply use linear fits. In our simulations, we are not really interested in *light* quantities *i.e.* those involving only up and/or down quarks. Our simulation also does not go to very light masses. Therefore we use linear fits for our results. However, sometimes we do use quadratic and/or chiral log fits to comment on the systematic uncertainty connected to the choice of extra/interpolation function

2.6.6 Continuum extrapolation

It is also important to work with more than one lattice spacing and then do a continuum extrapolation to $a \to 0$. However, it may be noted that often there are not enough computational resources to do this, as was the case with us. In such cases, the results reported are for some given lattice spacing.

2.6.7 Analysis of errors

One of the most important claims of lattice QCD is that, though there are errors, as in any other method, here the errors can be well-estimated and systematically reduced, apart from quenching and some symmetry breaking effects. Therefore in any calculation, a significant proportion of time and effort is spent on an analysis of the errors. This is discussed in a little bit more detail in the next section.

2.7 Errors in a simulation

Errors in a lattice calculation are of two main types: statistical and systematic. When two errors are reported after a result, conventionally, the first and second

ones are the statistical and systematic errors respectively. Sometimes, asymmetric errors are quoted for the systematic error. In some cases, results may be reported with only the statistical error.

2.7.1 Statistical error

This is the error arising from the limited statistics available. As already mentioned, this goes like the $1/\sqrt{N_{\text{conf}}}$ and is estimated using a jackknife or bootstrap method.

2.7.2 Systematic error

For the systematic error one attempts to quantify the possible variation due to choices made for the simulation/analysis. In some cases these choices are forced by practical constraints, whereas in other cases a degree of arbitrariness simply exists in the choices. Some of these are described below to illustrate the point.

Finite volume errors

This is an example of an error that is usually forced by computational constraints. As the cost of simulation grows with the number of points on the lattice, we always have a limited volume for our simulation, usually of something in the range of 2 fm in spatial dimension. Squeezing our physical system into such a finite box can affect the quantities we are trying to measure. Therefore, ideally one should work at more than one volume and look at the volume dependence of the results. Then one should work at a volume where there is no further variation and/or quote the variation in that region as a measure of the systematic error due to finite volume. In our case, unfortunately, we are restricted to using just one volume, but where possible we refer to other studies on finite volume effects in the relevant region.

Errors in the extrapolation or interpolation

As mentioned in sec. 2.6.5, in the simulations we cannot *a priori* sit on top of the realistic quark masses and have to extrapolate or interpolate to the physical masses.

The form of this extra(inter)polating function is not beyond question. This can become more of an issue at light masses, where one starts to expect to see *chiral logarithms*. Therefore, it often is an open question as to whether one should use a linear fit, some higher polynomial or some function suggested by chiral perturbation theory. In our case, since our focus is not on light quantities and since our simulations do not go to extremely light masses, we simply use linear fits for our main results. In the doublecharm baryon study we include variations from quadratic fits in the systematic error, whereas for the B_K study we do not quote a systematic error, but include quadratic and chiral log fits to illustrate the possible variation.

Continuum extrapolation

The true physical world is recovered only when we go to the continuum, otherwise there remain several artefacts of finite lattice spacing. Ideally, one should work with different lattice spacings (β values) and extrapolate to the continuum. In the absence of this continuum extrapolation, the result quoted is essentially the result for that finite value of the spacing and suffers from $\mathcal{O}(a^2)$ discretisation errors ($\mathcal{O}(a)$ for unimproved simulations). Here again, we are restricted to working with only one spacing and hence are unable to extrapolate to the continuum limit.

Choice of fit-window

As already mentioned, typically one looks at the correlation functions, sometimes in the form of effective mass plots or ratios of different correlators, and chooses a fit-window, where it is expected that contamination from higher states are negligible. This choice may be rather subjective and there are ideas of *sliding window* analysis etc. where the fit window is varied and the best window found in some iterative process. For the doublecharm study, we report results for one fit-window and then repeat the analysis for adjecent alternative windows and include the variation in the quoted systematic error.

Setting the spacing and scales with known quantities

In the analysis stage, one of our observables have to be sacrificed for the spacing and each scale (*e.g.* m_s or m_c) that we need to set. Again there is a choice of quantities that can be used and this leads to a variation. This can also be incorporated in the systematic error, by looking at the variation arising when alternative observables are used. This is indeed done in our doublecharm study.

Quenching

The error due to quenching is difficult to quantify. The only way to judge it is by looking *a posteriori* at the discrepancy between quenched estimates and experimental values and by ascribing it to quenching and any unaddressed systematic effects. A third error providing such an estimate is provided for our results in the doublecharm study.

2.8 Steps in a simulation

To summarise, below is the skeleton structure of the steps in a typical lattice simulation.

- Choice of action, appropriate volume and other parameters
- Generate gauge configurations using Monte Carlo algorithms
  - Metropolis
  - Heatbath - *this one is used for the doublecharm study*
  - Hybrid Monte Carlo
  - Multiboson
- Propagator inversion
  - Minimum Residue method

  - Stabilized Biconjugate Gradient method - *this one is used for these simulations*

- Correlator contraction
- Averaging and determination of statistical error by jackknife or bootstrap
- Chiral extrapolation
- Infinite volume extrapolation
- Continuum extrapolation
- Setting of the scales with known quantities
- Analysis of systematic errors

Chapter 3

Spectroscopy of double-charm baryons

This chapter is based on the published paper:
J.M. Flynn, F. Mescia and A.S.B. Tariq [UKQCD Collaboration], "Spectroscopy of doubly-charmed baryons in lattice QCD", JHEP **0307** (2003) 066 [arXiv:hep-lat/0307025].

3.1 Motivation and background

The baryon multiplets of flavour $SU(4)$ are plotted in fig. (3.1). For unbroken $SU(4)$, the masses of all the states in the multiplet would be degenerate. Since the mass of the charm quark is much greater than the other three, this breaks the degeneracy and splits it into sub-multiplets with different numbers of charm quarks. It is intriguing to note that, though the existence of all these states has been expected within QCD for decades, the first observation of a state with two charm quarks, was reported only in 2002 at the SELEX experiment in Fermilab [26] and still lacks sufficient experimental verification to find a place in the summary tables of the Particle Data Book 2004 [27].

Double charmed baryons combine the opposites of the slow relative motion of two heavy quarks with the fast motion of a light quark. They provide scope for testing ideas developed for single charm physics, such as the predicted hierarchies

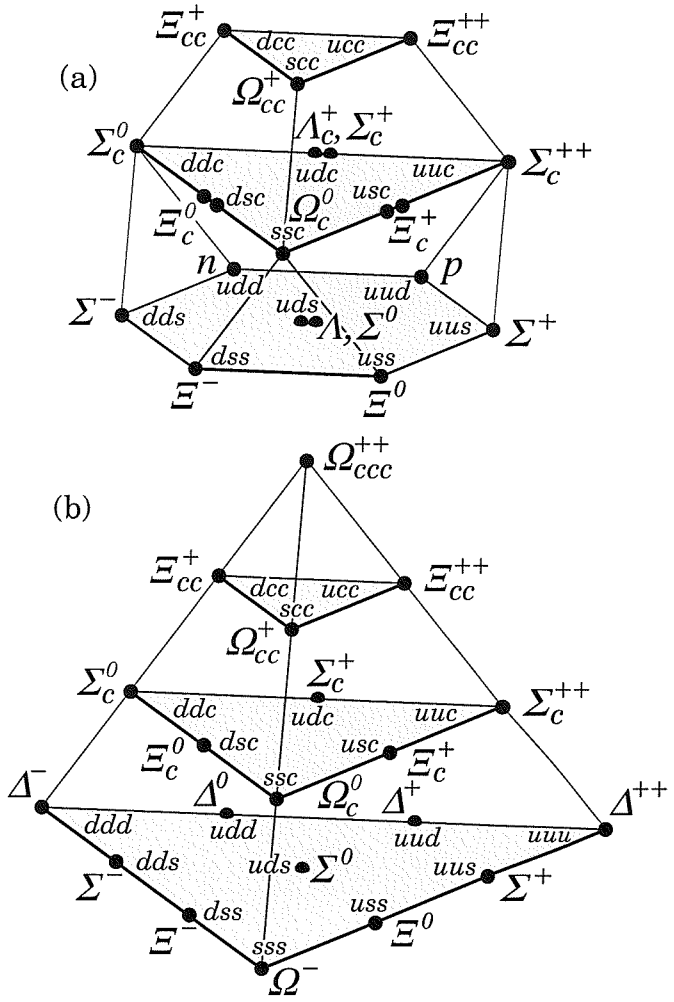

Figure 3.1: 20-plets of SU(4) [badly broken by m_{charm}]. Figure from [27].

in lifetimes and semi-leptonic branching ratios and give us more room to explore predictions of exotic tetra- and penta-quark states (see [28] for a review of the relevance of double-charm baryons).

3.1.1 Experimental status

As mentioned above, the first observation of double-charmed states was made in 2002 by the SELEX experiment in Fermilab. Initially there were three states observed at 3520, 3460 and 3780 MeV [29–31], with two more reported later at 3443 and 3541 MeV [32, 33]. All these were observed in decays to $\Lambda_c^+ K^-$ and one or two π^+'s. But of these, only one: the $\Xi_{cc}^+(3520)$ has been published [26] with a very recent confirmation of the observation of this state from the same experiment, but from a different channel pD^+K^- [34].

Unresolved issues regarding the confirmed SELEX observation itself include the fact that the observed lifetime of less than 30 fs is much less than the $\sim$ 400 fs predicted by quark models [35]. This has led [36] to cast some doubt over the observation. This state has also not been observed in any other experiment, particular candidates being FOCUS and E791, but SELEX claims that this does not contradict their result. According to their understanding, experimental detail, such as the fact that they themselves see the signal only in the case of baryonic beams (as opposed to pionic ones) and that only SELEX covers the forward hemisphere with baryon beams when these events are observed, might explain the non-observation of these states in other experiments.

The other states that have been reported by SELEX in more informal ways, but have not yet been published are summarised in fig. 3.2. SELEX proposes an understanding of these states in terms of two isodoublets, separated by the energy of a diquark orbital excitation with the higher mass states decaying weakly to the lower ones [32, 33]. It is to be noted that, in this picture, the Ξ_{cc}^+ ground state will be the 3443 MeV one. Moreover, the 3780 MeV state is interpreted as a light quark p-wave excitation. If this picture is correct, the isospin splitting is $\sim$ 20 MeV which

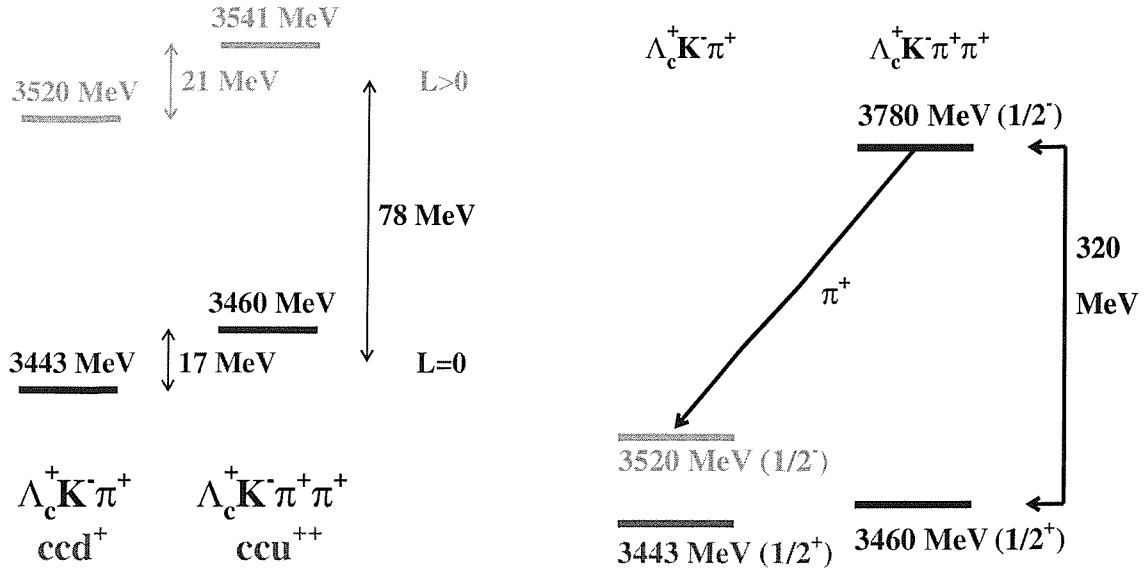

Figure 3.2: States observed by SELEX, including the non-published ones. [Figures from SELEX]

is about 15 times that for the nucleons and is also inverted, *i.e.* $m(ccu) > m(ccd)$. They suggest that this may be due to the fact that the core diquark charge here is 4/3 instead of 1/3. Also the isospin splitting for the single-charmed Ξ_c is itself more than four times that for the nucleons. Nevertheless, these issues require further understanding and this is perhaps the reason behind the delay in publication of the other states.

For the purpose of this study, we take only the published state of $\Xi_{cc}^+(3520)$ as observed and ignore the other states.

3.1.2 Previous theoretical studies

The first prediction for the masses of these double-charmed baryons comes from the early work of [37] around the days when charm was being discovered. This was followed by a more than a decade of relative inactivity. The subject seems to have livened up a bit over the last 15 years with a good number of further calculations from quark models and QCD sum rules [38–47]. Most of these calculations, in

general, predict a ground state around 3.6 GeV and a hyperfine splitting of 50-150 MeV. A good deal of work has been done as well on the lifetimes of these states, from the works of [48, 49] in the mid-80's to the more recent studies using quark models and sum rules [35, 50].

There have been only two lattice studies from one group before the one reported in this chapter. They use the D234 action [51] and NRQCD [52] and find numbers consistent with each other and also with the quark model predictions. There was another lattice NRQCD study that included double-heavy baryons, but was focused on hadrons with a b-quark [53].

3.1.3 Motivation for a lattice calculation

Almost all previous calculations are in the framework of various quark models, which can be quite subjective to tuning of parameters and over-simplifying assumptions. On the other hand, lattice QCD provides a method of calculating the masses of these baryons from first principles in a model-independent and non-perturbative manner.

It is also interesting to compare the results from different lattice calculational techniques. Previous lattice calculations have used the D234 action [51] and NRQCD [52]. NRQCD is less suitable for charm quarks than for beauty quarks, and furthermore charm quark masses are very accessible to lattice simulation without using an effective theory. In this calculation we use a non-perturbatively $\mathcal{O}(a)$-improved clover action [18].

These calculations performed on the Southampton PC cluster Iridis with the code FermiQCD [54, 55] were the first full-fledged ones using both of these (the cluster and the code).

3.1.4 An additional aspect: study of spin splittings

We also study spin-splittings for charmed baryons and mesons, where the leading charm quark mass dependence cancels. Historically, there has been a problem of a suppression of hyperfine splittings in lattice simulations. However, recent

calculations using the $\mathcal{O}(a)$ non-perturbatively improved clover action find vector-pseudoscalar meson splittings in better agreement [56, 57] with experiment than earlier calculations using less-improved clover actions [58].

For the single-charmed baryons, calculations with a tree-level clover action had difficulty reproducing the experimental splittings [59], while simulations using the D234 [51] or NRQCD [52] actions were compatible with experiment. For the single-charmed baryons we can compare with experiment, whereas, for the doubly-charmed baryons, experimental data are not yet available. However, we may compare our results with those from the other simulations for the doublecharm. Since the hyperfine splitting is sensitive to the chromomagnetic moment term in the improved clover fermion action, this could show the importance of using the non-perturbative value for its coefficient ($c_{\rm SW}$). A similar observation was made concerning the coupling with the chromomagnetic field in the NRQCD action [52] (c_4 in eq. (A5) in [52]).

Some interesting features are observed and predicted in heavy hadronic hyperfine splittings, *e.g.* the constancy of $M_V^2 - M_P^2$ for mesons [60–63], constancy of the ratio of mesonic and baryonic spin splittings [64, 65] etc. A good discussion from a lattice perspective is available in [51].

3.1.5 The charmed baryon states: some nomenclature

The double and single charmed baryons expected in QCD are summarised in tab. 3.1. Since on the lattice it is not possible to distinguish between u and d quarks, we have states in the isospin limit and, *e.g.* Ξ_{cc} refers to both the ccu and ccd states, which would otherwise be distinguished by their charges as Ξ_{cc}^{++} and Ξ_{cc}^{+}. Furthermore, we have spin-1/2 and 3/2 states. The spin-3/2 states are denoted by an asterisk. Operators creating spin-3/2 states [*e.g.* J_γ^μ in eq. (3.3)] also couple to spin-1/2, but for two identical quarks the diquark can only couple to spin 1 and there is only one spin-1/2 state. Therefore, the spin-1/2 state projected from a spin-3/2 operator is degenerate with the state produced by a spin-1/2 operator [*e.g.* J_γ in eq. (3.2)]. For three distinct quarks the diquark can be in spin 0 or 1, leading to two different

Baryon	Quark content	Mass [MeV]
	$s_{cc} = 1,\ J^P = 1/2^+$	
Ξ_{cc}	$ccu,\ ccd$	3519(5)
Ω_{cc}	ccs	
	$s_{cc} = 1,\ J^P = 3/2^+$	
Ξ^*_{cc}	$ccu,\ ccd$	
Ω^*_{cc}	ccs	
	$s_{ll} = 0,\ J^P = 1/2^+$	
Λ_c	cud	2285(1)
Ξ_c	$cus,\ cds$	2469(1)
	$s_{ll} = 1,\ J^P = 1/2^+$	
Σ_c	$cuu,\ cud,\ cdd$	2452(1)
Ξ'_c	$cus,\ cds$	2575(3)
Ω_c	css	2698(3)
	$s_{ll} = 1,\ J^P = 3/2^+$	
Σ^*_c	$cuu,\ cud,\ cdd$	2518(2)
Ξ^*_c	$cus,\ cds$	2646(2)
Ω^*_c	css	

Table 3.1: Summary of charmed baryons. Valence quark content and spin-parity are shown. The quantities s_{cc} and s_{ll} are the total spin of the charm and light quark pair respectively. The experimental values are from ref. [66], averaged over isospin multiplets. The Ξ_{cc} mass is from the recent observation of the $\Xi^+_{cc}(ccd)$ [26].

spin-1/2 states. Sometimes called the Λ- and Σ-like states [67], these states are distinguished either by Λ and Σ symbols or by a prime for the Σ-like states.

3.2 Calculation of the relevant baryon 2-pt functions on the lattice

On the lattice, the masses of these hadrons can be calculated in the usual way from the large time behaviour of two point correlation functions

$$C(t) = \sum_{\mathbf{x}} \langle 0|J(\mathbf{x},t)\bar{J}(0)|0\rangle \tag{3.1}$$

where the J's are interpolating operators with quantum numbers to create or annihilate the state of interest. The choice of operators is not unique.

For the spin-1/2 double-heavy baryon states, a simple operator is

$$J_\gamma = \epsilon_{abc}\, h^a_\gamma \left(h^{bT}\, \gamma_5 \mathcal{C}\, l^c \right), \qquad s_{hh} = 1 \tag{3.2}$$

where a, b, c are colour indices, $\mathcal{C}$ is the charge conjugation matrix and the h and l fields stand for generic heavy and light quarks.

In S-wave baryons with two identical quarks (heavy quarks in our case), the two quarks cannot couple to spin zero and the only possibility is $s_{hh} = 1$ (symmetric in both spin and flavour). The component $s_{hh} = 0$ as well as the operator $-\epsilon_{abc}\, l^a_\gamma\, (h^{bT}\, \gamma_5 \mathcal{C}\, h^c)$ vanish. The coupling of the light-quark spin to $s_{hh} = 1$, however, can also generate the spin 3/2 states, Ξ^*_{hh} and Ω^*_{hh} in tab. 3.1.

An interpolating operator for the spin-3/2 states can be obtained by replacing γ_5 with γ^μ in eq. (3.2).

$$J^\mu_\gamma = \epsilon_{abc}\, h^a_\gamma \left(h^{bT}\, \gamma^\mu \mathcal{C}\, l^c \right), \quad s_{hh} = 1. \tag{3.3}$$

This operator also couples to spin-1/2 and projections are needed to obtain the desired state. The spin-1/2 masses from J^μ_γ and J_γ are equal since there is only one spin 1/2 baryon in the situation where two quarks are identical. We have directly verified this property in our simulation.

Another operator, used for spin-3/2 double heavy baryons [52, 53] is

$$\widetilde{J}^{\mu}_{\gamma} = \epsilon_{abc}\, l^{c}_{\gamma}\, (h^{b^T}\, \gamma^{\mu} \mathcal{C}\, h^{a}). \tag{3.4}$$

We have also tried this operator and we see no reason to prefer one over the other. Indeed, both give a good overlap for the ground state and the masses extracted turn out to be equal as expected.

For the operators J_γ and J^{μ}_{γ} (or $\widetilde{J}^{\mu}_{\gamma}$) the 2-point functions in eq. (3.1) have the following large-time behaviour

$$\begin{aligned} C(t)_{\gamma\bar{\gamma}} &= \sum_{\mathbf{x}} \langle 0|J_\gamma(\mathbf{x},t)\bar{J}_{\bar{\gamma}}(0)|0\rangle \\ &\xrightarrow{t\gg 0} Z_{1/2}\ (P_+)_{\gamma\bar{\gamma}}\ e^{-m_{1/2}t} + Z^{P}_{1/2}\ (P_-)_{\gamma\bar{\gamma}}\ e^{-m^{P}_{1/2}t}. \end{aligned} \tag{3.5}$$

$$\begin{aligned} C_2(t)^{ij}_{\gamma\bar{\gamma}} &= \sum_{\mathbf{x}} \langle 0|J^{i}_\gamma(\mathbf{x},t)\bar{J}^{j}_{\bar{\gamma}}(0)|0\rangle \\ &\xrightarrow{t\gg 0} Z_{3/2}\left(P_+ P^{ij}_{3/2}\right)_{\gamma\bar{\gamma}} e^{-m_{3/2}t} + Z_{1/2}\left(P_+ P^{ij}_{1/2}\right)_{\gamma\bar{\gamma}} e^{-m_{1/2}t} \\ &\quad + Z^{P}_{3/2}\left(P_- P^{ij}_{3/2}\right)_{\gamma\bar{\gamma}} e^{-m^{P}_{3/2}t} + Z^{P}_{1/2}\left(P_- P^{ij}_{1/2}\right)_{\gamma\bar{\gamma}} e^{-m^{P}_{1/2}t} \end{aligned} \tag{3.6}$$

where the projection operators are defined by

$$\begin{aligned} P_- &= \frac{1+\gamma_0}{2}, & P_+ &= \frac{1-\gamma_0}{2}, \\ P^{ij}_{3/2} &= g^{ij} - \frac{1}{3}\gamma^i\,\gamma^j, & P^{ij}_{1/2} &= \frac{1}{3}\gamma^i\,\gamma^j. \end{aligned} \tag{3.7}$$

Details of the spin algebra involved in obtaining the intended states are given in appendix A. Contributions of negative parity states are removed by projection with P_+. The negative parity states can, in principle, be detected by using the projector P_-, but in our simulation they are much noisier. We show an example of the signals from the operators J_γ, J^{μ}_{γ} and $\widetilde{J}^{\mu}_{\gamma}$ in fig. 3.3. As stressed above, spin-1/2 masses extracted using the three operators are equal, while the choice between J^{μ}_{γ} and $\widetilde{J}^{\mu}_{\gamma}$ makes no difference for the spin-3/2 mass.

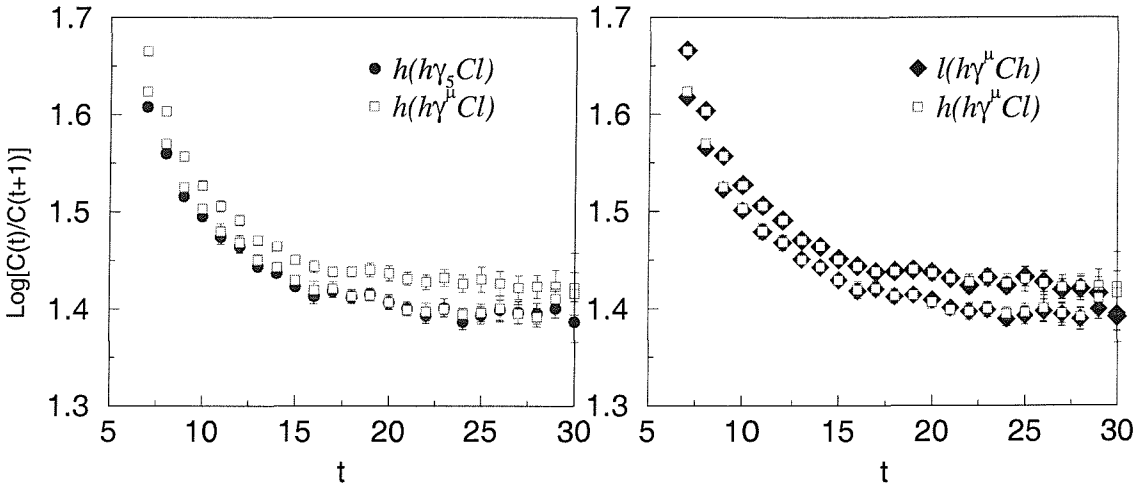

Figure 3.3: Comparison of the effective mass plots for the double heavy operators J_γ, J_γ^μ and $\widetilde{J}_\gamma^\mu$, with $\kappa_h = 0.1222$ and $\kappa_l = 0.1351$. In each plot the upper points are for spin-3/2 and the lower points for spin-1/2. The spin-1/2 plateaus are the the same for J_γ and J_γ^μ (left) while both plateaus coincide for the J_γ^μ and $\widetilde{J}_\gamma^\mu$ operators (right).

For a baryon containing a single heavy quark, a common choice of operators is

$$\mathcal{O}_\gamma = \epsilon_{abc}\, h^a_\gamma \left({l_1^b}^T \gamma_5 \mathcal{C}\, l_2^c \right), \quad s_{ll} = 0, \tag{3.8}$$

$$\mathcal{O}^\mu_\gamma = \epsilon_{abc}\, h^a_\gamma \left({l_1^b}^T \gamma^\mu \mathcal{C}\, l_2^c \right), \quad s_{ll} = 1, \tag{3.9}$$

for the states $s_{ll} = 0$ and $s_{ll} = 1$ in tab. 3.1, respectively. In our simulation, the light quarks l_1, l_2 carry different flavours but the same masses.

It should be noted that for baryons with three different quarks, *i.e.*, hl_1l_2 (or lh_1h_2), these two operators correspond to different physical spin-1/2 states with $s_{ll} = 0$ and 1 respectively, the latter one often being denoted by a prime. This is evident from the experimental masses of Ξ_c and Ξ'_c in tab. 3.1.

3.3 Numerical simulation and analysis

Our simulation was made using the code FermiQCD [54] on a PC cluster. In this study 100 quenched gauge configurations were generated at $\beta = 6.2$ on a volume of $24^3 \times 64$ with 1000 heatbath steps for the thermalisation followed by 200 heatbath steps to separate each gauge configuration. These numbers were decided upon after an autocorrelation study on the average plaquette values.

Four light quark propagators around the strange quark mass and three heavy quark propagators around the charm were calculated using the following values of the hopping parameters:

- $\kappa_l = 0.1344\,,\ 0.1346\,,\ 0.1351\,,\ 0.1353$;
- $\kappa_h = 0.1240\,,\ 0.1233\,,\ 0.1222$.

The propagators were generated by the Stabilised Biconjugate Gradient method [14] for the non-perturbatively improved clover action [18].

Since the signal is satisfactory with local interpolating operators, no smearing was required. The statistical errors were estimated by a jackknife procedure, removing 10 configurations at a time from the ensemble.

κ_l	am_P	am_V
0.1344	0.300(2)	0.397(4)
0.1346	0.276(2)	0.383(5)
0.1351	0.210(3)	0.352(11)
0.1353	0.177(2)	0.340(15)

Table 3.2: Light pseudoscalar and vector meson masses. The fit interval is [12 – 28]. Our time counting starts from 0.

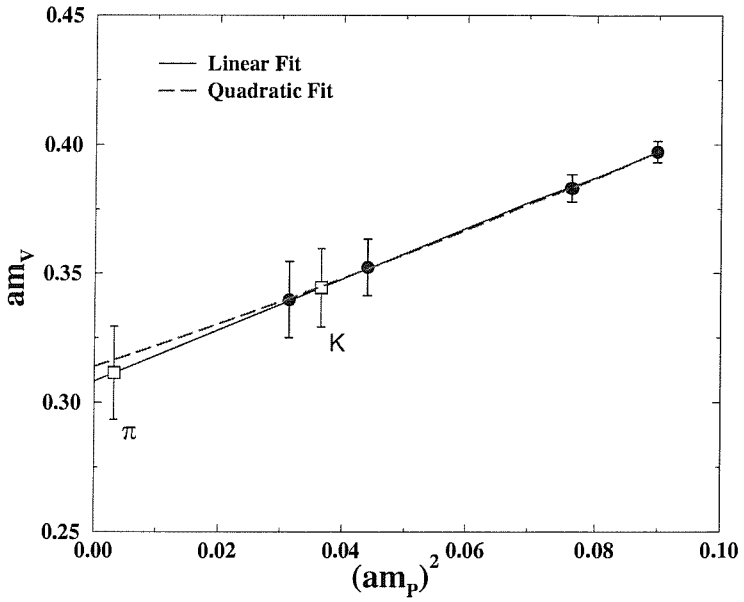

Figure 3.4: Light vector masses as a function of squared light pseudoscalar masses. The interpolated kaon and extrapolated pion masses are also shown.

3.3.1 Lattice spacing and quark masses

To fix the lattice spacing, we used the *method of lattice planes* [68]. In other words, we perform the following fit to the light vector and pseudoscalar masses in table 3.2,

$$am_V = C + L\,(am_P)^2. \tag{3.10}$$

This is shown in fig. 3.4. From the physical values of m_{K^*} and m_K, the inverse lattice spacing is found to be

$$a^{-1} = 2.6(1)\ \text{GeV}. \tag{3.11}$$

Terms of $\mathcal{O}((am_P)^4)$ in eq. (3.10) turn out to be irrelevant and do not affect the above estimate (compare the linear and quadratic fits in fig. 3.4). For illustration, the values of the pseudoscalar masses in tab. 3.2 converted to physical units are

$$m_P = \{779\,,\ 716\,,\ 546\,,\ 459\}\ \text{MeV}. \tag{3.12}$$

These span the kaon mass while the pion is instead quite far away. For this reason, we interpolate for the strange quark and extrapolate for the up/down masses. This is also the reason for using K, K^* to fix the lattice spacing.

For the heavy sector, the D_s-meson mass is within our range of simulation. This is evident once the heavy-light pseudoscalar masses in tab. 3.3 are interpolated to the strange mass (through the lattice plane method) and expressed in physical units

$$m_{P,hs} = \{1.83\,,\ 1.89\,,\ 1.98\}\ \text{GeV}. \tag{3.13}$$

3.3.2 Analysis of the baryon masses

Since κ_{charm} is rather close to our third $\kappa_h = 0.1222$[1], as the first step in our analysis, we interpolate the quantities of interest, *viz.* the single and double heavy baryon masses, to the charm mass. In practice, this procedure is implemented by doing for each κ_l the following fits:

$$am_{hhl} = C_l + L_l\, am_{P,hs}\,, \quad am_{hll} = C'_l + L'_l\, am_{P,hs}. \tag{3.14}$$

Quantities at the charm mass, m_{ccl} and m_{cll} are obtained by putting $m_{P,hs} = m_{D_s}$. This interpolation is shown for the double heavy case in fig. 3.5. With the charm mass fixed, the light quark mass dependence is studied using

$$am_{cll} = A + B\,(am_{P,ll})^2\,, \quad am_{ccl} = A' + B'\,(am_{P,ll})^2. \tag{3.15}$$

This fit is shown for the spin-1/2 double charm case in fig. 3.6. The masses of charmed baryons containing strange and/or up/down quarks are obtained by the following substitutions for m_P in the above equations:

[1] A naive linear fit in $1/\kappa_h$ to the masses in eq. (3.13) gives $\kappa_{\text{charm}} = 0.1224(9)$.

$\kappa_h - \kappa_l$	$am_{P,hl}$	$am_{hll'}$			am_{hhl}	
		$J^P = \frac{1}{2}^+$	$J^P = \frac{1}{2}^+$	$J^P = \frac{3}{2}^+$	$J^P = \frac{1}{2}^+$	$J^P = \frac{3}{2}^+$
		$s_{ll'} = 0$	$s_{ll'} = 1$	$s_{ll'} = 1$	$s_{hh} = 1$	$s_{hh} = 1$
0.1240-0.1344	0.718(2)	0.954(5)	0.988(6)	1.008(6)	1.326(3)	1.354(3)
0.1233-0.1344	0.740(2)	0.975(5)	1.010(6)	1.029(6)	1.368(3)	1.395(3)
0.1222-0.1344	0.775(2)	1.008(6)	1.044(6)	1.062(6)	1.433(3)	1.459(3)
κ_{charm}-0.1344		1.003(28)	1.039(33)	1.057(32)	1.055(31)	1.442(57)
0.1240-0.1346	0.710(2)	0.934(6)	0.972(7)	0.992(7)	1.318(4)	1.347(4)
0.1233-0.1346	0.733(2)	0.956(6)	0.994(7)	1.013(7)	1.360(4)	1.388(3)
0.1222-0.1346	0.767(2)	0.989(6)	1.028(7)	1.046(7)	1.425(3)	1.452(3)
κ_{charm}-0.1346		0.984(28)	1.023(34)	1.041(33)	1.416(57)	1.442(57)
0.1240-0.1351	0.691(3)	0.878(10)	0.929(13)	0.945(10)	1.297(4)	1.329(5)
0.1233-0.1351	0.714(3)	0.900(10)	0.951(13)	0.966(10)	1.339(5)	1.370(5)
0.1222-0.1351	0.748(3)	0.934(10)	0.984(14)	0.998(10)	1.404(5)	1.434(5)
κ_{charm}-0.1351		0.928(27)	0.979(39)	0.993(34)	1.395(58)	1.425(58)
0.1240-0.1353	0.683(3)	0.854(13)	0.903(17)	0.915(12)	1.287(5)	1.322(6)
0.1233-0.1353	0.706(3)	0.876(13)	0.923(17)	0.935(12)	1.330(5)	1.363(6)
0.1222-0.1353	0.740(3)	0.910(13)	0.956(18)	0.967(12)	1.395(6)	1.427(6)
κ_{charm}-0.1353		0.904(28)	0.951(43)	0.962(34)	1.385(58)	1.418(58)

Table 3.3: Double and single-heavy baryon masses in lattice units, together with pseudoscalar masses. The fit intervals are [16−28] for double and [15−25] for single-heavy baryons.

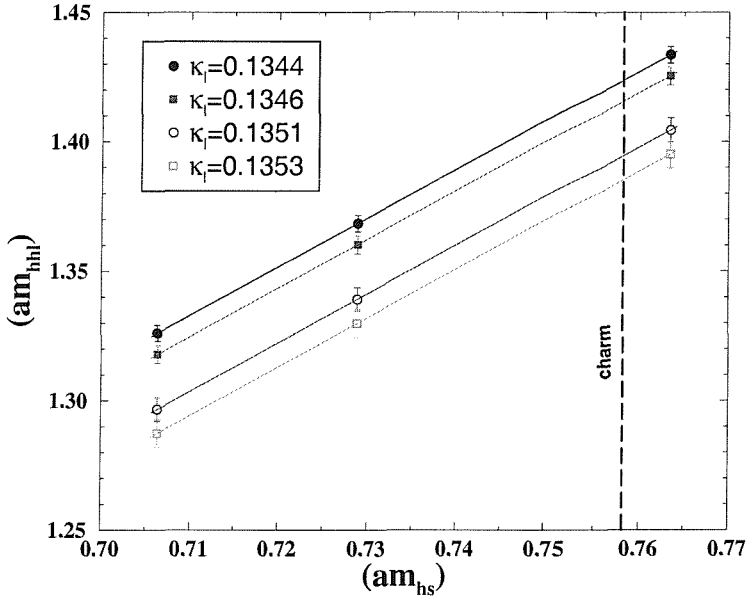

Figure 3.5: Spin-1/2 double-heavy baryon masses for all κ combinations. For each κ_l we fit the heavy quark mass dependence using the heavy-strange pseudoscalar meson mass. The fit function is given in equation (3.14). The vertical dashed line indicates the D_s meson mass (in lattice units) used to fix the masses of the *ccl* spin-1/2 baryons.

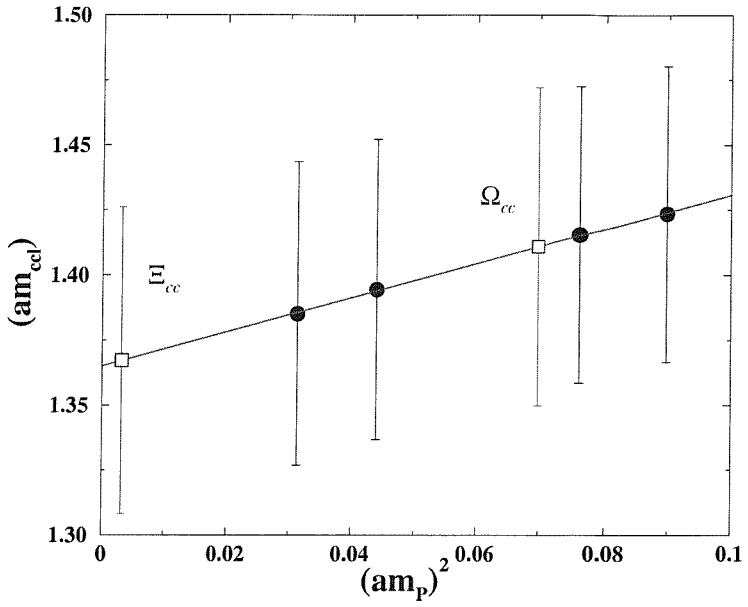

Figure 3.6: Spin-1/2 double charm state masses as a function of the square of the light pseudoscalar masses. The values at strange and up/down masses are shown.

- $m_P = m_\pi$ for m_{cud}, m_{ccu};
- $m_P = m_K$ for m_{csu};
- $m_P = m_{\eta_{ss}}$ for m_{css}, m_{ccs},

where $m^2_{\eta_{ss}} = 2m^2_K - m^2_\pi$. In the second case, we suppose that $SU(3)$ breaking terms are negligible and obtain our estimate from states containing two mass-degenerate light quarks [53, 68].

3.4 Results and discussion

Here we collect our final values for the double-charm baryon masses.

$$\begin{array}{ll} \Xi_{cc} = 3549(13)(19)(92)\ \text{MeV} & \Omega_{cc} = 3663(11)(17)(95)\ \text{MeV} \\ \Xi^*_{cc} = 3641(18)(8)(95)\ \text{MeV} & \Omega^*_{cc} = 3734(14)(8)(97)\ \text{MeV} \end{array} \tag{3.16}$$

The first error is statistical. The second error is systematic, estimated by combining in quadrature the effects of the following variations in our analysis:

- changing the time fit-ranges — this contributes up to 35% of the quoted error;
- using single or double exponential fits — we saw no change in our lowest state masses;
- linear versus quadratic chiral extrapolations — in the worst case this gives three-quarters of the quoted error;
- interchanging the order of light quark extrapolations and charm quark interpolation — this produces no change in our results.

Only one volume and lattice spacing was studied; investigation of discretization errors, the continuum limit and finite volume effects are not addressed. One can then consider the remaining discrepancy between any experimental value and its simulated counterpart due to these as well as quenching effects. One idea is to try to estimate this systematic error by setting one of these simulated masses to the experimental mass and rescale the others by the same amount. The third quoted error is obtained in this manner using the experimental Λ_c mass.

The Ξ_{cc} mass is in good agreement with the experimental value [26]

$$(\Xi_{cc})_{\text{expt}} = 3519 \pm 1 \pm 5 \text{ MeV} \tag{3.17}$$

Other masses are consistent with the lattice estimates using NRQCD [52] or D234 [51] actions [tab. 3.4]. For recent estimates in quark models or QCD Sum Rules we refer the reader to [47] and [45] respectively. For completeness, our estimates for the single charm baryon masses are given in tab. 3.5 along with the experimental results. Values turn out to be compatible with previous lattice calculations [52, 53, 59]. It may be noted that in ref. [59], a perturbative value for the coefficient c_{SW} was used in the clover action.

We now turn to the baryon and meson spin-splittings. Our results for these are given in tab. 3.6. The values are obtained either from the difference in individually fitted masses (labelled "Diff" in the table), or by directly fitting a ratio of correlators

	This work [MeV]	D234 [51] [MeV]	NRQCD [52] [MeV]
Ξ_{cc}	3549(13)(19)(92)	$3595(12)(^{21}_{22})$	$3588(66)(^{32}_{27})$
Ω_{cc}	3663(11)(17)(95)	$3727(9)(^{16}_{40})$	$3698(60)(^{26}_{23})$
$\Xi^*_{cc} - \Xi_{cc}$	87(13)(13)(2)	$83(8)(^{7}_{10})$	$70(11)(^{7}_{7})$
$\Omega^*_{cc} - \Omega_{cc}$	67(9)(13)(2)	$72(5)(^{4}_{5})$	$63(7)(^{5}_{5})$

Table 3.4: Our estimates for the double charm baryon masses and splittings compared to previous calculations for the available cases. The splittings in this table from our work are from the ratio method described in this section. The numbers from the other two works are taken from their simulations at $\beta = 2.3$ (for a different gauge action).

	This work [MeV]	Expt [MeV]
Λ_c	2227(50)(57)(58)	2285(1)
Ξ_c	2374(34)(23)(61)	2469(1)
Σ_c	2377(38)(84)(62)	2452(1)
Ξ'_c	2502(26)(40)(65)	2575(3)
Ω_c	2627(16)(48)(68)	2698(3)
Σ^*_c	2396(42)(122)(62)	2518(2)
Ξ^*_c	2532(31)(62)(66)	2646(2)
Ω^*_c	2669(21)(26)(70)	

Table 3.5: Our estimates for the single charm baryon masses compared to experimental values.

	Diff [MeV]	Ratio [MeV]	Expt [MeV]
$\Xi^*_{cc} - \Xi_{cc}$	89(15)	87(13)(13)(2)	
$\Omega^*_{cc} - \Omega_{cc}$	69(10)	67(9)(13)(2)	
$\Sigma^*_c - \Sigma_c$	18(51)	49(39)(12)(1)	66(2)
$\Xi^*_c - \Xi'_c$	30(33)	47(27)(4)(1)	71(3)
$\Omega^*_c - \Omega_c$	43(17)	44(16)(15)(1)	
$D^* - D$		127(14)(1)(3)	142(2)
$D^*_s - D_s$		123(11)(1)(3)	138(2)

Table 3.6: Our results for the single- and double-charm mass splittings.

(labelled "Ratio" in the table). When using the ratio the noise starts to dominate earlier so we restrict our fit to a shorter time-slice window. For the baryons we find a better signal using the ratio method and the difference between the two approaches becomes more apparent as we move away from our region of simulation to lighter quarks. We use the numbers from the ratio as our best estimates.

For the double-charm baryons we observe a good signal for non-zero splittings. For the single-charm baryons, where experimental data is available, our results are compatible. This distinguishes our results from earlier ones using a less-improved clover action [59]. Our values are also compatible with those found using the D234 [51] or NRQCD [52] actions. For the mesons too our results are compatible with experiment: this improved agreement is also found in other recent non-perturbatively improved clover simulations [56, 57]. This may suggest that the suppression of the spin-splittings observed in earliers works is more of a lattice discretisation artefact than anything else.

The predictions are more precise for (Ω^*_c, Ω_c) and the double charm spin doublets $(\Omega^*_{cc}, \Omega_{cc})$ and (Ξ^*_{cc}, Ξ_{cc}), where less extrapolation is needed, but experimental numbers are still awaited.

3.5 Conclusion

Exploratory quenched lattice results are reported for double charm baryon masses. The calculation is done with non-perturbatively $\mathcal{O}(a)$-improved Wilson fermions at $\beta = 6.2$ and on a large lattice. Good signals for the positive parity ground states are observed without any smearing. In addition, we have reported the masses of single charm baryons. We also see a definite signal for non-zero baryon and meson spin splittings and do not observe any suppression of the splittings and taking other works together, we conclude that the previously observed suppression was a discretisation artefact. The calculated masses and splittings look quite reasonable and, where available, agree with experiment and other simulations.

Finer lattice spacing, examination of chiral logarithms in the light extrapolations and simulations with chiral fermions and dynamical quarks are required for a more reliable simulation.

Meanwhile, experimental observations of the remaining double charmed baryon states and, in particular their spin-splittings, would allow the lattice predictions to be checked.

Chapter 4

Sea quark effects in B_K

This chapter is based on the paper:

J.M. Flynn, F. Mescia and A.S.B. Tariq [UKQCD Collaboration], "Sea quark effects in B_K from $N_f = 2$ clover-improved Wilson fermions", [arXiv:hep-lat/0406013], submitted to JHEP, also presented at Lattice 2004 [arXiv:hep-lat/0409075].

4.1 Motivation and background

The Cabibbo-Kobayashi-Maskawa (CKM) matrix [69, 70] gives the rotation between the weak and the mass eigenstates.

$$\begin{pmatrix} d' \\ s' \\ b' \end{pmatrix} = \begin{pmatrix} V_{ud} & V_{us} & V_{ub} \\ V_{cd} & V_{cs} & V_{cb} \\ V_{td} & V_{ts} & V_{tb} \end{pmatrix} \begin{pmatrix} d \\ s \\ b \end{pmatrix} \equiv \hat{V}_{\rm CKM} \begin{pmatrix} d \\ s \\ b \end{pmatrix} . \tag{4.1}$$

Though the weak neutral current interactions turn out to be flavour diagonal, the weak charged current (with a W-exchange) comes with factors of these matrix elements.

The standard parametrisation of this matrix is given by:

$$\hat{V}_{\rm CKM} = \begin{pmatrix} c_{12}c_{13} & s_{12}c_{13} & s_{13}e^{-i\delta} \\ -s_{12}c_{23} - c_{12}s_{23}s_{13}e^{i\delta} & c_{12}c_{23} - s_{12}s_{23}s_{13}e^{i\delta} & s_{23}c_{13} \\ s_{12}s_{23} - c_{12}c_{23}s_{13}e^{i\delta} & -s_{23}c_{12} - s_{12}c_{23}s_{13}e^{i\delta} & c_{23}c_{13} \end{pmatrix} , \tag{4.2}$$

where $c_{ij} = \cos\theta_{ij}$ and $s_{ij} = \sin\theta_{ij}$ $(i, j = 1, 2, 3)$. Since s_{13} and s_{23} are $\mathcal{O}(10^{-3})$ and $\mathcal{O}(10^{-2})$, respectively it is convenient to choose $s_{12} = |V_{us}|$, $s_{13} = |V_{ub}|$, $s_{23} = |V_{cb}|$ and δ as the four independent parameters.

The CKM matrix elements have a hierarchy in the values with $|V_{us}|$ and $|V_{cd}|$ being of order 0.2, the elements, $|V_{cb}|$ and $|V_{ts}|$ of order $4 \cdot 10^{-2}$ whereas $|V_{ub}|$ and $|V_{td}|$ are of order $5 \cdot 10^{-3}$. This is used in the Wolfenstein parametrisation [71] to expand the elements in terms of a power series in the small parameter $\lambda = |V_{us}| \approx 0.22$,

$$\hat{V} = \begin{pmatrix} 1 - \frac{\lambda^2}{2} & \lambda & A\lambda^3(\rho - i\eta) \\ -\lambda & 1 - \frac{\lambda^2}{2} & A\lambda^2 \\ A\lambda^3(1 - \rho - i\eta) & -A\lambda^2 & 1 \end{pmatrix} + \mathcal{O}(\lambda^4), \tag{4.3}$$

The free parameters now are (λ, A, ρ, η). It may be noted that this is an approximate parametrisation, and the $\mathcal{O}(\lambda^4)$ terms may differ, according to the definitions of the parameters. But this has been put into an exact form by defining them through [72, 73]

$$s_{12} = \lambda, \qquad s_{23} = A\lambda^2, \qquad s_{13}e^{-i\delta} = A\lambda^3(\rho - i\eta) \tag{4.4}$$

through all orders in λ. These leaves us with a simple recipe to expand any CKM matrix element in a consistent manner up to any power of λ. Including $\mathcal{O}(\lambda^4)$ and $\mathcal{O}(\lambda^5)$ terms we find

$$\hat{V} = \begin{pmatrix} 1 - \frac{1}{2}\lambda^2 - \frac{1}{8}\lambda^4 & \lambda + \mathcal{O}(\lambda^7) & A\lambda^3(\rho - i\eta) \\ -\lambda + \frac{1}{2}A^2\lambda^5[1 - 2(\rho + i\eta)] & 1 - \frac{1}{2}\lambda^2 - \frac{1}{8}\lambda^4(1 + 4A^2) & A\lambda^2 + \mathcal{O}(\lambda^8) \\ A\lambda^3(1 - \bar{\rho} - i\bar{\eta}) & -A\lambda^2 + \frac{1}{2}A\lambda^4[1 - 2(\rho + i\eta)] & 1 - \frac{1}{2}A^2\lambda^4 \end{pmatrix} \tag{4.5}$$

where,

$$\bar{\rho} = \rho\left(1 - \frac{\lambda^2}{2}\right), \qquad \bar{\eta} = \eta\left(1 - \frac{\lambda^2}{2}\right). \tag{4.6}$$

The unitarity of the matrix leads to six relations of the type

$$V_{ud}V_{ub}^* + V_{cd}V_{cb}^* + V_{td}V_{tb}^* = 0. \tag{4.7}$$

These can be expressed in the form of triangle in the complex $(\bar{\rho}, \bar{\eta})$ plane [fig. 4.1] with a normalisation by $1/V_{cd}V_{cb}^*$ to make the base of unit length. The vectors should meet up in a triangle for unitarity to be fulfilled. To look for physics beyond the standard model, one approach has been to over-constrain these triangles in search for any sign of non-unitarity.

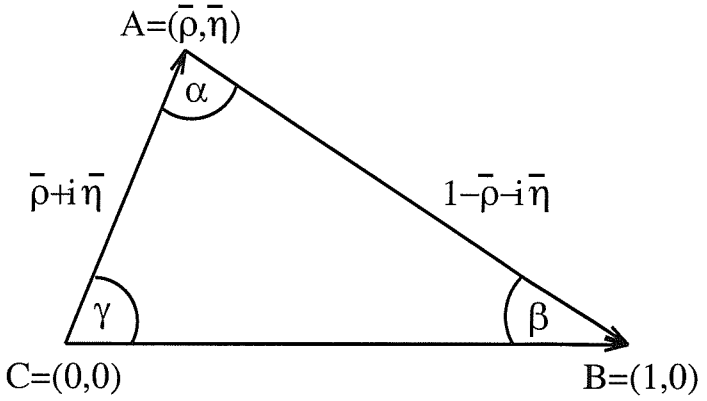

Figure 4.1: Unitarity triangle.

One of these constraints [fig. 4.2] comes from the indirect CP-violation parameter ε_K occuring in the mixing of neutral kaons. B_K parametrises the non-perturbative matrix element in ε_K. Experimentally, ε_K is very accurately determined, with

$$\varepsilon_K^{\text{expt}} = 2.280(13) \times 10^{-3} e^{i\pi/4} \qquad \text{(PDG)}. \tag{4.8}$$

ε_K is related to the unitarity triangle parameters $\bar{\eta}$ and $\bar{\rho}$ [71] through the relation [75] as quoted in [76]

$$\begin{aligned} \varepsilon_K &= \bar{\eta} A^2 \hat{B}_K \left[1.11(5) \cdot A^2(1-\bar{\rho}) + 0.31(5)\right] \\ &\sim \hat{B}_K \bar{\eta}(1-\bar{\rho}), \end{aligned} \tag{4.9}$$

giving a hyperbola in the $(\bar{\rho}, \bar{\eta})$ plane. Here $\hat{B}_K$ is the renormalisation group invariant (RGI) definition of B_K which will be related to other scheme- and scale-dependent definitions later in this chapter.

Pinning down the value of $\hat{B}_K$ has not been an easy process. In fact, if we look at the evolution of the constraints over the last years in fig. 4.3 it is noticeable that there has been almost no progress in the ε_K direction in the last few years partly due to lack of progress in determining a better value of $\hat{B}_K$. In fact, this is one of the areas of major uncertainty in CKM inputs.

The value of $\hat{B}_K$ used in present CKM fits is usually $0.86 \pm 0.06 \pm 0.14$ and since the accuracy here is not even 20%, despite the 0.5% experimental precision,

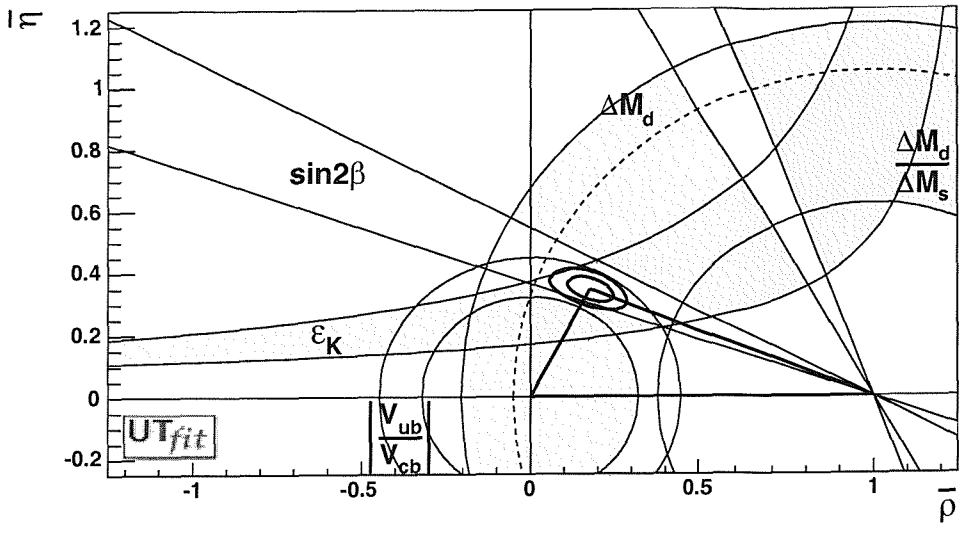

Figure 4.2: Different constraints on the unitarity triangle. [Figure from [74]]

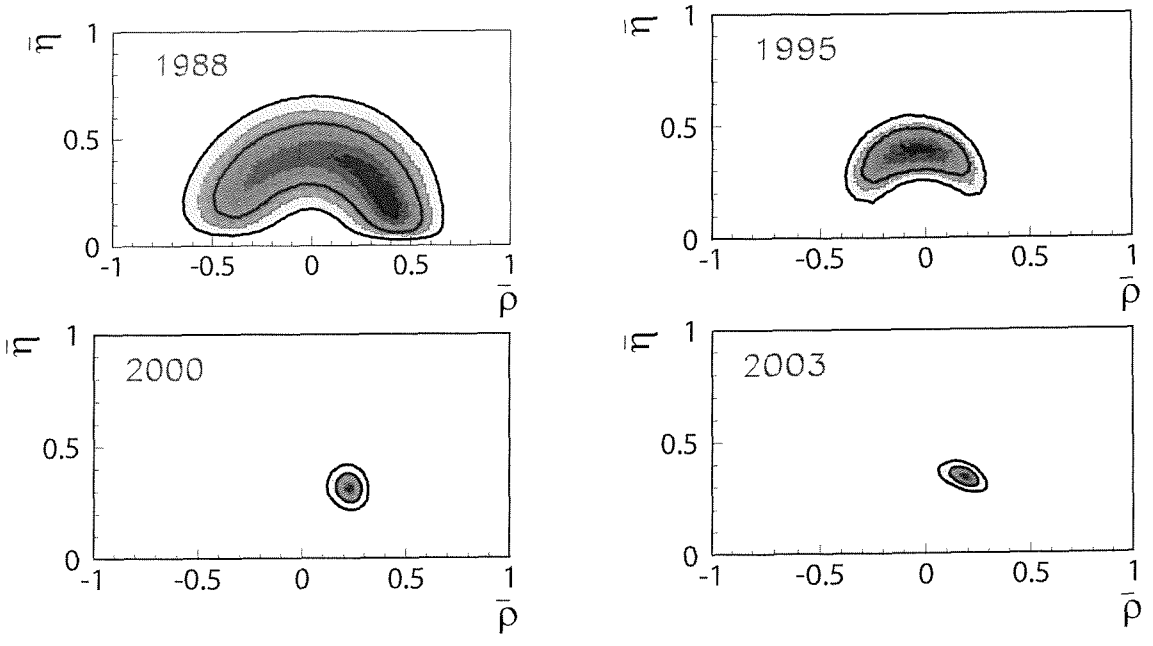

Figure 4.3: Evolution of the unitarity triangle constraints. Noticeably in the last interval there has been no progress in the ε_K direction, partly owing to the lack of a better determination of $\hat{B}_K$. [Figure from [74]]

Table 4.1: Some previous lattice calculations of B_K. NP refers to non-perturbative renormalisation. Only the last number is unquenched.

	B_K $\overline{\text{MS}}$, 2 GeV	Fermion Action	Ren	a^{-1} (GeV)
Kilcup *et al.*(1997) [77]	0.62(2)(2)	Staggered	Pert	∞
JLQCD (1997) [78]	0.63(4)	Staggered	Pert	∞
SPQcdR (2002) [79]	0.66(7)	Clover	NP	∞
JLQCD (1999) [80]	0.69(7)	Wilson	NP	∞
CP-PACS (2001) [81]	0.57(1)	DW	Pert	1.8, 2.8
RBC (2002) [82]	0.53(1)	DW	NP	1.9
MILC (2003) [83]	0.55(7)	Overlap	Pert	∞
Garron *et al.*(2003) [84]	0.63(6)(1)	Overlap	NP	2.1
ALPHA (2003) [85]	0.66(6)(2)	Tw Mass	NP	2.1
RBC (2003) [86]	0.50(2)	Dyn DW	NP	1.8

the constraints from ε_K on the unitarity triangle are not very stringent. This has resulted in a great deal of activity in the lattice community to refine the calculation.

There is a relatively long history of B_K calculations in different frameworks. A more comprehensive summary can be found in [87, 88]. It is noticeable that numbers from other methods *e.g.* large-N_c, sum rules and quark models are dispersed over a relatively wide range. Here it should be stressed, however, that the only rigorous way to reach a numerical estimate from first principles is through lattice calculations.

Some of the recent lattice calculations are listed in table 4.1. Over the years the quenched lattice value of B_K has more or less settled down. The 1997 quenched value of $B_K(\overline{\text{MS}}, 2\,\text{GeV}) = 0.63(4)$, corresponding to $\hat{B}_K = 0.86(6)$, using staggered fermions [78] remains the benchmark and is the value usually quoted for phenomenology. Other quenched numbers are more or less consistent with this. The additional systematic error has been estimated by taking into account possible effects of unquenching (15%) and SU(3)$_f$ breaking (5%), and for phenomenology the general practice is to take a conservative viewpoint and add these two in quadrature

making the value $\hat{B}_K = 0.86(6)(14)$ [87, 89]. A more aggressive estimate makes it $\hat{B}_K = 0.86(6)(6)$, but as already mentioned, the first one is the one used for most of phenomenology. Unquenching, therefore remains the primary systematic effect to be addressed.

Now let us come to what we know about unquenching effects. There have been a few quenched studies that have additionally performed $N_f = 2$ calculations for somewhat heavy sea quark masses. These works, *e.g.* [76, 90–95] using Wilson or staggered fermions, in general find the unquenched numbers to be consistent with the quenched ones. Intriguingly it was noted in the LAT95 review that, though the unquenched numbers are always within the errors of the quenched ones, they are systematically lower [96]. This statement is valid for works subsequent to [96] as well.

There has been one preliminary report of an unquenched calculation using Domain Wall (DW) fermions from the RBC collaboration [86] where they have a few sea quark masses allowing an extrapolation to lighter sea quarks. Though the central values for B_K from DW fermions have often been on the lower side, the unquenched DW preliminary number is really at the lower end of the spectrum [table 4.1].

However, one of the above works [91] also includes a simulation with $N_f = 4$ and finds the values there to be higher. Their $N_f = 2$ value, as stated before, is lower but consistent within errors with $N_f = 0$, but then they interpolate to $N_f = 3$ and suggest that the unquenched number should be greater by 5%. In most present day reviews, the accepted statement one finds about unquenching effects originates from [89] adding on the estimated 15% unquenching and 5% SU(3) breaking uncertainty onto this 5% increase, giving a factor of 1.05(15)(5). Despite the large errors, this has led to the lore that the unquenched number should be higher.

In this situation, it is difficult to reach an unambiguous conclusion on the true effect of dynamical fermions on this quantity and even questions such as whether unquenching will change the value, and if so, in which direction, are still to be answered.

It is well-understood that doing a dynamical simulation on a large set of parameters with increasingly light quarks and a well-controlled chiral extrapolation is not easy and will require a much greater effort to make a robust quantitative estimate. But, given the level of our present understanding of the situation (or rather, the lack of it), there is room for a study aiming to make even some qualitative remark on what to expect from dynamical quarks.

In this spirit, the calculation reported in this chapter is undertaken as an intermediate step towards a complete unquenched evaluation of B_K. In the near future one might hope to perform detailed studies over lighter and larger samples of sea quark masses at different lattice spacings in order to make the continuum extrapolation. In the meantime, exploratory studies may help as a guide to those regions of parameter space accessible today.

Keeping this in mind we may now proceed to set up our calculation, starting again from the indirect CP violation problem in $K^0 - \overline{K^0}$ mixing.

4.2 Theoretical setup

Within the standard model, the box diagrams in fig. 4.4 provide leading order contributions to CP-violation from flavour mixing in the neutral kaon sector. Integrating out the degrees of freedom above the charm mass in the part of the electroweak Hamiltonian responsible for these diagrams, we get the $\Delta S = 2$ effective weak Hamiltonian.

$$\begin{aligned}
\mathcal{H}_{\text{eff}}^{\Delta S=2} &= \frac{G_{\text{F}}^2}{16\pi^2} M_W^2 \\
&\quad \times \left[\lambda_c^2 \eta_1 S_0(x_c) + \lambda_t^2 \eta_2 S_0(x_t) + 2\lambda_c \lambda_t \eta_3 S_0(x_c, x_t)\right] \\
&\quad \times \left[\alpha_s^{(n_f)}(\mu)\right]^{-\gamma_0/2\beta_0} \left[1 + \frac{\alpha_s^{(n_f)}(\mu)}{4\pi} J(n_f)\right] Q^{\Delta S=2}(\mu) + \text{h.c.} \\
&\sim C(\alpha_s(\mu)) \cdot Q^{\Delta S=2}(\mu) \\
&= C'(\alpha_s(\mu)) \left[\alpha_s^{(n_f)}(\mu)\right]^{-\frac{\gamma_0}{2\beta_0}} \left[1 + \frac{\alpha_s^{(n_f)}(\mu)}{4\pi} J(n_f)\right] Q^{\Delta S=2}(\mu).
\end{aligned} \tag{4.10}$$

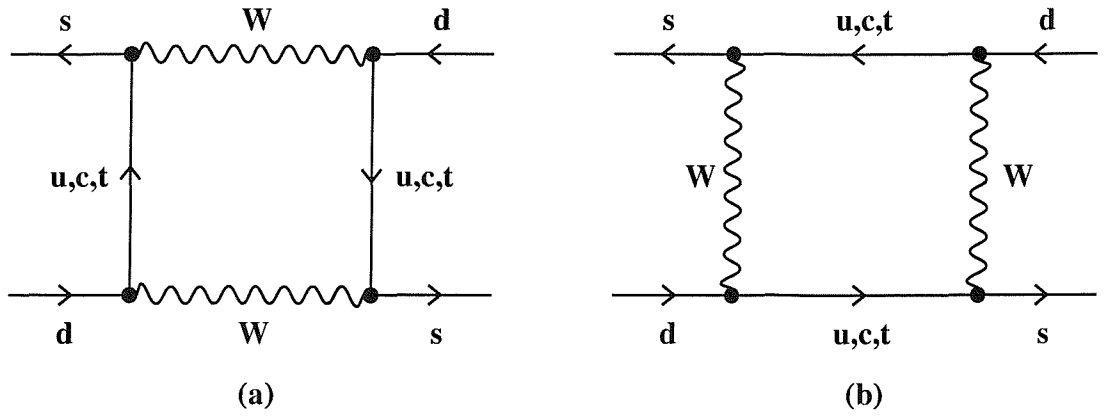

Figure 4.4: Box diagrams contributing to $K^0 - \overline{K^0}$ mixing in the Standard Model.

Here $\gamma_0 = 4$ and $\beta_0 = (11 - 2n_f)/3$ are the scheme-independent leading order anomalous dimension and beta function respectively, $\alpha_s^{(n_f)}(\mu)$ is the strong coupling while $J(n_f)$ is a scheme-dependent NLO renormalisation coefficient, n_f being the number of active flavours. In this expression, $\lambda_i = V_{is}^* V_{id}$ comes from the CKM matrix elements, while the S's are the perturbatively calculated Inami-Lim coefficients [97] for contributions from the cases with charm, top and charm-top in the loop with $x_i = m_i^2/m_W^2$. The η terms are short-distance QCD corrections. $C(\alpha_s(\mu))$ embodies the constants and all that can be calculated perturbatively, leaving the operator $Q^{\Delta S=2}(\mu)$ as the focus of our attention. Notice that now we have a local four quark operator [fig. 5.2]. In the last line the renormalisation group running has been factored out. This is useful for the renormalisation group invariant (RGI) definition of $\hat{B}_K$ and will be explained in somewhat greater detail later.

For the expectation value of oscillations between the neutral kaon states for this Hamiltonian, we have

$$\begin{aligned} \langle \overline{K^0} \mid \mathcal{H}_{\text{eff}}^{\Delta S=2} \mid K^0 \rangle &= C'(\alpha_s(\mu)) \left[\alpha_s^{(n_f)}(\mu)\right]^{-\frac{\gamma_0}{2\beta_0}} \left[1 + \frac{\alpha_s^{(n_f)}(\mu)}{4\pi} J(n_f)\right] \\ &\quad \times \langle \overline{K^0} \mid Q^{\Delta S=2}(\mu) \mid K^0 \rangle \end{aligned} \tag{4.11}$$

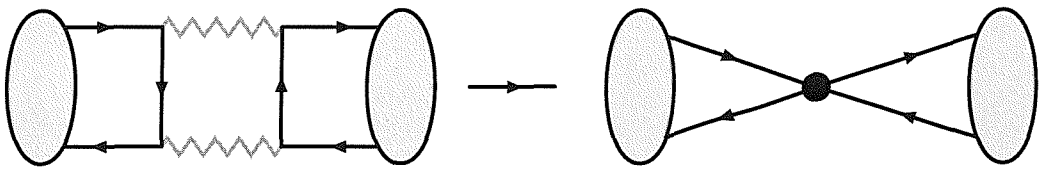

Figure 4.5: An operator product expansion reduces the box diagram to one with an effective four-quark interaction.

with our operator of interest

$$Q^{\Delta S=2}(\mu) = [\bar{s}\gamma_\mu(1-\gamma_5)d]\,[\bar{s}\gamma_\mu(1-\gamma_5)d]\,. \tag{4.12}$$

So, it all boils down to calculating

$$\langle \overline{K^0} \mid [\bar{s}\gamma_\mu(1-\gamma_5)d]\,[\bar{s}\gamma_\mu(1-\gamma_5)d] \mid K^0\rangle. \tag{4.13}$$

The soft gluon exchanges shown in fig. 4.6 make the calculation of this matrix element non-perturbative and naturally leads one to a lattice calculation of $\hat{B}_K$.

Now, we may proceed to define B_K. In the Vacuum Saturation Approximation (VSA), *i.e.* when instead of inserting a complete set of states, one considers inserting the vacuum alone to be sufficient, one gets

$$\begin{aligned} \langle \overline{K^0} \mid Q^{\Delta S=2}(\mu) \mid K^0\rangle &= \langle \overline{K^0}|\bar{s}\gamma_\mu(1-\gamma_5)d \mid 0\rangle\langle 0 \mid \bar{s}\gamma_\mu(1-\gamma_5)d \mid K^0\rangle \\ &= \frac{8}{3} f_K^2 m_K^2 \end{aligned} \tag{4.14}$$

where f_K is the kaon decay constant defined by $\langle 0|\bar{s}\gamma_\mu\gamma_5 d|K^0(p)\rangle = i f_K p_\mu$. B_K is the correction factor for this value and is then defined as

$$\langle \overline{K^0} \mid Q^{\Delta S=2}(\mu) \mid K^0\rangle = \frac{8}{3} f_K^2 m_K^2 B_K(\mu). \tag{4.15}$$

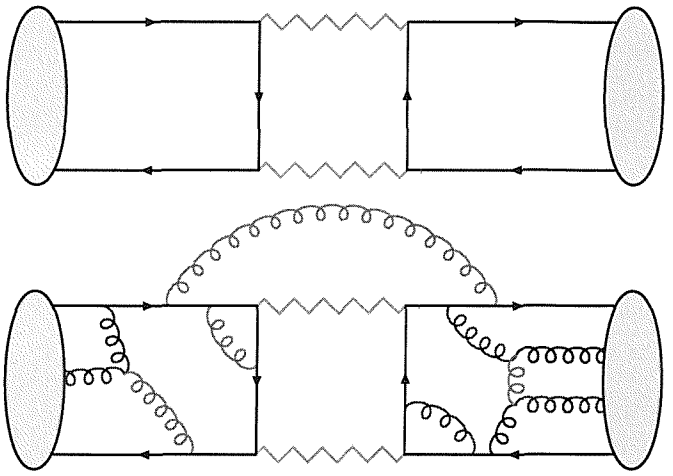

Figure 4.6: In QCD the leading order diagram is not the simple box diagram (top), rather there are soft gluon interactions all over the place (bottom) to make the process non-perturbative.

Therefore, we end up with

$$\begin{aligned}
\langle \overline{K^0} \mid \mathcal{H}_{\text{eff}}^{\Delta S=2} \mid K^0 \rangle &= C'(\alpha_s(\mu)) \left[\alpha_s^{(n_f)}(\mu)\right]^{-\frac{\gamma_0}{2\beta_0}} \left[1 + \frac{\alpha_s^{(n_f)}(\mu)}{4\pi} J(n_f)\right] \\
&\quad \times \langle \overline{K^0} \mid Q^{\Delta S=2}(\mu) \mid K^0 \rangle \\
&= C'(\alpha_s(\mu)) \left[\alpha_s^{(n_f)}(\mu)\right]^{-\frac{\gamma_0}{2\beta_0}} \left[1 + \frac{\alpha_s^{(n_f)}(\mu)}{4\pi} J(n_f)\right] \\
&\quad \times \frac{8}{3} f_K^2 m_K^2 B_K(\mu) \\
&= C'(\alpha_s(\mu)) \frac{8}{3} f_K^2 m_K^2 \hat{B}_K.
\end{aligned} \tag{4.16}$$

$\hat{B}_K$ is the renormalisation group invariant quantity, whereas B_K has a scheme dependence and

$$\hat{B}_K = \left[\alpha_s^{(n_f)}(\mu)\right]^{-\frac{\gamma_0}{2\beta_0}} \left[1 + \frac{\alpha_s^{(n_f)}(\mu)}{4\pi} J(n_f)\right] B_K(\mu), \tag{4.17}$$

where n_f is the number of active flavours at the relevant scale, and γ_0 and β_0 have the scheme independent values of 4 and $11 - 2n_f/3$. The first factor is related to

the scale-dependence while the second one has both scale- and scheme-dependence, with J being the explicitly scheme-dependent factor. We use the $\overline{\text{MS}}$ scheme for which J is calculated to NLO in [98] and can be written in a concise form as

$$J_{\overline{\text{MS}}}(n_f) = \frac{13095 - 1626\, n_f + 8\, n_f^2}{6(33 - 2\, n_f)^2}. \tag{4.18}$$

To go from $\overline{\text{MS}}$ at 2 GeV to the RGI value we note that there are four active flavours and $J_{\overline{\text{MS}}}(4) = 1.792$. The remaining choice to be made is for the strong coupling. In our case we take the PDG expression for running of the strong coupling to two loops and starting from the PDG value of $\Lambda^{(5)}_{\text{QCD}} = 216$ MeV[1] [66], we match the value of the strong coupling at the charm threshold and then run it down to 2 GeV. Thus, we obtain $\hat{B}_K = 1.404\, B_K(\overline{\text{MS}}, 2\,\text{GeV})$. In this running, one may ask what value of n_f should be used for Λ_{QCD}. In our case, though we have $n_f = 2$ in the simulations, once we have our estimate of $B_K(\overline{\text{MS}}, 2\,\text{GeV})$ we consider this to be a measure of the true $B_K(\overline{\text{MS}}, 2\,\text{GeV})$ for the physical number of flavours and proceed with the remaining matching likewise. Here, it is relevant to note that the final matching factor is rather insensitive to the value of n_f [99] and therefore the effect of any ambiguity in the value of n_f should not a be a cause for concern.

With all the peripheral machinery set up, we can now concentrate on how to calculate our matrix element of interest

$$\langle \overline{K^0} \mid [\bar{s}\gamma_\mu(1-\gamma_5)d]\,[\bar{s}\gamma_\mu(1-\gamma_5)d] \mid K^0 \rangle$$

on the lattice.

4.3 Calculation of the 3-pt function for $K^0 - \overline{K^0}$ oscillations on the lattice

The standard procedure for calculating our matrix element is spelt out in [100]. We study

$$\langle 0 | J_{\overline{K^0}}(y) Q_{4q}(z) J_{K^0}(x) | 0 \rangle \tag{4.19}$$

[1]This is the PDG(2002) value. The recently appeared PDG(2004) [27] quote $\Lambda^{(5)}_{\text{QCD}}$ to be 217 MeV.

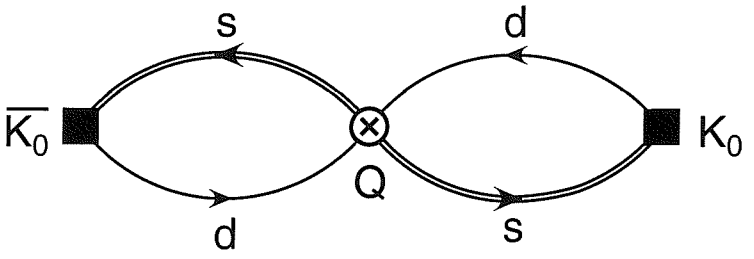

Figure 4.7: 3-pt function evaluated in a calculation of B_K. Typically the 4-quark operator is at the origin and one of the kaon sources is fixed.

with the kaon source, the four-quark operator and the the anti-kaon source (essentially a kaon annihilation operator – hermitian conjugate of the kaon source) at three different points, hence a 3-pt function. Since, our quark propagators have one end fixed at the origin, it is convenient to put the four-quark operator at the origin. For the kaon sources, we take one of them at negative time and the other at positive time and therefore we actually have a system where a kaon is created at a point, then it propagates to the origin, it is converted to an anti-kaon and then that propagates for a while and is eventually annihilated. This gives us the *figure of eight* diagram of fig. 4.7.

The kaon interpolating operators can be of the pseudoscalar or axial vector type; we use pseudoscalars and denote the sources as J_5 and use P for a generic pseudoscalar meson (π, K etc.). They can also be local or smeared. It is also possible to inject some discrete momenta in the kaon sources, something that we will find useful.

In practice, t_y is kept fixed at a particular value, while t_x is varied over the full temporal range of the lattice. For the momentum configurations, we have chosen $\{p_x, p_y\} = \{(0,0,0),(0,0,0)\}, \{(0,0,0),(1,0,0)\}$ and $\{(1,0,0),(0,0,0)\}$ where the average over equivalent configurations is understood. It may be noted this momentum is added by weighting the sum over spatial sites $\vec{x}$ with factors of $\exp(i\vec{p}\cdot\vec{x})$ whereas an unweighted sum isolates the zero-momentum ground state. With all

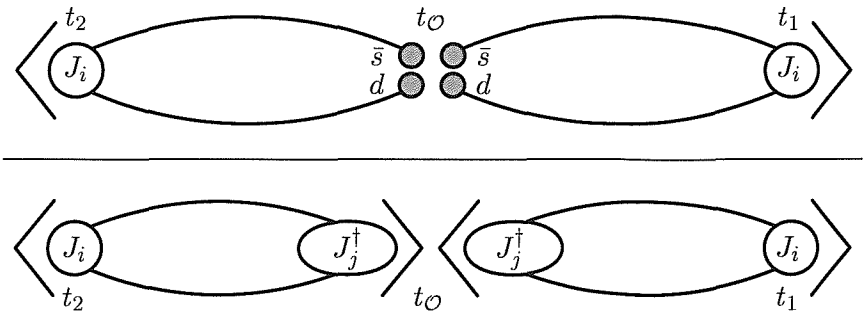

Figure 4.8: Ratio of lattice correlation functions used to calculate B_K.

these ingredients the 3-pt function is given by

$$\begin{aligned} C^{(3)}(t_x, t_y; p_x, p_y; \mu) &= \sum_{\vec{x},\vec{y}} \langle\, J_5(\vec{x}, t_x) Q(\vec{0}, 0; \mu) J_5(\vec{y}, t_y)\, \rangle e^{i\vec{p}_x\vec{x}}\, e^{i\vec{p}_y\vec{y}} \\ &\xrightarrow{-t_y, t_x \gg 0} \mathcal{Z}_P e^{-E_x t_x} \langle \overline{P}|Q(\mu)|P\rangle \mathcal{Z}_P e^{-E_y t_y}. \end{aligned} \tag{4.20}$$

To cancel the exponentials and the normalisation factor at the ends, this is divided by two 2-pt functions [fig. 4.8] of the form

$$\begin{aligned} C^{(2)}_{J_i J_j}(t; p_x) &= \sum_{\vec{x}} \langle\, J_i(\vec{x}, t) J_j^\dagger(0, 0)\, \rangle e^{i\vec{p}_x\vec{x}} \\ &\xrightarrow{t_x \gg 0} \mathcal{Z}_{J_i} \mathcal{Z}_{J_j} e^{-E_x t}. \end{aligned} \tag{4.21}$$

The labels for the interpolating operators in the 2-pt function are kept generic to cater for the possibility of pseudoscalar-axial current operators.

4.3.1 The operator

In the continuum, the operator of interest in eq. (4.15) is

$$Q^{\Delta S=2}(\mu) \equiv Q_1(\mu) = \bar{s}\gamma_\mu d\, \bar{s}\gamma_\mu d + \bar{s}\gamma_\mu\gamma_5 d\, \bar{s}\gamma_\mu\gamma_5 d, \tag{4.22}$$

which is the parity conserving part of $Q(\mu)$ in eq. (4.12). For Wilson fermions, the Wilson term in the fermion action explicitly breaks chiral symmetry leading to an extra mixing with other dimension-6 operators. Therefore one has to work with a complete basis of operators and subtract contributions from the extra ones. One

such set is

$$\begin{aligned} Q_1(\mu) &= \overline{s}\gamma_\mu d\ \overline{s}\gamma_\mu d + \overline{s}\gamma_\mu\gamma_5 d\ \overline{s}\gamma_\mu\gamma_5 d \\ Q_2(\mu) &= \overline{s}\gamma_\mu d\ \overline{s}\gamma_\mu d - \overline{s}\gamma_\mu\gamma_5 d\ \overline{s}\gamma_\mu\gamma_5 d \\ Q_3(\mu) &= \overline{s}d\ \overline{s}d + \overline{s}\gamma_5 d\ \overline{s}\gamma_5 d \\ Q_4(\mu) &= \overline{s}d\ \overline{s}d - \overline{s}\gamma_5 d\ \overline{s}\gamma_5 d \\ Q_5(\mu) &= \overline{s}\sigma_{\mu\nu} d\ \overline{s}\sigma_{\mu\nu} d. \end{aligned} \tag{4.23}$$

For simulation, we use the simpler basis of

$$\begin{aligned} Q_V(\mu) &= \overline{s}\gamma_\mu d\ \overline{s}\gamma_\mu d \\ Q_A(\mu) &= \overline{s}\gamma_\mu\gamma_5 d\ \overline{s}\gamma_\mu\gamma_5 d \\ Q_S(\mu) &= \overline{s}d\ \overline{s}d \\ Q_P(\mu) &= \overline{s}\gamma_5 d\ \overline{s}\gamma_5 d \\ Q_T(\mu) &= \overline{s}\sigma_{\mu\nu} d\ \overline{s}\sigma_{\mu\nu} d, \end{aligned} \tag{4.24}$$

which is related to our renormalisation basis introduced in the previous section through a simple rotation.

$$\begin{aligned} Q_1 &= Q_V + Q_A \\ Q_2 &= Q_V - Q_A \\ Q_3 &= Q_S - Q_P \\ Q_4 &= Q_S + Q_P \\ Q_5 &= Q_T. \end{aligned} \tag{4.25}$$

Once the simulations are complete we can rotate back to our renormalisation basis where we now have contributions from Q_i $(i = 2, 3, 4, 5)$ mixing with contributions from Q_1. Together with the overall multiplicative renormalisation, the subtraction of the unwanted operators may be expressed in a compact form as

$$Q^{\text{cont}}(\mu) = Z(\mu, g_0^2) \left(Q_1^{\text{latt}} + \sum_{i \neq 1} \Delta_i(g_0^2) Q_i^{\text{latt}} \right). \tag{4.26}$$

The renormalisation coefficients Z and Δ_i have been determined perturbatively for $\overline{\text{MS}}$-NDR in [101, 102] and the expressions relevant to our calculation are given in appendix B . Once the renormalisation and subtraction of eq. (4.26) is carried through, we have the matrix element for our desired operator in eq. (4.12).

4.3.2 Contractions

Let us start now by writing out our 3-pt function in its full glory. We will be using pseudoscalar kaon sources $J_5 = \bar{d}\gamma_5 s$ at x and y and for the operator $d\Gamma_1\bar{s}d\Gamma_2\bar{s}$ at the origin, where the suffixes on the Γ are just to identify separate contractions and do not imply that the γ-matrices are different. In fact, for our simulations they refer to the operators in eq. (4.24). This leads to

$$C_i^{(3)}(t_x, t_y; \mu) = \sum_{\vec{x},\vec{y}} \langle \bar{d}(y)\gamma_5 s(y) d(0)\Gamma_1 \bar{s}(0) d(0)\Gamma_2 \bar{s}(0) \bar{d}(x)\gamma_5 s(x)\rangle. \tag{4.27}$$

The correlators in eq. (4.20) have two independent Wick contractions,

$$\begin{aligned} C_i^{(3)}(t_x, t_y; \mu) \;=\; & 2 \sum_{\vec{x}\vec{y}} \left[\mathrm{Tr}\left[S_d(0,x)\,\gamma_5\, S_s(x,0)\Gamma_1\right] \mathrm{Tr}\left[S_d(0,y)\,\gamma_5\, S_s(y,0)\,\Gamma_2\right]\right. \\ & \left. - \mathrm{Tr}\left[S_d(0,x)\,\gamma_5\, S_s(x,0)\Gamma_1\, S_d(0,y)\,\gamma_5\, S_s(y,0)\,\Gamma_2\right]\right] \end{aligned} \tag{4.28}$$

the capitalised Tr indicates that it is over both the colour and Dirac indices. Since, the propagators in the simulation are of the form $S(z,0)$, *i.e.* outgoing from origin, one may use the γ_5-conjugation $S(0,z) = \gamma_5 S^\dagger(z,0)\gamma_5$ along with $\gamma_5\gamma_5 = 1$ to obtain

$$\begin{aligned} C_i^{(3)}(t_x, t_y; \mu) \;=\; & 2 \sum_{\vec{x}\vec{y}} \left[\,\mathrm{Tr}\left[S_d^\dagger(x,0)\, S_s(x,0)\Gamma_1\,\gamma_5\right] \mathrm{Tr}\left[S_d^\dagger(y,0)\, S_s(y,0)\,\Gamma_2\,\gamma_5\right]\right. \\ & \left. - \mathrm{Tr}\left[S_d^\dagger(x,0)\, S_s(x,0)\Gamma_1\,\gamma_5\, S_d^\dagger(y,0)\, S_s(y,0)\,\Gamma_2\,\gamma_5\right]\right]. \end{aligned} \tag{4.29}$$

We notice objects of the form $S^\dagger(z,0)S(z,0)$ occurring repeatedly. For conciseness of notation and convenience in coding, let us introduce the following matrices,

$$A_{ab}^{\alpha\beta}(t_z) = \sum_{\vec{z}} \left(S_d^\dagger(z,0)\, S_s(z,0)\right)_{ab}^{\alpha\beta}. \tag{4.30}$$

This reduces the 3-pt function to

$$C_i^{(3)}(t_x, t_y; \mu) = 2\left[\Big(A(t_x)\Gamma_1\gamma_5\Big)_{aa}^{\alpha\alpha}\Big(A(t_y)\Gamma_2\gamma_5\Big)_{bb}^{\beta\beta} - \Big(A(t_x)\Gamma_1\gamma_5\Big)_{ab}^{\alpha\beta}\Big(A(t_y)\Gamma_2\gamma_5\Big)_{ba}^{\beta\alpha}\right]. \tag{4.31}$$

With this, we are now ready for the simulation, with eqs. (4.30) and (4.31) spelling out the basic building blocks for the code. But before we proceed let us look at the energy (four-momentum) dependence of the matrix elements and set out the methods of analysis.

4.4 Mass/momentum dependence of the matrix elements and methods of analysis

For fermion implementations which (nearly) respect chiral symmetry, *e.g.* in [77, 82, 84], the chiral behaviour is not modified by lattice artefacts and $B_K(\mu)$ can be obtained from matrix elements of kaons at rest. But for Wilson fermions as, for example, in [76, 90], lattice artefacts introduce chiral symmetry breaking contributions to B_K in the chiral limit. In our case, even though we use a clover-improved action, four-fermion operators are unimproved and $\mathcal{O}(a)$ artefacts may be present. To partially remove them at finite lattice spacing another degree of freedom is required and this requires the introduction of non-zero momentum kaons.

Keeping this in mind, let us now consider matrix elements with non-vanishing external momenta, generic pseudoscalar mesons and in the presence of extra lattice artefacts that arise for non-chiral fermions. On the lattice, the chiral behaviour of the matrix element in such cases can be parametrised as [89]

$$\begin{aligned}\langle \bar{P}^0, \vec{p}\,|Q(\mu)|P^0, \vec{q}\,\rangle \;&=\; \alpha' + \beta' m_P^2 + \delta' m_P^4 \\ &\quad + (p\cdot q)\left(\gamma + \gamma' + (\epsilon+\epsilon')m_P^2 + (\xi+\xi')(p\cdot q)\right) + \cdots\end{aligned} \tag{4.32}$$

where all the quantities are expressed in lattice units and the ellipsis stands for higher-order terms in $p\cdot q$ and m_P^2. All the primed coefficients are lattice artefacts.

However, while γ' and ϵ' are corrections of $\mathcal{O}(a)$ to the corresponding physical contributions, the parameters α', β' and δ' are absent in the continuum limit and have to be subtracted from the estimate of B_K in eq. (4.15). In particular the α' term makes B_K divergent in the chiral limit. The γ term is the one of interest and B_K is determined by γ to leading order in momentum and mass.

For our calculation with Wilson fermions, we neglect higher order terms and use the following expression for the matrix elements:

$$\langle \bar{P}^0, \vec{p} \,|Q(\mu)|P^0, \vec{q}\,\rangle = \alpha' + \beta' m_P^2 + (\gamma + \gamma')(p \cdot q). \tag{4.33}$$

Now, there is more than one way to extract the value of B_K from this. The one adopted in most of the early works is to use 2-pt correlators with the axial current at the origin in the denominator of the ratio [fig. 4.8]. This leads to a cancellation of the factors of $f_K m_K$ and gives $\frac{8}{3}B_K$ directly. However, as we too have ourselves noticed, 2-pt correlation functions with an axial current can be noisier than those with pseudoscalar currents.

An alternative procedure, followed by [79, 100, 103] is where first the following ratios are formed.

$$R_3 = \frac{\mathcal{C}^{(3)}(t_x, t_y; p_x, p_y; \mu)}{Z_A^2 \mathcal{C}^{(2)}_{PP}(t_x; p_x)\mathcal{C}^{(2)}_{PP}(t_y; p_y)} \longrightarrow \frac{1}{Z_A^2 \mathcal{Z}_P^2} \langle \bar{P}^0, \vec{p}_x|Q(\mu)|P^0, \vec{p}_y\rangle, \tag{4.34}$$

$$X(0) = \frac{8}{3}\left|\frac{\mathcal{C}^{(2)}_{A_0 P}(t_x)}{\mathcal{C}^{(2)}_{PP}(t_x)}\right|^2 \longrightarrow \frac{1}{Z_A^2 \mathcal{Z}_P^2}\frac{8}{3} f_P^2 m_P^2, \tag{4.35}$$

$$X(\vec{p}) = X(0) \cdot \frac{(p_x \cdot p_y)}{m_P^2} \longrightarrow \frac{1}{Z_A^2 \mathcal{Z}_P^2}\frac{8}{3} f_P^2 (p_x \cdot p_y), \tag{4.36}$$

where Z_A is the axial current renormalisation. This, effectively is a change of variables

$$\begin{aligned} \langle \bar{P} \mid Q \mid P \rangle &\Rightarrow R_3 \\ m_P^2 &\Rightarrow X \\ p \cdot q &\Rightarrow Y. \end{aligned} \tag{4.37}$$

At this stage, instead of eq. (4.33), one may fit the equation

$$R_3 = \widetilde{\alpha}' + \widetilde{\beta}' X(0) + (\widetilde{\gamma} + \widetilde{\gamma}') X(\vec{p}) \tag{4.38}$$

to obtain estimates for B_K from $\widetilde{\gamma}$ [79, 100, 103], by neglecting $\widetilde{\gamma}'$. In fact, the way it has been set up here, one may identify B_K with $\widetilde{\gamma}$ directly. We refer to this as Method I.

One, point of caution identified in this type of fit is that, the parameters with tildes are fitted by taking them to be constant. However if we look carefully at the transformation between eqs. (4.33) and (4.38)

$$\widetilde{\alpha}' \equiv \frac{\alpha'}{Z_A^2 \mathcal{Z}_P^2}, \quad \widetilde{\beta} \equiv \frac{3\beta'}{8 f_P^2}, \quad \widetilde{\gamma} \equiv \frac{3\gamma}{8 f_P^2} \text{ and } \widetilde{\gamma}' \equiv \frac{3\gamma'}{8 f_P^2}, \tag{4.39}$$

we notice the dependence on $\mathcal{Z}_{\mathcal{P}}$ and f_P, both of which may vary significantly over the fit-range. Hence the estimates are for effective values of $\mathcal{Z}_{\mathcal{P}}$ and f_P in our range of simulation. In this manner, for a set of different valence quarks on a given sea quark mass, this approach gives an estimate of the leading term in an expansion of B_K for that set with the kaons not necessarily being at the physical kaon mass but at a mass around the simulated region.

However, ideally we would like to have estimates for B_K not for pseudoscalar masses in our simulated region, but for physical kaon masses. Therefore, it is useful to have estimates of B_K for each $(\kappa_{\text{sea}}, \kappa_{\text{val}})$ combination, which will then allow us to extrapolate in the quark masses. For this, we follow the approach of [90, 101]. Let us call the non-zero- and zero-momentum R_3's $R_3(\vec{p})$ and $R_3(0)$ respectively, corresponding to $X(\vec{p})$ and $X(0)$ defined in eq. 4.34. The two non-zero momenta $\{p_x, p_y\} = \{(0,0,0),(1,0,0)\}$ and $\{(1,0,0),(0,0,0)\}$, have been averaged, since they are estimates of the same matrix elements in the continuum and indeed numerically are found to be very similar. Then we have

$$\left.\frac{R_3(\vec{p}) - R_3(0)}{X(\vec{p}) - X(0)}\right|_{(\kappa_{\text{sea}}, \kappa_{\text{val}})} = B_K(\mu, \kappa_{\text{sea}}, \kappa_{\text{val}}). \tag{4.40}$$

These can then be used in our chiral extrapolations in the sea and valence quarks. We refer to this method of analysis as Method II.

Table 4.2: The configurations used. Values for lattice spacings are as calculated from the value of the scale, r_0, in lattice units from the UKQCD set [104, 105].

Set	β	$c_{\rm SW}$	$\kappa_{\rm sea}$	a(fm)[GeV^{-1}]	$(m_P/m_V)_{\kappa_{\rm sea}=\kappa_{\rm val}}$	No. of configs
I	5.20	2.0171	0.1350	0.103(2) [1.91(2)]	0.70(1)	100
II	5.26	1.9497	0.1345	0.104(1) [1.90(2)]	0.78(1)	100
III	5.29	1.9192	0.1340	0.102(2) [1.94(2)]	0.83(1)	80

Here, it may be noted that, fitting these values to a constant for a given sea quark is similar to estimating $\widetilde{\gamma}$ from a fit of eq. (4.38). Also to be noted is the fact that for higher orders of momentum, this expression differs from the correct dependence of B_K by a term like $\widetilde{\xi} m_P E(\vec{p})$ [101] [see eq. (4.32)]. We have found the coefficient $\widetilde{\xi}$ of this term difficult to determine, particularly for our limited set of momenta. However, if we were able to make this correction, it would simply change our values of B_K within our systematics, leaving our conclusions unchanged.

4.5 Lattice simulation

In this work, B_K is calculated using Clover-improved Wilson fermions [18] with two degenerate flavours of dynamical quarks on the UKQCD set of unquenched configurations listed in table 4.2 The simulations are in the region $m_P/m_V \geq 0.7$ on a volume of $16^3 \times 32$ ($m_P L \geq 7$). In order to look for sea-quark dependence in B_K we use three different sea quark masses but a nearly constant lattice spacing. Details of the generation of the gauge configurations can be found in [104, 105]. To have a decorrelated sample, configurations separated by 40/50 trajectory steps are used.

The lattice spacings determined from the Sommer scale, r_0, are very similar for these sets. It may be noted that, for these configurations, a sea quark dependence of the lattice spacing has been noticed. Ideally, perhaps, one would expect the spacing

to depend only on the coupling, and it remains an open question as to what is the origin of this dependence. There are concerns that the $\kappa_{\rm sea}$-dependence of the lattice spacing observed in these configurations is due to the proximity to a phase transition around $a \simeq 0.1$ fm where there may be large cutoff effects in the dynamical case [106–108] and therefore needs to be considered with caution. However, to keep the lattice spacing, defined using the scale r_0 [109], as fixed as possible, a set of values of the bare coupling and bare dynamical quark mass have been chosen in [104, 105].

We take the view that, nevertheless, these sets of configurations do have some degree of matching according to a valence-quark-independent definition of an effective lattice spacing, and thus, unless our physics is completely overwhelmed by any nearby phase transition, a combined analysis of the data as a function of $\kappa_{\rm sea}$ is worthwhile. It may be noted that since B_K is dimensionless, the lattice spacing enters through discretisation errors but not via an overall power of a. Moreover, when analysing the sea quark mass dependence, we use the variable $(am_P)^2(\kappa_{\rm sea}, \kappa_{\rm sea})$ which in our case is equivalent to using $(r_0 m_P)^2$ since our lattice spacing is defined through r_0 and $r_0 m_P = (r_0/a) \times am_P$ with (r_0/a) fixed to a constant for these lattices [104, 105].

Propagators and correlators were calculated using the FermiQCD [54, 55] code. Five valence quark propagators at $\kappa = 0.1356$, 0.1350, 0.1345, 0.1340 and 0.1335 were generated for each sea quark using the Stabilised Biconjugate Gradient method [14]. Smearing was tried, but since it did not give any significant improvement in the signal, the results presented here are for the local case (see comments in the next section).

In the 3-pt functions, the operator is fixed at the origin and t_y is kept fixed at a particular value, while t_x is varied over the full temporal range of the lattice. The main reported results are for $t_y = 10$. We have checked with other neighbouring values of t_y but observe no dependence, implying that the ground state is reasonably well isolated by this time. For the momentum configurations, we have chosen $\{p_x, p_y\} = \{(0,0,0),(0,0,0)\}, \{(0,0,0),(1,0,0)\}$ and $\{(1,0,0),(0,0,0)\}$ where the

average over equivalent configurations is understood.

Fitted ratios for this basis that give us the matrix elements in lattice units, $Q_i^{\rm latt}$, $(i = V, A, S, P, T)$ are plotted in fig. 4.9. We now need to perform the renormalisation and subtraction of eq. (4.26). To go directly to $\overline{\rm MS}$ at $\mu = 2$ GeV, we note that in our case $(a\mu) \approx 1$ and we can naively use standard perturbation theory at one-loop. For the coupling there is a range of choices that may lead to different numerical values. We use the boosted bare lattice coupling, $g_0^2 = 6/\beta\langle P\rangle$, where $\langle P\rangle$ is value of the relevant average plaquette and our values are {0.5336, 0.5399, 0.5424}. For c_{SW} we used the tree-level value of 1.0 in eqs. (B.1) and (B.2) in appendix B. The perturbative matching coefficients thus obtained are listed in table 4.3. However, looking at fig. 4.9 one can notice that all the contributions, including those from the extra operators, are of comparable order. Hence the subtraction is very important and is likely to be sensitive to the subtraction coefficients, Δ_i, $(i = 1, 2, 3, 4)$. Therefore, a non-perturbative determination of the matching coefficients would probably have been better.

Once we have our renormalised (and subtracted) matrix element, we are ready to obtain the values of B_K from eqs. (4.38) and (4.40) for our analysis.

4.6 Analysis and discussion

The values obtained for $B_K(\overline{\rm MS}, 2\text{ GeV})$ for our sets of masses are tabulated in table 4.4. As mentioned before, we refer to the ones quoted from eq. (4.38) follow-

Table 4.3: Perturbative matching coefficients to go from $B_K^{\rm latt}(\mu = 1/a)$ to $B_K^{\overline{\rm MS}}(\mu = 2\text{ GeV})$.

Set	g_0^2	$Z(2\text{ GeV}, g_0^2)$	$Z\,\Delta_2(g_0^2)$	$Z\,\Delta_3(g_0^2)$	$Z\,\Delta_4(g_0^2)$	$Z\,\Delta_5(g_0^2)$	Z_A
I	2.162	0.4959	-0.0385	-0.0070	0.0140	0.0140	0.7482
II	2.113	0.5072	-0.0376	-0.0068	0.0137	0.0137	0.7540
III	2.091	0.5133	-0.0372	-0.0068	0.0135	0.0135	0.7565

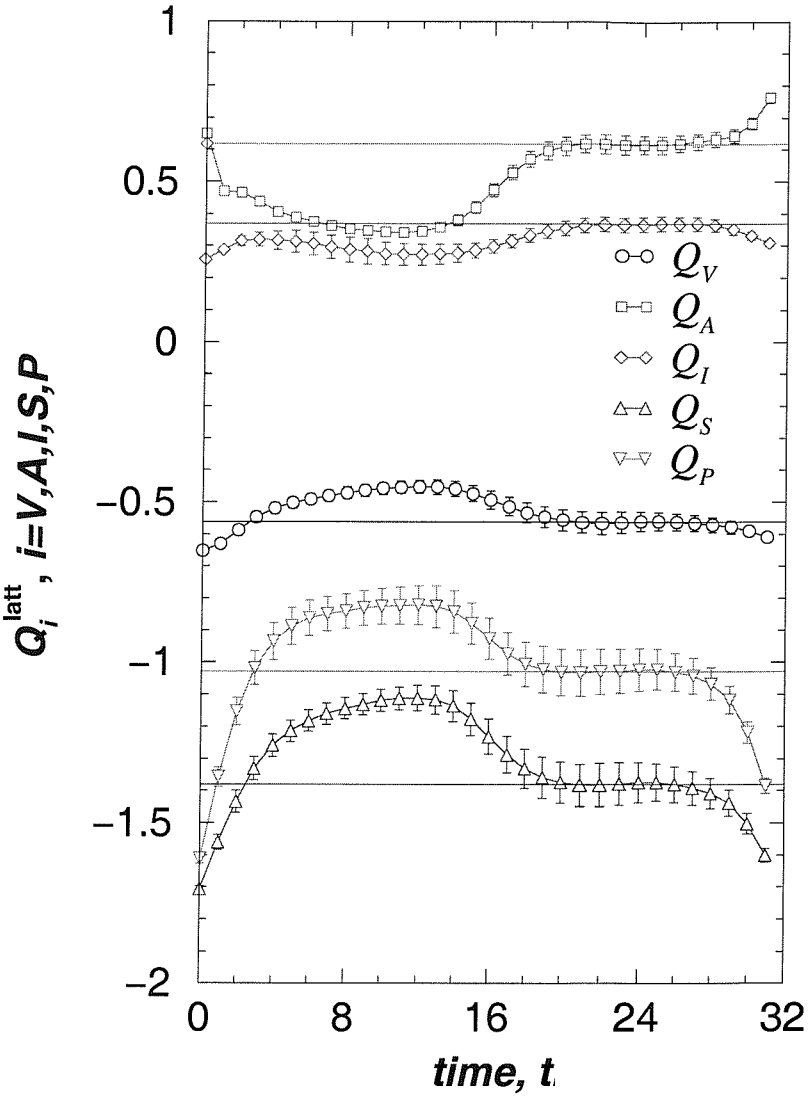

Figure 4.9: Fits for lattice matrix elements for the complete set of bare operators for a sample of our data (set I, $\kappa_{\rm val} = 0.1350$). Ratios of the 3-pt correlators to two 2-pt $\langle PP \rangle$ correlators are fitted in the interval $t_x = 22 - 27$ for $t_y = 10$ (see eq. 4.34). Correlators are shown for zero momentum. The fitted ones are those of interest $\langle \bar{P}^0 | Q_i | P^0 \rangle$ while the other plateau in the first half of the lattice corresponds to the off-shell $\langle \bar{P}^0 \bar{P}^0 | Q_i | 0 \rangle$ matrix elements.

ing [79, 100, 103] and from eq. (4.40) following [90, 101] as method I and II respectively.

We have degenerate valence quarks. So, SU(3) breaking effects due to $m_s \neq m_{u,d}$ are not accounted for. Rather, our kaon is made up of two quarks around $m_s/2$. Moreover, the results in table 4.4 are obtained for local sources. Indeed, we have not seen any significant improvement of the signal from smearing. This is not unexpected since we have a local operator at the origin and can smear only at the the sink, which is usually less effective than source smearing. It may also be due to a lack of optimisation of the smearing parameters. However, results were fully compatible with those using local operators and we have restricted the presentation to the simpler case.

In fig. 4.10, we plot $B_K(\overline{\text{MS}}, 2\text{ GeV})$ from eq. (4.40) as a function of the corresponding squared pseudoscalar masses over the complete set of our valence and sea quark masses. We observe the points for the lightest valence quarks diverging for the different sea quarks. It is known that finite volume effects can obscure the chiral behaviour in B_K [110]. The JLQCD collaboration [111] observes finite volume effects for lighter sea quarks for the same action, but for our parameters they have excluded finite volume effects for pseudoscalar meson correlators down to just beyond our lightest point in set I. Indeed we find the finite volume correction from [110] to be -0.1% for this point.

Nonetheless, we note that, contrary to the other sets, for set I, the $\mathcal{O}(a)$ discretisation error parameters $\widetilde{\alpha}$ and $\widetilde{\beta}$ turn out to have finite values of $-0.06(2)$ and $0.23(8)$. The effects of these terms are greater at lighter quark masses and we cannot be sure that the curvature observed here is due to a true chiral behaviour. As can be seen from our values of m_P/m_V, the lightest point of Set I is at a considerably lighter mass than all the other points. Therefore, we choose to be cautious and exclude it from our analysis. It would be interesting to know if non-perturbative renormalisation [112, 113], and/or the improvement programme of [114, 115] could lead to better chiral behaviour.

Table 4.4: Simulated values of $B_K(\overline{\text{MS}}, 2\text{ GeV})$. method I refers to a direct fit of eq. (4.38); while in method II, eq. (4.40) is used to obtain values for each $(\kappa_{\text{sea}}, \kappa_{\text{val}})$ combination.

				Method I	Method II
$(\beta, \kappa_{\text{sea}})$	κ_{val}	$m_P/m_V(\kappa_{\text{sea}}, \kappa_{\text{val}})$	$m_P^2(\kappa_{\text{sea}}, \kappa_{\text{val}})$	$B_K(\kappa_{\text{sea}})$	$B_K(\kappa_{\text{sea}}, \kappa_{\text{val}})$
(5.20, 0.1350)	0.1356	0.62(3)	0.106(5)	0.64(7)	0.41(12)
	0.1350	0.72(2)	0.166(4)		0.57(9)
	0.1345	0.77(1)	0.218(4)		0.63(7)
	0.1340	0.80(1)	0.270(4)		0.66(6)
	0.1335	0.83(1)	0.324(4)		0.69(5)
(5.26, 0.1345)	0.1356	0.67(2)	0.151(3)	0.69(8)	0.70(16)
	0.1350	0.74(1)	0.206(3)		0.71(10)
	0.1345	0.77(1)	0.255(3)		0.71(8)
	0.1340	0.81(1)	0.306(4)		0.72(7)
	0.1335	0.83(1)	0.359(4)		0.72(6)
(5.29, 0.1340)	0.1356	0.72(2)	0.170(5)	0.79(4)	0.81(6)
	0.1350	0.77(1)	0.229(5)		0.79(4)
	0.1345	0.80(1)	0.280(5)		0.78(4)
	0.1340	0.83(1)	0.332(6)		0.77(4)
	0.1335	0.85(1)	0.386(6)		0.77(4)

To look at the divergence of the three sets of data points at light quark masses, the data for the full matrix element $\langle \overline{K^0} \mid Q(\mu) \mid K^0 \rangle \equiv \frac{8}{3} f_P^2 m_P^2 B_P(\mu)$ and that of $f_P^2 B_P(\mu)$ are plotted against am_P^2 in fig. (4.11). It is noticeable that the full matrix element seems to show a more consistent valence quark dependence for the different fixed sea masses. Looking at $f_P^2 B_P(\mu)$, it can be noted that the divergence here is no worse than $B_P(\mu)$ itself. This suggests that, probably f_P is not the source of the divergence. However, one notices that the $f_P^2 B_P(\mu)$ curves are going to lower values at higher quark mass, implying that, in this data f_P decreases with mass, which is not the expected behaviour. This may suggest that the truncation of eq. (4.32) to eq. (4.33) is leading to non-negligible errors.

Let us proceed to consider the values from method I. It is notable that for these rather heavy sea quarks these numbers are compatible with quenched estimates.

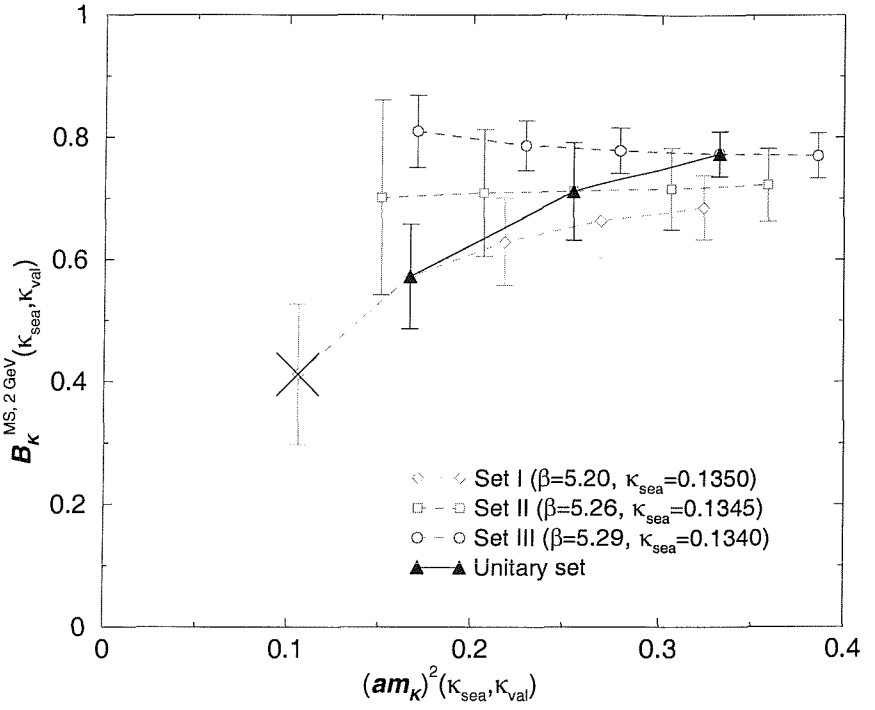

Figure 4.10: Values of $B_K(\overline{\text{MS}}, 2\text{ GeV})$ for each $(\kappa_{\text{sea}}, \kappa_{\text{val}})$ combination plotted as a function of the corresponding squared pseudoscalar masses. The dashed lines joining the points are just for a visual guide separating the sets with different sea quarks. The filled points joined by a solid line are the unitary ones for which $\kappa_{\text{sea}} = \kappa_{\text{val}}$. The lightest point for Set I (marked by a large cross) is excluded from the analysis.

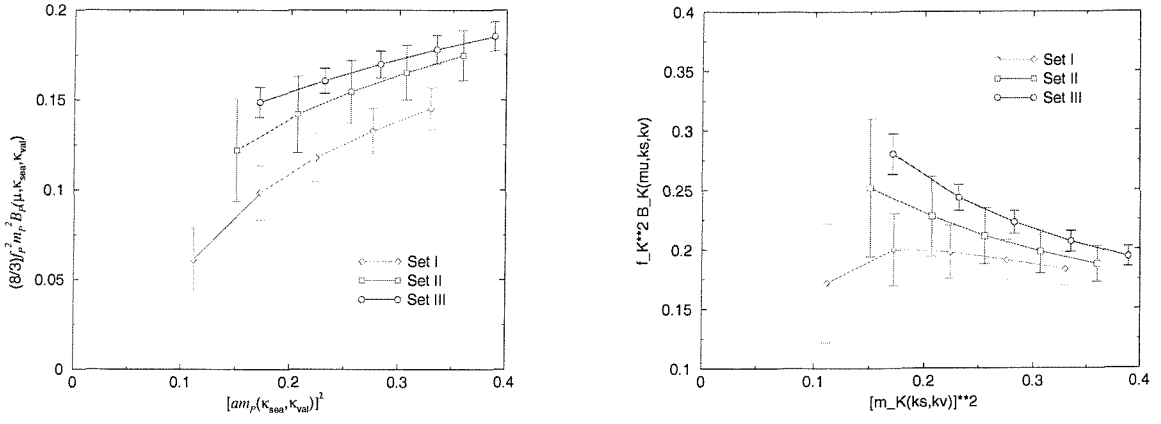

Figure 4.11: Plots of $\langle \overline{K^0} \mid Q(\mu) \mid K^0 \rangle \equiv \frac{8}{3} f_P^2 m_P^2 B_P(\mu)$ and $f_P^2 B_P(\mu)$ against am_P^2. The full matrix element seems to show a more consistent valence quark dependence for the different fixed sea masses.

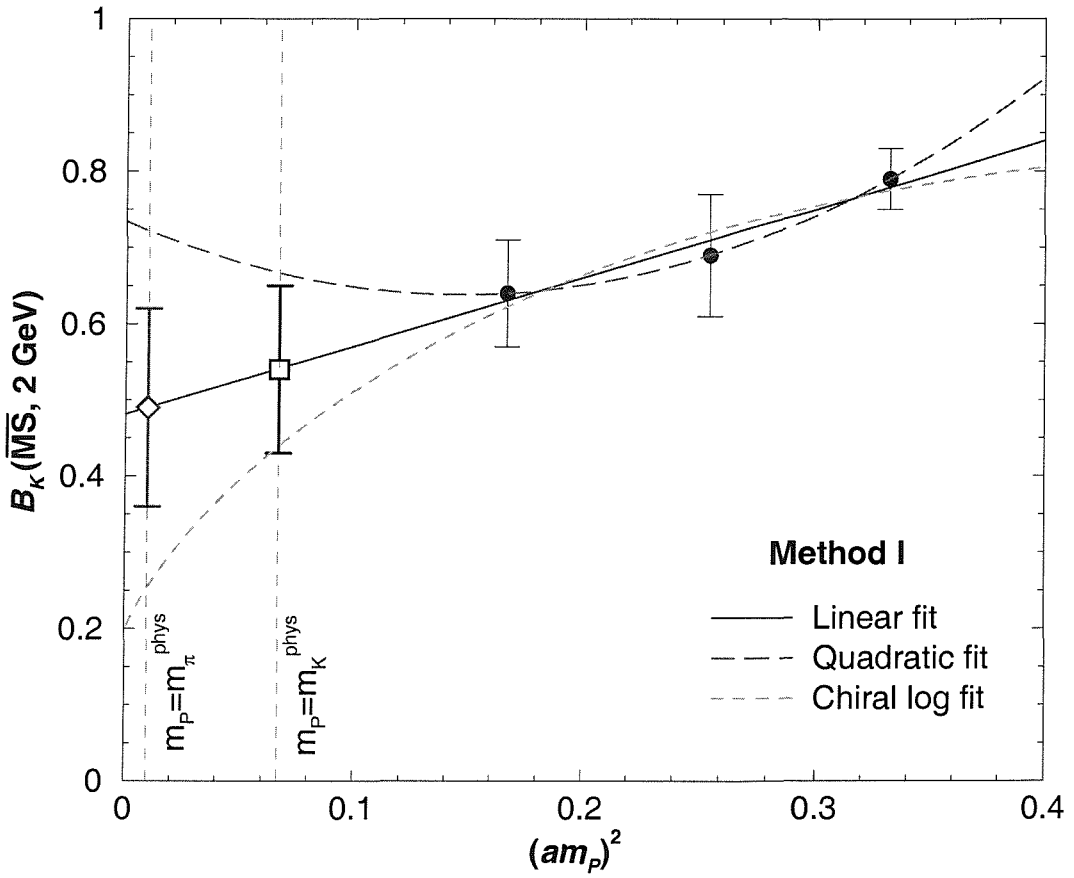

Figure 4.12: Fit to the data from method I. The values quoted is from the linear extrapolation in sea quark mass, whereas the quadratic and chiral log-type fits are added for illustration. The extrapolated points at $m_P = m_\pi^{\rm phys}$ (the result from this method) and $m_K^{\rm phys}$ are also shown.

This is the reason that previous attempts to unquench for a fixed heavy sea quark mass have found it difficult to disentangle the unquenching effects. Since we have more than one sea quark mass in our simulation, we can attempt to extrapolate these numbers to realistically light sea quarks. We use a linear fit versus the unitary pseudoscalar masses $(am_P)^2(\kappa_{\rm sea} = \kappa_{\rm val})$ and go to the up/down limit. This gives us

$$B_K(\overline{\rm MS},\ 2\ {\rm GeV}) = 0.49(13), \tag{4.41}$$

which corresponds to $\hat{B}_K = 0.69(18)$.

In this method we estimate $\widetilde{\gamma}$ in eq. 4.38. Here, we know the masses of the sea

quarks for each set. But, it is reasonable to ask, what valence quark masses do these values of B_K (for the individual sets) correspond to. As mentioned in the previous section, the valence quarks are not necessarily such that $m_P = m_K^{\rm phys}$. In fact one can note by comparing with the last column of table 4.4 that the values from method I are comparable to those obtained in method II for valence quarks in the simulated region. Therefore one may think of the extrapolated estimate in method I as one of B_K where the sea quarks are realistically light but the valence quarks are in our simulated region of masses, *i.e.* heavier than the physical strange quark.

A somewhat complementary approach, would be to follow the route of [86] and take the unitary points, *i.e.* the points with $\kappa_{\rm sea} = \kappa_{\rm val}$ from method II, for extrapolation to the physical kaon mass [fig. 4.13]. This leads to

$$B_K(\overline{\rm MS},\ 2\ {\rm GeV}) = 0.48(13), \tag{4.42}$$

Corresponding to $\hat{B}_K = 0.67(18)$. Here we have a more reasonable valence $m_P = m_K^{\rm phys}$, but on the other hand the sea and valence quarks are degenerate and hence the sea content is not as light as the up/down quarks. To understand how much this may affect us we note that if we take all the quark masses (both valence and sea) to light quarks our value of B_K goes down to 0.40(17) and $\hat{B}_K = 0.56(24)$.

A combined analysis of valence and sea quarks has been tried for the spectroscopy studies in [105, 111]. With a larger sample of sea and valence quark masses, this would be a possible route to an estimate of B_K at the physical valence and sea masses. But, for our data such a fit produces unstable parameters and hence these are not reported.

Owing to the exploratory nature of our analysis and the already large statistical errors, a study of systematic errors such as those connected to choices of fit window, chiral extrapolation, renormalisation method, the fixed time at one end, the strong coupling, Λ_{QCD}, etc. has not been addressed.

Even though we recognise that the presence of several artefacts does not allow a quantitative estimate of the sea quark dependence, it does seem that dynamical

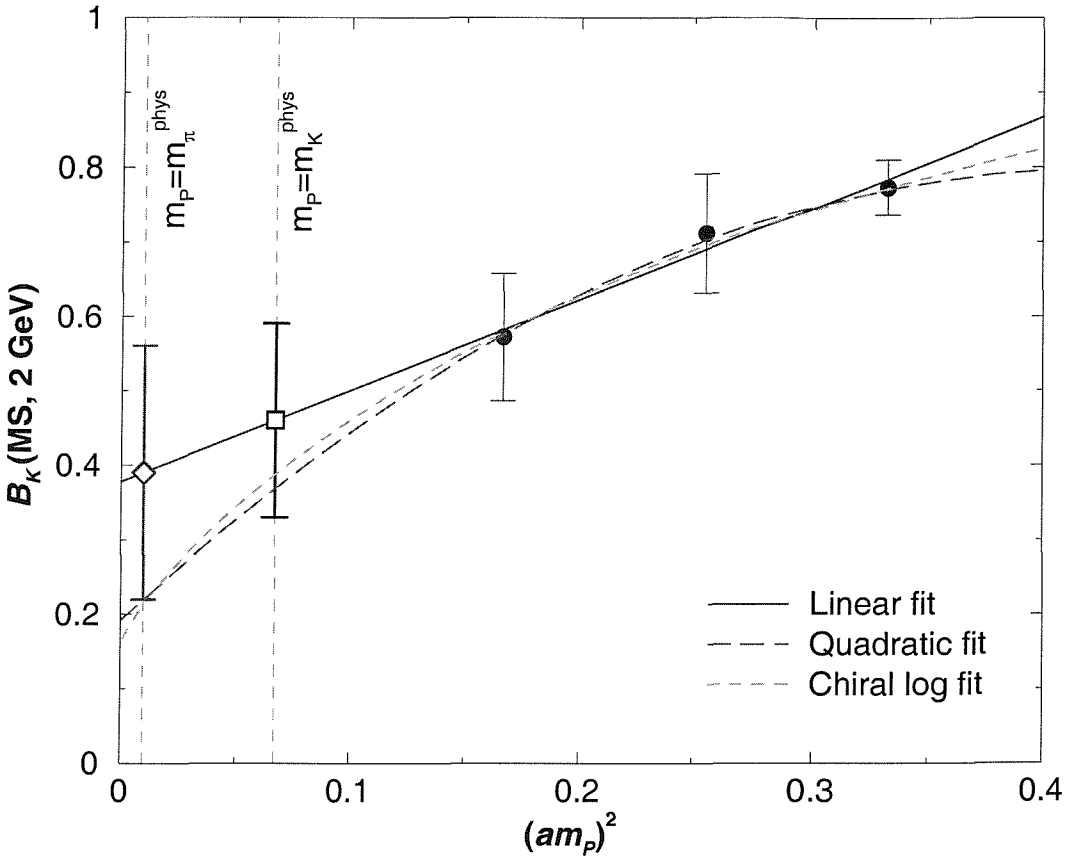

Figure 4.13: Unitary fit of the data. The value quoted is from the linear extrapolation in both sea and valence quark masses, whereas the quadratic and chiral log-type fits are added to illustrate that, from the available data it is not possible to infer any non-linearity. The vertical lines show the position where $m_K = m_K^{\rm phys}$ (the result in this method) and $m_\pi^{\rm phys}$.

Table 4.5: Table reproduced from [96] showing that $N_f = 2$ numbers are systematically lower than the quenched ones.

Ref.	Action	$\frac{B_K(N_f=0)}{B_K(N_f=2)}$
[93]	Staggered	$\sim 1.09(7)$
[92]	Staggered	$\sim 1.03(5)$
[94]	Staggered	$\sim 1.06(10)$
[95]	Wilson	$\sim 1.08(15)$

quark effects can be quite significant. There also seem to be indications that, incorporating dynamical quarks lowers the value of B_K. It is also intriguing to note that in recent studies where $\hat{B}_K$ is taken as a free parameter and fitted using the other unitarity triangle constraints, the values obtained are $\hat{B}_K = 0.69(11)$ [116] and $\hat{B}_K = 0.65(10)$ [117], again lower than the usual quenched lattice value and more in line with our numbers.

Now, we come to the question of how to understand this suggested lowering of the value of B_K in the backdrop of the lore since the works of [89, 91] that the unquenched B_K will probably be higher. First of all, it needs to be kept in mind, that this is based only on [91] where they found B_K to get slightly lower for $N_f = 2$ and higher for $N_f = 4$. Then they interpolated to $N_f = 3$, which is something that is probably not beyond question.

For us, it is not possible to comment on $N_f = 3$. For $N_f = 2$ a table is reproduced from [96] with the observation that the $N_f = 2$ numbers are always lower than those for $N_f = 0$. This statement also valid for subsequent works [79, 91]. So, now we can see that when one has two finite-mass but still heavy sea quarks, B_K starts to decrease but is still consistent with the quenched value within errors. This is why previous works have failed to see unquenching effects. Even within our simulated range, we see the same. But, when the sea quarks can be taken to the massless limit, the value of B_K becomes distinctly lower than the quenched result.

Putting all the pieces together, including the RBC dynamical DW results [86]

and the UT fits with B_K as a free parameter [116, 117], there seems to be emerging evidence in favour of a lower value value of B_K as indicated in our analysis.

4.7 Conclusion

We have presented results for an unquenched calculation of B_K with non-perturbatively $\mathcal{O}(a)$-improved Wilson fermions for three sets of sea quarks on relatively small volume lattices of matched spacing. This allows us to look at the variation of B_K with sea quark mass. There is some concern about the robustness of the estimates due to various lattice uncertainties. Hence we do not emphasise our final number. Nevertheless, there are indications that dynamical quark effects are important and lead to a lower value of B_K. Connections are also made to previous unquenching attempts and in new light those works are also understood to be giving similar indications.

Chapter 5

Extracting signals from static quarks for the Λ_b lifetime problem

In this chapter we report progress in an ongoing calculation of spectator effects in Λ_b lifetime. Correlators with static quarks are known for their noise. Findings are presented on possible approaches to extract a signal along with an outlook for the future directions of this calculation.

5.1 Motivation

The Λ_b-lifetime problem is usually discussed in terms of the ratio of the lifetimes of Λ_b and B_d. In the Heavy Quark Expansion, making use of the fact that $m_b \gg \Lambda_{\rm QCD}$, this ratio can be expressed as [118, 119]:

$$\begin{aligned} \frac{\tau(\Lambda_b)}{\tau(B_d)} &= 1 + \frac{\Lambda^2}{m_b^2}\left[\left(\Gamma_2^{(0)} + \frac{\alpha_s}{4\pi}\Gamma_2^{(1)} + \ldots\right) + \frac{\Lambda}{m_b}\left(\Gamma_3^{(0)} + \cdots + \right) + \ldots\right] \\ &\approx 0.98 + \frac{\Lambda^3}{m_b^3}\left[\left(\Gamma_3^{(0)} + \frac{\alpha_s}{4\pi}\Gamma_3^{(1)} + \ldots\right) + \frac{\Lambda}{m_b}\left(\Gamma_4^{(0)} + \cdots + \right) + \ldots\right]. \end{aligned} \tag{5.1}$$

Here in the last step the leading order QCD value of the $\mathcal{O}(1/m_b^2)$ term has been used [120].

The experimental value [121] [as cited in [87]]

$$\left.\frac{\tau(\Lambda_b)}{\tau(B_d)}\right|_{\rm expt} = 0.786(34). \tag{5.2}$$

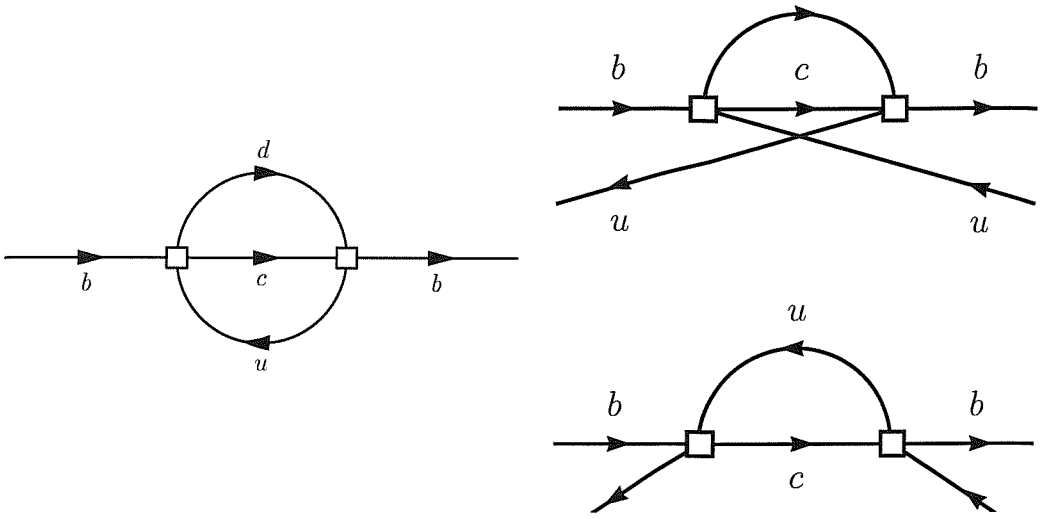

Figure 5.1: Non-spectator contributions (left) correspond to $1 \to 3$ particle processes, whereas spectator effects come in as $2 \to 2$ body, giving the latter a phase space advantage. Non-spectator processes are also two-loop compared to the one-loop spectator contributions.

is significantly lower, pointing to large higher order corrections. This has received significant attention as it has so far not been possible to find a theoretical value to satisfactorily match the experimental one.

However, the $\mathcal{O}(1/m_b^3)$ corrections contain spectator contributions (*i.e.* ones where a light spectator quark gets involved) that correspond to $2 \to 2$ particle processes compared with $1 \to 3$ particle processes for the non-spectator terms, with a corresponding enhancement in the phase space. This means that the $\mathcal{O}(1/m_b^3)$ corrections could be larger than simple power counting would suggest. An exploratory study [122] for two different pion masses and without chiral extrapolation indicates that the $\mathcal{O}(1/m_b^3)$ spectator contribution is significant, but probably not large enough to account for the difference. This expectation is also supported by sum rule results [123].

An updated theoretical value taking into account calculations $\mathcal{O}(m_b^3)$ contributions [122, 124, 125] and a partial estimate of $\mathcal{O}(m_b^4)$ [126] in [127] gives

$$\left.\frac{\tau(\Lambda_b)}{\tau(B_d)}\right|_{\text{theory}} = 0.88(5). \tag{5.3}$$

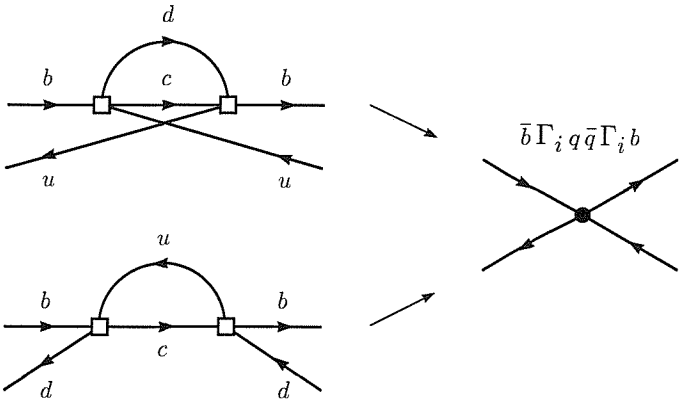

Figure 5.2: Spectator contributions to the decay width. In the OPE these can be written as matrix elements of four-fermion operators with Γ_i denoting some combination of Dirac and colour matrices.

However, some of the inputs here, particularly the exploratory values of the $\mathcal{O}(m_b^3)$ baryonic matrix elements and the $\mathcal{O}(m_b^4)$ contribution, are rather preliminary.

Keeping the above issues in mind, the aim of this project was to calculate the lifetime ratio to order $\mathcal{O}(1/m_b^3)$ on a large number of configurations and including a chiral extrapolation to verify the conclusions of the exploratory study [122].

5.2 Theoretical setup

The formalism for this calculation is spelt out in [120]. Using the optical theorem, the inclusive decay width of the Λ_b can be written as

$$\Gamma(\Lambda_b \to X) = \frac{1}{m_{\Lambda_b}} \mathrm{Im}\, \langle \Lambda_b | \mathbf{T} | \Lambda_b \rangle, \tag{5.4}$$

with the transition operator

$$\mathbf{T} = i \int \mathrm{d}^4 x\, T \left\{ \mathcal{L}_{\mathrm{eff}}(x) \mathcal{L}_{\mathrm{eff}}(0) \right\}, \tag{5.5}$$

where T denotes time ordering and $\mathcal{L}_{\mathrm{eff}}$ denotes the effective weak Lagrangian, renormalised at $\mu = m_b$. In the Operator Product Expansion this non-local operator is expanded in terms of local four-quark operators.

Table 5.1: Mesonic B-parameters in previous calculations.

Ref.	$B_1^d(m_b)$	$B_2^d(m_b)$	$\varepsilon_1^d(m_b)$	$\varepsilon_2^d(m_b)$
[124]	1.06(8)	1.01(6)	−0.01(3)	−0.03(2)
[128]	1.2(2)	0.7(1)	0.03(2)	0.04(1)

For details of $\mathcal{O}(1/m_b^2)$ terms we refer the reader to [120, 125] and proceed straight to the $\mathcal{O}(1/m_b^3)$ terms.

5.2.1 Matrix elements contributing at $\mathcal{O}(1/m_b^3)$

At next-to-leading order, spectator contributions ($\propto 1/m_b^3$) can be written as [125]

$$\begin{aligned}\frac{\tau(\Lambda_b)}{\tau(B_d)} &= 0.98 - \Delta_{\text{spec}} \\ \Delta_{\text{spec}} &= -0.08(2)L_1 + 0.33(8)L_2 \\ &\quad +0.008(2)B_1^d - 0.008(2)B_2^d + 0.16(4)\varepsilon_1^d - 0.16(4)\varepsilon_2^d. \end{aligned} \tag{5.6}$$

The mesonic B-parameters are defined as follows:

$$\begin{aligned} B_1^d(m_b) &= \frac{2}{f_B^2 m_{B_d}} \frac{\langle B_d|\bar{b}\gamma^\mu(1-\gamma_5)d\,\bar{d}\gamma^\mu(1-\gamma_5)b|B_d\rangle}{2m_{B_d}}, \\ B_2^d(m_b) &= \frac{2}{f_B^2 m_{B_d}} \frac{\langle B_d|\bar{b}(1-\gamma_5)d\,\bar{d}(1+\gamma_5)b|B_d\rangle}{2m_{B_d}}, \\ \varepsilon_1^d(m_b) &= \frac{2}{f_B^2 m_{B_d}} \frac{\langle B_d|\bar{b}\gamma^\mu(1-\gamma_5)\,t^a d\,\bar{d}\gamma^\mu(1-\gamma_5)t^a b|B_d\rangle}{2m_{B_d}}, \\ \varepsilon_2^d(m_b) &= \frac{2}{f_B^2 m_{B_d}} \frac{\langle B_d|\bar{b}(1-\gamma_5)\,t^a d\,\bar{d}(1+\gamma_5)\,t^a b|B_d\rangle}{2m_{B_d}}, \end{aligned} \tag{5.7}$$

with the argument m_b referring to the fact that they are renormalised (in the $\overline{\text{MS}}$ scheme) at the scale $\mu = m_b$. Here the t's are generators of $SU(3)_c$. The values of these matrix elements calculated in [122, 124, 128] are given in table 5.1

For the baryon, due to heavy quark symmetry relations [120]

$$\begin{aligned} \langle\Lambda_b|\bar{b}\gamma^\mu(1-\gamma_5)d\,\bar{d}\gamma^\mu(1-\gamma_5)b|\Lambda_b\rangle &= -2\,\langle\Lambda_b|\bar{b}(1-\gamma_5)d\,\bar{d}(1+\gamma_5)b|\Lambda_b\rangle, \\ \langle\Lambda_b|\bar{b}\gamma^\mu(1-\gamma_5)t^a d\,\bar{d}\gamma^\mu(1-\gamma_5)t^a b|\Lambda_b\rangle &= -2\,\langle\Lambda_b|\bar{b}(1-\gamma_5)t^a d\,\bar{d}(1+\gamma_5)t^a b|\Lambda_b\rangle \end{aligned}$$

there are only two, rather than four, independent matrix elements. These can be taken as

$$L_1(m_b) = \frac{2}{f_B^2 m_{B_d}} \frac{\langle \Lambda_b | \bar{b}\gamma^\mu(1-\gamma_5) d\, \bar{d}\gamma^\mu(1-\gamma_5) b | \Lambda_b \rangle}{2m_{\Lambda_b}}, \tag{5.8}$$

$$L_2(m_b) = \frac{2}{f_B^2 m_{B_d}} \frac{\langle \Lambda_b | \bar{b}\gamma^\mu(1-\gamma_5)\, t^a d\, \bar{d}\gamma^\mu(1-\gamma_5)\, t^a b | \Lambda_b \rangle}{2m_{\Lambda_b}}.$$

However, for Wilson fermions, in the absence of explicit chiral symmetry, similar to the B_K study, the operators mix with other ones of the same dimension. Therefore, again it will be necessary to work with a complete basis of operators and then subtract the contributions from the extra ones during tbe renormalisation process.

The values of the matrix elements of eq. (5.9) from the exploratory study [122] at $a^{-1} \approx 1.1\text{GeV}$ are

$$L_1(m_b) = \begin{cases} -0.31(3) & \text{for} \quad am_\pi = 0.52(3) \\ -0.22(4) & \text{for} \quad am_\pi = 0.74(4), \end{cases} \tag{5.9}$$

$$L_2(m_b) = \begin{cases} 0.23(2) & \text{for} \quad am_\pi = 0.52(3) \\ 0.17(2) & \text{for} \quad am_\pi = 0.74(4). \end{cases} \tag{5.10}$$

The recalculation of these matrix elements in a more rigorous way is the ultimate goal of this study. In the process, the mesonic B-parameters are also to be calculated. But the main focus remains these two baryonic matrix elements. This corresponds to calculating the so-called *crab diagram* of fig. 5.3.

It is a well-recognised fact that using some kind of smearing, or an insertion of a wave-function in the operator, can improve the signal by improving the overlap with the desired state, while reducing the overlap with the unwanted ones [see, for example [129]].

Working with ordinary lattice propagators that originate from the origin, for this type of 3-pt function calculation, one practically has to put the four-quark operator at the origin. Since this operator is local we cannot smear there. Moreover, since our heavy quarks are static, they are fixed at the other ends as well. Therefore the only smearing that is possible is for the light quarks at points away from the origin. These are represented by the wiggly lines in fig. 5.4.

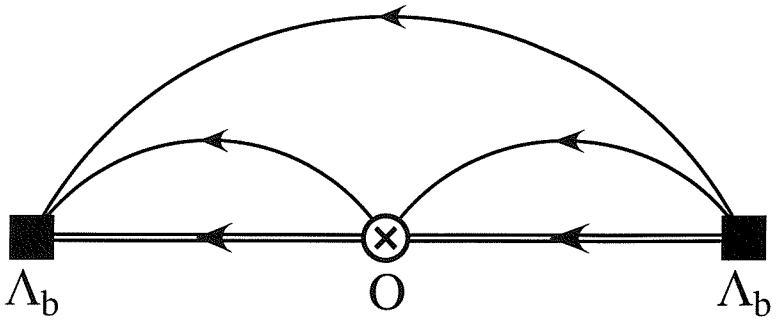

Figure 5.3: The baryon 3-pt function that is to be calculated. The double lines represent the b quarks and it is drawn straight to indicate that it is static, *i.e.* it propagates only in time.

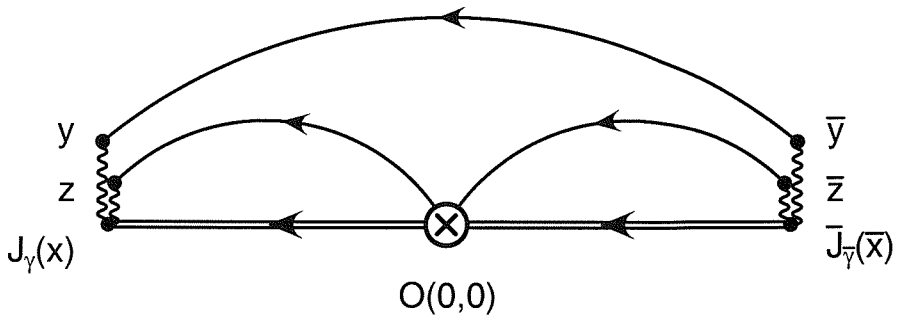

Figure 5.4: The 3-pt function with smearing. The wiggly lines represent the smearing functions and are drawn vertical to emphasise that the smearing is only along spatial directions, as opposed to the static quark that propagates only in the time direction, hence drawn horizontal.

Now, we may focus on the heavy quark. It should be noted here that the b-quark is too heavy ($\geq 1/a$) to simulate on a typical lattice, and therefore is defined in leading order in the Heavy Quark Effective Theory as a static quark with the Eichten-Hill action [130]. This is denoted by the horizontal double lines in fig. 5.4. On the lattice, the discrete version can be expressed as

$$\begin{aligned} S^{ab}_{\alpha\beta}(x,y,[U]) &= \left(\frac{1+\gamma_0}{2}\right)_{\alpha\beta}\left[U_0^\dagger(x-a\hat{0})...U_0^\dagger(y)\right]\theta(t_x-t_y)\delta_{\mathbf{x},\mathbf{y}} \\ &+\left(\frac{1-\gamma_0}{2}\right)_{\alpha\beta}\left[U_0(x)...U_0(y-a\hat{0})\right]\theta(t_y-t_x)\delta_{\mathbf{x},\mathbf{y}}. \end{aligned} \tag{5.11}$$

Here we have both forward propagating quark and backward propagating anti-quark. The Dirac structure is such that, in practice it is efficient to initially use just the colour matrix formed by the product of links and then pick out by hand the only Dirac components that survive. Correlators with static quarks are on the one hand computationally much less expensive to compute, but notorious for their noise. The following sections describe how different approaches have fared in our attempts of calculating our required baryonic correlation functions with a static quark.

5.3 Approach I: Using an extended propagator

As opposed to stochastic all-to-all propagators, one of the main restrictions with ordinary propagators generated by a inversion is that these have one end fixed at the origin. This does not allow us to use the light propagator from $\bar{y}$ to y in a simple way. One approach is to build an extended or generalised propagator as shown in fig. (5.5) which then has one end at the origin.

Now, for our correlation function let us first introduce the following interpolation operators

$$\begin{aligned} J_\gamma(x) &= -\varepsilon_{abc}(\gamma_5 C)_{\beta\alpha}\sum_{\mathbf{y},\mathbf{z}} b^c_\gamma(\mathbf{x},t)g(\mathbf{x},\mathbf{z})_{bb'}d^{b'}_\beta(\mathbf{z},t)h(\mathbf{x},\mathbf{y})_{aa'}u^{a'}_\alpha(\mathbf{y},t) \\ \bar{J}_{\bar{\gamma}}(\bar{x}) &= \epsilon_{\bar{a}\bar{b}\bar{c}}(\gamma_5 C)_{\bar{\alpha}\bar{\beta}}\sum_{\bar{\mathbf{y}},\bar{\mathbf{z}}} h^*(\bar{\mathbf{x}},\bar{\mathbf{y}})_{\bar{a}\bar{a}'}\bar{u}^{\bar{a}'}_{\bar{\alpha}}(\bar{\mathbf{y}},t)\, g^*(\bar{\mathbf{x}},\bar{\mathbf{z}})_{\bar{b}\bar{b}'}\bar{d}^{\bar{b}'}_{\bar{\beta}}(\bar{\mathbf{z}},t)\,\bar{b}^{\bar{c}}_{\bar{\gamma}}(\bar{\mathbf{x}},t), \end{aligned} \tag{5.12}$$

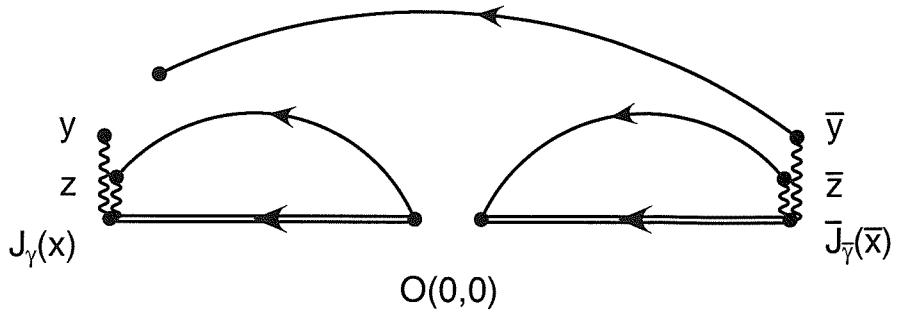

Figure 5.5: The extended propagator is the separated object on the right.

which can destroy or create the Λ_b baryon. Here, g and h are smearing functions and a sum over colour indices is understood. Moreover, the four-fermion operators we are interested in are of the form

$$\mathcal{O}(x) = \left(\bar{b}^d_\delta \, \Gamma^{de}_{\delta\varepsilon} \, d^e_\varepsilon\right) \left(\bar{d}^f_\eta \, \widetilde{\Gamma}^{fg}_{\eta\zeta} \, b^g_\zeta\right). \tag{5.13}$$

Substituting these into our correlator

$$C_3(\mathcal{O}, t, \bar{t})_{\gamma\bar{\gamma}} = \sum_{\mathbf{x},\bar{\mathbf{x}}} \langle 0 | J_\gamma(\mathbf{x}, t) \mathcal{O}(0) \bar{J}_{\bar{\gamma}}(\bar{\mathbf{x}}, \bar{t}) | 0 \rangle \qquad \text{with } t > 0 > \bar{t} \tag{5.14}$$

we get

$$\begin{aligned} C_3(\mathcal{O}, t, \bar{t})_{\gamma\bar{\gamma}} \;=\; & -\varepsilon_{abc}\varepsilon_{\bar{a}\bar{b}\bar{c}} (\gamma_5 C)_{\beta\alpha} (\gamma_5 C)_{\bar{\alpha}\bar{\beta}} \Gamma^{de}_{\delta\varepsilon} \widetilde{\Gamma}^{fg}_{\eta\zeta} \\ & \sum_{\substack{\mathbf{x},\mathbf{y},\mathbf{z} \\ \bar{\mathbf{x}},\bar{\mathbf{y}},\bar{\mathbf{z}}}} g(\mathbf{x}, \mathbf{z})_{bb'} h(\mathbf{x}, \mathbf{y})_{aa'} h^*(\bar{\mathbf{x}}, \bar{\mathbf{y}})_{\bar{a}\bar{a}'} g^*(\bar{\mathbf{x}}, \bar{\mathbf{z}})_{\bar{b}\bar{b}'} \\ & \langle 0 | b^c_\gamma(x) d^{b'}_\beta(z) u^{a'}_\alpha(y) \bar{b}^d_\delta(0) d^e_\varepsilon(0) \bar{d}^f_\eta(0) b^g_\zeta(0) \bar{u}^{\bar{a}'}_{\bar{\alpha}}(\bar{y}) \bar{d}^{\bar{b}'}_{\bar{\beta}}(\bar{z}) \bar{b}^{\bar{c}}_{\bar{\gamma}}(\bar{x}) | 0 \rangle. \end{aligned}$$

And after the contractions, this can be expressed in terms of propagators as

$$\begin{aligned} C_3(\mathcal{O}, t, \bar{t})_{\gamma\bar{\gamma}} \;=\; & \varepsilon_{abc}\varepsilon_{\bar{a}\bar{b}\bar{c}} (\gamma_5 C)_{\beta\alpha} (\gamma_5 C)_{\bar{\alpha}\bar{\beta}} \Gamma^{de}_{\delta\varepsilon} \widetilde{\Gamma}^{fg}_{\eta\zeta} \qquad (5.15) \\ & \sum_{\substack{\mathbf{x},\mathbf{y},\mathbf{z} \\ \bar{\mathbf{x}},\bar{\mathbf{y}},\bar{\mathbf{z}}}} g(\mathbf{x}, \mathbf{z})_{bb'} h(\mathbf{x}, \mathbf{y})_{aa'} h^*(\bar{\mathbf{x}}, \bar{\mathbf{y}})_{\bar{a}\bar{a}'} g^*(\bar{\mathbf{x}}, \bar{\mathbf{z}})_{\bar{b}\bar{b}'} \\ & S_b(x, 0)^{cd}_{\gamma\delta} S_b(0, \bar{x})^{g\bar{c}}_{\zeta\bar{\gamma}} S_u(y, \bar{y})^{a'\bar{a}'}_{\alpha\bar{\alpha}} S_d(0, \bar{z})^{e\bar{b}'}_{\varepsilon\bar{\beta}} S_d(z, 0)^{b'f}_{\beta\eta}. \qquad (5.16) \end{aligned}$$

This may be written in a more compact form by defining the smeared propagators

$$\begin{aligned} S_d^g(x,0)^{bf}_{\beta\eta} &\equiv \sum_z g(\mathbf{x},\mathbf{z})_{bb'} S_d(z,0)^{b'f}_{\beta\eta} \\ S_d^{g\dagger}(0,\bar{x})^{e\bar{b}}_{\varepsilon\bar{\beta}} &\equiv \sum_{\bar{z}} S_d(0,\bar{z})^{e\bar{b}'}_{\varepsilon\bar{\beta}} g^*(\bar{\mathbf{x}},\bar{\mathbf{z}})_{\bar{b}\bar{b}'}, \end{aligned}$$

leading to

$$\begin{aligned} C_3(\mathcal{O},t,\bar{t})_{\gamma\bar{\gamma}} &= \varepsilon_{abc}\varepsilon_{\bar{a}\bar{b}\bar{c}}(\gamma_5 C)_{\beta\alpha}(\gamma_5 C)_{\bar{\alpha}\bar{\beta}}\Gamma^{de}_{\delta\varepsilon}\widetilde{\Gamma}^{fg}_{\eta\zeta}\sum_{\bar{\mathbf{x}},\bar{\mathbf{y}}}^{\mathbf{x},\mathbf{y}} h(\mathbf{x},\mathbf{y})_{aa'}h^*(\bar{\mathbf{x}},\bar{\mathbf{y}})_{\bar{a}\bar{a}'} \\ &\quad S_b(x,0)^{cd}_{\gamma\delta}S_b(0,\bar{x})^{g\bar{c}}_{\zeta\bar{\gamma}}S_d^g(x,0)^{bf}_{\beta\eta}S_d^{g\dagger}(0,\bar{x})^{e\bar{b}}_{\varepsilon\bar{\beta}}S_u(y,\bar{y})^{a'\bar{a}'}_{\alpha\bar{\alpha}}. \end{aligned}$$

We may now identify the extended propagator

$$E_{\bar{\gamma}}(\mathbf{y},t;\bar{t})^{a'eg}_{\alpha\varepsilon\zeta} \equiv \sum_{\bar{\mathbf{x}},\bar{\mathbf{y}}} S_u(y,\bar{y})^{a'\bar{a}'}_{\alpha\bar{\alpha}}h^*(\bar{\mathbf{x}},\bar{\mathbf{w}})_{\bar{a}\bar{a}'}\varepsilon_{\bar{a}\bar{b}\bar{c}}S_b(0,\bar{x})^{g\bar{c}}_{\zeta\bar{\gamma}}S_d^{g\dagger}(0,\bar{x})^{e\bar{b}}_{\varepsilon\bar{\beta}}(\gamma_5 C)_{\bar{\alpha}\bar{\beta}}$$

which solves

$$\sum_y M(v,y)^{ha'}_{\xi\alpha}\,E_{\bar{\gamma}}(\mathbf{y},t;\bar{t})^{a'eg}_{\alpha\varepsilon\zeta} = \sum_{\bar{\mathbf{x}},\bar{\mathbf{y}}} h^*(\bar{\mathbf{x}},\mathbf{v})_{\bar{a}h}\varepsilon_{\bar{a}\bar{b}\bar{c}}S_b(0,\bar{x})^{g\bar{c}}_{\zeta\bar{\gamma}}S_d^{g\dagger}(0,\bar{x})^{e\bar{b}}_{\varepsilon\bar{\beta}}(\gamma_5 C)_{\xi\bar{\beta}}\,\delta(t_v-\bar{t}).$$

So, finally we have

$$\begin{aligned} C_3(\mathcal{O},t,\bar{t})_{\gamma\bar{\gamma}} &= \sum_{\bar{\mathbf{x}},\bar{\mathbf{y}}}\varepsilon_{abc}(\gamma_5 C)_{\beta\alpha}h(\mathbf{x},\mathbf{y})_{aa'}\Gamma^{de}_{\delta\varepsilon}\widetilde{\Gamma}^{fg}_{\eta\zeta}S_b(x,0)^{cd}_{\gamma\delta}S_d^g(x,0)^{bf}_{\beta\eta}E_{\bar{\gamma}}(\mathbf{y},t;\bar{t})^{a'eg}_{\alpha\varepsilon\zeta} \\ &= \sum_{\bar{\mathbf{x}},\bar{\mathbf{y}}} h(\mathbf{x},\mathbf{y})_{aa'}\left(S_b^f(x,0)\Gamma\right)^{ce}_{\gamma\varepsilon}\left(S_d^g(x,0)\widetilde{\Gamma}\right)^{bg}_{\beta\zeta}\varepsilon_{abc}(\gamma_5 C)_{\beta\alpha}E_{\bar{\gamma}}(\mathbf{y},t;\bar{t})^{a'eg}_{\alpha\varepsilon\zeta}. \end{aligned}$$

Now with the extended propagator $E_{\bar{\gamma}}(\mathbf{y},t;\bar{t})^{a'eg}_{\alpha\varepsilon\zeta}$, the baryon 3-pt correlation function is written just in terms of propagators coming out from the origin. Once the static quark is used the calculation of $E_{\bar{\gamma}}(\mathbf{y},t;\bar{t})$ requires the equivalent of three extra inversions and takes three times the memory to store compared to an ordinary propagator.

5.3.1 Smearing study

As just stated, the first approach was to calculate the extended propagator. In this approach, to extract a signal, the idea was to use smearing as extensively as

possible. Since we have a local four-quark operator fixed at the origin, the best that is possible, is to smear the light propagators at the baryon sources.

Initially a smearing study was undertaken mainly on hl meson and hll baryon 2-pt functions. Though for the actual calculation the static could not be smeared, but for the smearing study we did explore that option as well. Boyle smearing [131] was used and typically we had 30 quenched configurations at volume 48×24^3 and $\beta = 6.2$ and the light propagator at $\kappa = 0.1346$. First we tried the combinations:

- source smeared, sink local
- sink smeared, source local
- source and sink both smeared

It may be mentioned here that when a propagator is inverted, for the local case, one uses a delta function source. For source smearing, instead of the delta function, one has the smearing function. Whereas, for sink smearing, a local inversion is performed and then the smearing function is appended by hand to the sink.

One subsidiary, but sometimes practically important, consequence of this is that, if only sink smeared propagators are needed, one needs to generate and save only one set of (local) propagators and the sink smearing can be added while building the correlation functions. On the other hand if one needs source smeared and local propagators, two sets of inversions are required and this has ramifications on the computation time and storage requirements.

It was observed that source smearing, is more effective than sink smearing, however, the signal is most improved when both ends are smeared. Though, it was known that we can only smear at one end, for the smearing study, to enhance the visibility of the effect, we used smearing at both ends. Next, we tried to optimise the smearing radius, r. We looked at the cases:

- $r = 1.0$

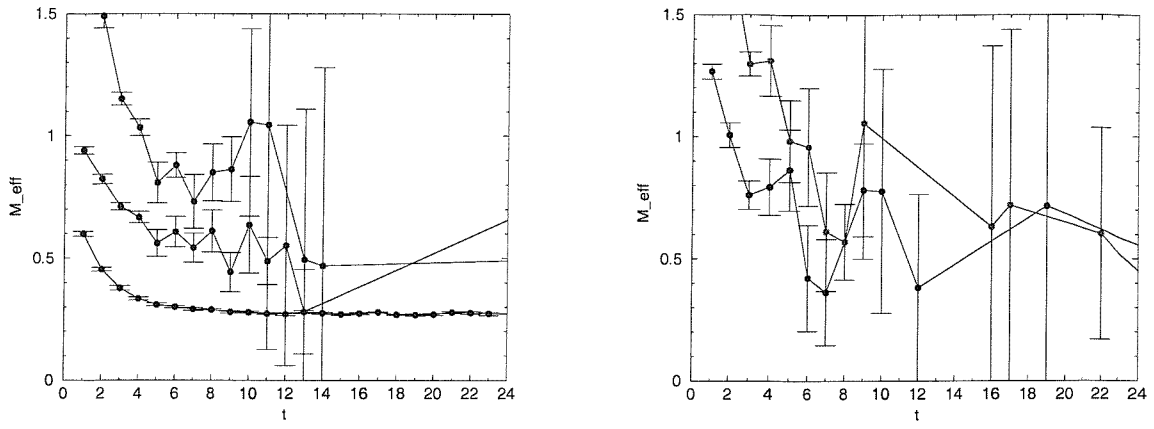

Figure 5.6: 30 configurations with (a) both static and light smeared at both ends [figure on left] and (b) a local static and light smeared at both ends [figure on right]. The correlators are for (from the top) a *hll* baryon and a *hl* meson, with a *ll* meson included in one case for reference. The signal is evidently much better when the static quark is smeared as well.

- $r = 2.0$
- $r = 3.0$

$r = 1.0$ was worst, with $r = 2.0$ looking marginally better than $r = 3.0$. However, while there was a definite difference between smearing and not smearing, there did not seem to be too much sensitivity to the smearing radius. So, there did not seem to be much point in tuning it further and $r = 2.0$ was chosen for the remaining work. Next we tried

- light smeared, static local
- static smeared, light local
- light and static both smeared

When everything is smeared we can just about see a signal for a few timeslices. But, when we remove the smearing on the static the signal gets significantly weaker

[Fig. 5.6]. As mentioned before, this was in a sense of academic interest only, as we cannot smear the static while the other end is pinned down to the origin.

In summary, though we were able to see Λ_b-baryon signal, the case in which the signal was more or less satisfactory was when both the static and the light quarks were smeared at both ends. This could have been alright if we were calculating baryon masses, but for the additional constraints in a matrix element 3-pt calculation, there seemed to be little hope to see a signal.

5.3.2 Conclusion for this approach

It was eventually concluded that to complete this calculation in this method requires a few thousand gauge configurations if not more. Since there are four propagator inversions to be performed for each configuration, this makes it a mammoth calculation, beyond our scope. Therefore, this approach does not seem to be feasible. However, if one intends to undertake such a calculation in the future with greater computational power at hand, the information extracted above, may be helpful.

5.4 Approach II: Using static with alternative discretisation

The second approach concerns with a recent development reported by the ALPHA collaboration [132, 133]. They have observed that the signal can be significantly enhanced if the usual Eichten-Hill discretisation of the static action

$$S_h^{\mathrm{EH}} = a^4 \sum_x \bar{\psi}_h(x) D_0 \psi_h(x)\,, \tag{5.17}$$

$$D_0\psi_h(x) = \frac{1}{a}\left[\psi_h(x) - U^\dagger(x - a\hat{0}, 0)\psi_h(x - a\hat{0})\right], \tag{5.18}$$

is replaced, preserving some of the desired symmetries, by discretisations of the form

$$D_0\psi_h(x) = \frac{1}{a}\left[\psi_h(x) - W^\dagger(x - a\hat{0}, 0)\,\psi_h(x - a\hat{0})\right], \tag{5.19}$$

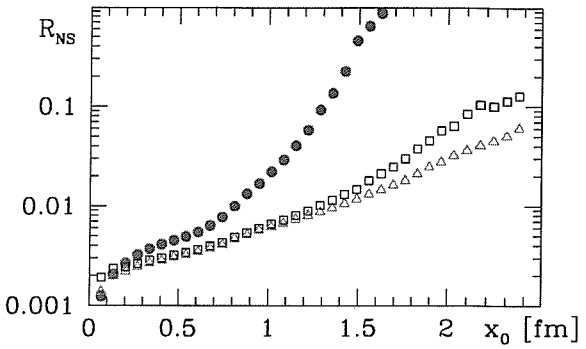

Figure 5.7: Improvment in the signal-to-noise ratio using alternative discretisations of the static action [Figure from [132]]. The filled circles are the usual EH [eq. 5.18], open squares are for APE type [eq. 5.21], while the open triangles are for HYP type statics [eq. 5.22]

where $W(x,0)$ is a generalised gauge parallel transporter with the gauge transformation properties of $U(x,0)$. $W(x,0)$ is a function of the link variables in the neighborhood of x invariant under spatial cubic rotations and with the correct classical continuum limit. W can then be taken of the forms:

$$W_{\rm S}(x,0) = V(x,0)\left[\frac{g_0^2}{5} + \left(\frac{1}{3}{\rm tr}V^\dagger(x,0)V(x,0)\right)^{1/2}\right]^{-1}, \tag{5.20}$$

$$W_{\rm APE}(x,0) = V(x,0), \tag{5.21}$$

$$W_{\rm HYP}(x,0) = V_{\rm HYP}(x,0), \tag{5.22}$$

where

$$V(x,0) = \frac{1}{6}\sum_{j=1}^{3} \; [\; U(x,j)U(x+a\hat{j},0)U^\dagger(x+a\hat{0},j) \tag{5.23}$$

$$+U^\dagger(x-a\hat{j},j)U(x-a\hat{j},0)U(x+a\hat{0}-a\hat{j},j)\;] \tag{5.24}$$

Here the so-called HYP-link, $V_{\rm HYP}(x,0)$, described further in appendix C is a function of the gauge links located within a hypercube [134, 135]. In the latter case they recommend the parameter values $\alpha_1 = 0.75$, $\alpha_2 = 0.6$, $\alpha_3 = 0.3$ [134] [See appendix C]. It may be noted that, albeit in a different context, a covariant derivative of the general type used above was first introduced in [136]. These effectively fatten the link and is similar to the fuzzing done on the gauge links in Boyle smearing. Fig. 5.7

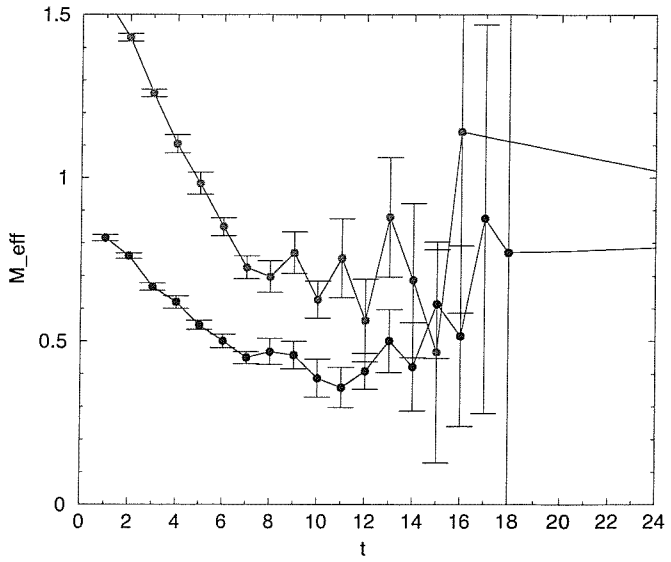

Figure 5.8: 100 configurations with APE-type fat static (light smeared at one end) shows a much better signal for hl-meson (lower set) and hll-baryon (upper set) correlators in comparison with those in fig. (5.6).

from the ALPHA studies shows how the noise to signal ratio stays low for longer in this improved discretisation.

We have tried the APE and HYP [eqs. (5.21, 5.22)] type fattening and indeed do observe a significant improvement of signal. It may be noted here, that this was also the first time that this procedure is used for baryonic correlators. However, for our purpose the APE and HYP types give similar signals. Perhaps, this is due to the fact that the difference between the two surfaces only at large times.

In fig. 5.8, we have the APE-type fat static and the light quark smeared at the sink, which is the maximum we can do for the Λ_b lifetime calculation. Here, though there is some fluctuation around the plateau, it seems there really is a signal.

We did explore a calculation of the matrix element in this approach. Though the situation is much better, the signal still gets drowned in noise for up to 100 configurations. Here, the feeling is that maybe with several hundreds of configurations, rather than thousands, it will be possible to see something.

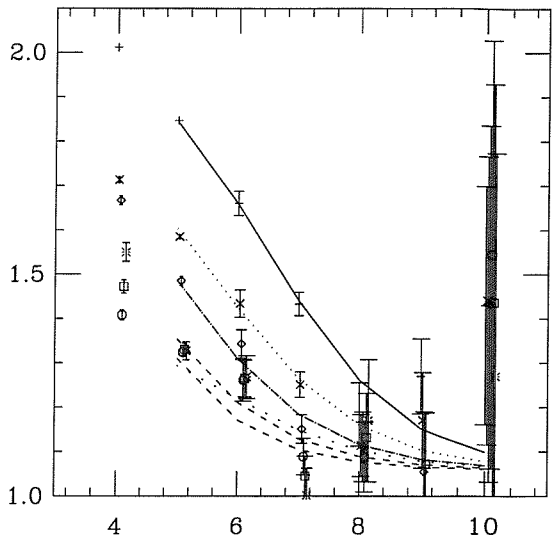

Figure 5.9: Static baryon 2-pt function signal from only one gauge configuration using maximal variance reduced all-to-all propagators [Courtesy: C. Michael]

5.5 Approach III: Using all-to-all propagators

This brings us to our final approach of using stochastically generated all-to-all propagators. Due to the stochastic nature, these have more intrinsic noise, but since it is now possible to average over all spatial sites, that is a huge gain in statistics that more than compensates for the stochastic nature. Furthermore, by using maximal variance reduced all-to-all propagators [137] there is a further significant gain in signal. So much so, that it is possible to extract a baryon 2-pt signal from only one configuration [fig. (5.9)].

In this formalism, rather than generating the full propagator matrices it is far more efficient to generate the pseudo-fermion fields that can be tied up directly in the correlator code. Moreover, initially due to the requirement of a significant number of gauge configurations the calculation was intended to be done in the quenched approximation. This is due to the fact that, at least when this calculation was planned, it was difficult/expensive to obtain/generate dynamical configuration in

sufficient number at suitable volumes. However, when using all-to-all propagators one gains a huge amount of statistics by allowing the operator to move over the spatial sites and averaging. Not only that, one may even rotate the gauge fields by a few time slices and gain further statistics. This makes it possible to extract an otherwise impossible amount of information from even a single gauge configuration. It may even be possible to do the calculation well with less than 100 configuration. This makes the prospect of using dynamical configurations much more feasible.

Again, for the generation of dynamical configurations itself, there is a practical new idea that can speed up the equilibration a great deal. That is to equilibrate on a smaller volume and then replicate it to get a bigger volume and then proceed some more steps [108]. This should make dynamical configurations more easily available at a suitable volume.

5.6 Outlook

The extended propagator approach to calculating the lifetime appears to be inefficient and not feasible. However, it appears that there seems to be reasonably good promise in going through this calculation using these maximal variance reduced all-to-all propagators. An addition of the new fat static propagators should improve the signal further. And to try both of these together is the plan for the future of this project. With a few other practical new ideas it may even be possible to do this calculation on dynamical configurations.

Chapter 6

Conclusions

Conclusions for the three studies have been given at the end of the relevant chapters. But, to summarise our results:

In the doublecharm baryon study the expected states, both double- and single-charm were identified with masses consistent with the experimental values where available. Spin-splittings were also observed without any noticeable suppression, leading to a confirmation of the idea that the suppression observed in some early works were due to discretisation errors. Further predictions are provided and hopefully now that the first states are experimentally identified there will be further experimental verification of the lattice predictions. Overall there seems to be some interesting phenomelogy ahead of us in double charm physics.

In the B_K study, looking at the sea quark mass dependence, it appears that there is growing evidence of a significant effect of sea quarks on the value of B_K. Moreover the unquenched value seems to be lower than the quenched one. There are concerns about lattice artefacts, but taken together with an aggregate account of previous works, it seems all the more plausible that unquenching, at least for $N_f = 2$, will lower the value of B_K.

In the last project related to the Λ_b-lifetime, it seems quite evident that the extended propagator approach is not efficient. However, there seems to be considerable promise in completing the calculation with maximal variance reduced all-to-all propagators. The novel techniques of using static propagators *fattened* by APE or

HYP type smearing should also augment the improvement in the signal. With a few other developments, it may also be possible to do this calculation on dynamical, rather than quenched, configurations. Overall there seem to be exciting days ahead for more involved calculations like this one using static quarks.

It is probably also worth mentioning that the code FermiQCD was found to be extremely useful and user-friendly, allowing us to concentrate on the physics and write our codes almost directly off our notebooks in a very transparent way. The University of Southampton cluster Iridis also seemed reasonably adequate for lattice calculations of this level. Though, there is no doubt that gigantic purpose-built machines are still needed for precision lattice QCD, the wider availability of these general-purpose clusters are indeed making lattice calculations much more accessible.

To conclude, some useful results have been obtained in these studies in lattice phenomenology and hopefully more rigorous calculations and experimental evidence will take these further in our understanding of non-perturbative QCD.

Appendix A

Spin algebra for the baryon states

For the spin $\frac{1}{2}$ state we have

$$C(t)_{\gamma\bar{\gamma}} = \sum_{\mathbf{x}} \langle 0|J_\gamma(\mathbf{x},t)\bar{J}_{\bar{\gamma}}(0)|0\rangle \tag{A.1}$$

$$\begin{aligned} J_\gamma(x) &= -\varepsilon_{abc}(\gamma_5 C)_{\beta\alpha} q^c_\gamma(\mathbf{x},t) Q^b_\beta(\mathbf{x},t) Q^a_\alpha(\mathbf{x},t) \\ (\bar{J})_{\bar{\gamma}}(\bar{x}) &= \varepsilon_{\bar{a}\bar{b}\bar{c}}(\gamma_5 C)_{\bar{\alpha}\bar{\beta}} \bar{Q}^{\bar{a}}_{\bar{\alpha}}(\bar{\mathbf{x}},t)\, \bar{Q}^{\bar{b}}_{\bar{\beta}}(\bar{\mathbf{x}},t)\, \bar{q}^{\bar{c}}_{\bar{\gamma}}(\bar{\mathbf{x}},t) \end{aligned} \tag{A.2}$$

C is the charge conjugation operator $\gamma_0\gamma_2$

$$\begin{aligned} C_2(t)_{\gamma\bar{\gamma}} &= -\varepsilon_{abc}\varepsilon_{\bar{a}\bar{b}\bar{c}}(\gamma_5 C)_{\beta\alpha}(\gamma_5 C)_{\bar{\alpha}\bar{\beta}} \sum_{\mathbf{x}} S_q(x,0)^{c\bar{c}}_{\alpha\bar{\alpha}} \\ &\quad \times \left(S_Q(x,0)^{b\bar{b}}_{\beta\bar{\beta}}\, S_Q(x,0)^{a\bar{a}}_{\gamma\bar{\gamma}} - S_Q(x,0)^{b\bar{a}}_{\beta\bar{\gamma}}\, S_Q(x,0)^{a\bar{b}}_{\gamma\bar{\beta}} \right) \end{aligned} \tag{A.3}$$

For the spin $\frac{3}{2}$ states

$$\begin{aligned} J_\gamma(x) &= -\varepsilon_{abc}(\gamma_i C)_{\beta\alpha} q^c_\gamma(\mathbf{x},t) Q^b_\beta(\mathbf{x},t) Q^a_\alpha(\mathbf{x},t) \\ (\bar{J})_{\bar{\gamma}}(\bar{x}) &= \varepsilon_{\bar{a}\bar{b}\bar{c}}(\gamma_j C)_{\bar{\alpha}\bar{\beta}} \bar{Q}^{\bar{a}}_{\bar{\alpha}}(\bar{\mathbf{x}},t)\, \bar{Q}^{\bar{b}}_{\bar{\beta}}(\bar{\mathbf{x}},t)\, \bar{q}^{\bar{c}}_{\bar{\gamma}}(\bar{\mathbf{x}},t) \end{aligned} \tag{A.4}$$

$$\begin{aligned} C_2(t)^{ij}_{\gamma\bar{\gamma}} &= -\varepsilon_{abc}\varepsilon_{\bar{a}\bar{b}\bar{c}}(\gamma_i C)_{\beta\alpha}(\gamma_j C)_{\bar{\alpha}\bar{\beta}} \sum_{\mathbf{x}} S_q(x,0)^{c\bar{c}}_{\alpha\bar{\alpha}} \\ &\quad \times \left(S_Q(x,0)^{b\bar{b}}_{\beta\bar{\beta}}\, S_Q(x,0)^{a\bar{a}}_{\gamma\bar{\gamma}} - S_Q(x,0)^{b\bar{a}}_{\beta\bar{\gamma}}\, S_Q(x,0)^{a\bar{b}}_{\gamma\bar{\beta}} \right) \end{aligned} \tag{A.5}$$

A.1 Symmetry for spin 1/2 baryons

Let us define the projectors

$$\begin{aligned} P_- &= \frac{1+\gamma_0}{2} \\ P_+ &= \frac{1-\gamma_0}{2} \\ P^{ij}_{3/2} &= g^{ij} - \frac{1}{3}\gamma^i\,\gamma^j \\ P^{ij}_{1/2} &= \frac{1}{3}\gamma^i\,\gamma^j \end{aligned} \tag{A.6}$$

At large time

$$\begin{aligned} C_2(t)_{\gamma\bar{\gamma}} &= \sum_{\mathbf{x}} \langle 0|J_\gamma(\mathbf{x},t)\bar{J}_{\bar{\gamma}}(0)|0\rangle \overset{t\gg 0}{\longrightarrow} \\ & Z^2\,(P_-)_{\gamma\bar{\gamma}}\,e^{-mt} + Z^2\,(P_+)_{\gamma\bar{\gamma}}\,e^{-mt}. \end{aligned} \tag{A.7}$$

we can exploit the following relation

$$C_2(t)_{00} = C_2(t)_{11} \quad , \quad C_2(t)_{22} = C_2(t)_{33} = 0 \tag{A.8}$$

for positive-parity states and

$$C_2(t)_{00} = C_2(t)_{11} = 0 \quad , \quad C_2(t)_{22} = C_2(t)_{33} \tag{A.9}$$

for negative-parity states.

A.2 Symmetries for spin 3/2 baryons

In the region $0 \ll t \ll T$ the correlation $C_2(t)^{ij}_{\gamma\bar{\gamma}}$

$$\begin{aligned} C_2(t)^{ij}_{\gamma\bar{\gamma}} &= \sum_{\mathbf{x}} \langle 0|J^i_\gamma(\mathbf{x},t)\bar{J}^j_{\bar{\gamma}}(0)|0\rangle \overset{t\gg 0}{\longrightarrow} \\ & Z^{3/2}\left(P_+\,P^{ij}_{3/2}\right)_{\gamma\bar{\gamma}} e^{-m_{3/2}t} + Z^{1/2}\left(P_+\,P^{ij}_{1/2}\right)_{\gamma\bar{\gamma}} e^{-m_{1/2}t} \\ & + Z_p^{3/2}\left(P_-\,P^{ij}_{3/2}\right)_{\gamma\bar{\gamma}} e^{-m^p_{3/2}t} + Z_p^{1/2}\left(P_-\,P^{ij}_{1/2}\right)_{\gamma\bar{\gamma}} e^{-m^p_{1/2}t} \end{aligned} \tag{A.10}$$

For spin $1/2^-$ and $3/2^+$ contributions we have the following relations

$$\begin{aligned} C_{01}^{13} &= \frac{1}{4}\left(C_{01}^{13} - C_{10}^{13} - C_{01}^{31} + C_{10}^{31}\right) \\ C_{11}^{12} &= \frac{1}{8}\left(-C_{00}^{12} + C_{11}^{12} + C_{00}^{21} - C_{11}^{21} - C_{01}^{23} - C_{10}^{23} + C_{01}^{32} + C_{10}^{32}\right) \\ C_{00}^{11} &= \frac{1}{6}\left(C_{00}^{11} + C_{11}^{11} + C_{00}^{22} + C_{11}^{22} + C_{00}^{33} + C_{11}^{33}\right) \end{aligned} \tag{A.11}$$

For spin $1/2^+$ and $3/2^-$ contributions we have the following relations

$$\begin{aligned} C_{23}^{13} &= \frac{1}{4}\left(C_{23}^{13} - C_{32}^{13} - C_{23}^{31} + C_{32}^{31}\right) \\ C_{33}^{12} &= \frac{1}{8}\left(-C_{22}^{12} + C_{33}^{12} + C_{22}^{21} - C_{33}^{21} - C_{23}^{23} - C_{32}^{23} + C_{23}^{32} + C_{32}^{32}\right) \\ C_{22}^{11} &= \frac{1}{6}\left(C_{22}^{11} + C_{33}^{11} + C_{22}^{22} + C_{33}^{22} + C_{22}^{33} + C_{33}^{33}\right) \end{aligned} \tag{A.12}$$

Moreover

$$\begin{aligned} C_{01}^{13} &= \frac{1}{3}\left(Z^{1/2}\, e^{-m_{1/2}\, t} - Z^{3/2}\, e^{-m_{3/2}\, t}\right) \\ C_{11}^{12} &= \frac{i}{3}\left(Z^{1/2}\, e^{-m_{1/2}\, t} - Z^{3/2}\, e^{-m_{3/2}\, t}\right) \\ C_{00}^{11} &= -\frac{1}{3}\left(Z^{1/2}\, e^{-m_{1/2}\, t} + 2\, Z^{3/2}\, e^{-m_{3/2}\, t}\right) \end{aligned} \tag{A.13}$$

$$\begin{aligned} C_{23}^{13} &= \frac{1}{3}\left(Z_p^{1/2}\, e^{-m_{1/2}^p\, t} - Z_p^{3/2}\, e^{-m_{3/2}^p\, t}\right) \\ C_{33}^{12} &= \frac{i}{3}\left(Z_p^{1/2}\, e^{-m_{1/2}^p\, t} - Z_p^{3/2}\, e^{-m_{3/2}^p\, t}\right) \\ C_{22}^{11} &= -\frac{1}{3}\left(Z_p^{1/2}\, e^{-m_{1/2}^p\, t} + 2\, Z_p^{3/2}\, e^{-m_{3/2}^p\, t}\right) \end{aligned} \tag{A.14}$$

Finally spin $1/2$ and spin $3/2$ contributions can be isolated through the following combinations.

$$\begin{aligned} C_{00}^{11} + i\, C_{11}^{12} - C_{01}^{13} &= -e^{-m_{1/2}\, t}\, Z^{1/2} \\ C_{00}^{11} - \frac{1}{2}\left(i\, C_{11}^{12} - C_{01}^{13}\right) &= -e^{-m_{3/2}\, t}\, Z^{3/2} \\ C_{22}^{11} + i\, C_{33}^{12} - C_{23}^{13} &= -e^{-m_{1/2}\, t}\, Z^{1/2} \\ C_{22}^{11} - \frac{1}{2}\left(i\, C_{33}^{12} + C_{23}^{13}\right) &= -e^{-m_{3/2}\, t}\, Z^{3/2} \end{aligned} \tag{A.15}$$

Appendix B

Perturbative renormalisation coefficients for 4-quark operators relevant to B_K

We use the perturbative expressions of ref. [101], and combine them with the results of [102]. In the $\overline{\text{MS}}$ scheme they read:

$$Z(\mu, g_0^2) = 1 - \frac{g_0^2}{4\pi}(4\log(a\mu) + 50.839 - 9.33c_{SW} - 4.88c_{SW}^2) \ ,$$

$$Z(\mu, g_0^2) \cdot \Delta_i(g_0^2) = c_i \frac{g_0^2}{4\pi}(0.767 - 0.795c_{SW} + 0.272c_{SW}^2) \ , \tag{B.1}$$

where $c_2 = -11/12$, $c_3 = -1/6$, $c_4 = c_5 = 1/3$. Here the indices refer to operators in the basis of eq. (4.23). In the numerical computations, we use the boosted coupling, $g_0^2 \to g_0^2 = 6/(\beta\langle P\rangle)$

We can follow the standard pertubation theory, since in our case $\log(a\mu)$ is small. In this case, using $\mu = 2$ GeV, we can directly obtain the renormalisation constants for $\overline{\text{MS}}$ at $\mu = 2$ GeV. Using the one-loop perturbative value of $c_{SW} = 1$ and the average plaquette values of $\{0.533644, 0.539863, 0.542384\}$ in the boosted coupling we get the values in Table 4.3.

Moreover, Z_A is evaluated perturbatively from

$$Z_A(g_0^2) = 1 + \frac{g_0^2}{4\pi}(15.7963 - 0.2478c_{SW} - 2.2514c_{SW}^2). \tag{B.2}$$

Appendix C

Hypercubic blocking

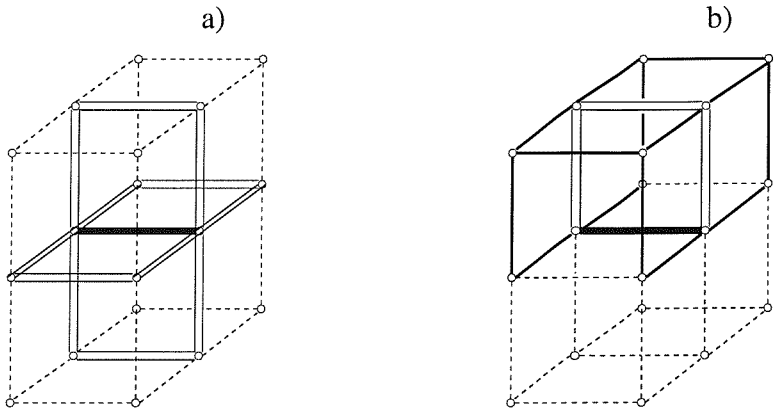

Figure C.1: Schematic representation of the hypercubic blocking in three dimensions. a) The fat link is built from the four double-lined staples. b) Each of the double-lined links is built from two staples which extend only in the hypercubes attached to the original link. An important point is that the links entering the staples are projected onto SU(3).

[Note: This appendix is taken from [134]]

The fat links of the hypercubic blocking (HYP) are constructed in three steps. At the final level the blocked link $V_{i,\mu}$ is constructed via projected APE blocking [138] from a set of decorated links $\tilde{V}_{i,\mu;\nu}$ as

$$V_{i,\mu} = Proj_{SU(3)}[(1-\alpha_1)U_{i,\mu} + \frac{\alpha_1}{6}\sum_{\pm\nu\neq\mu}\tilde{V}_{i,\nu;\mu}\tilde{V}_{i+\hat{\nu},\mu;\nu}\tilde{V}^{\dagger}_{i+\hat{\mu},\nu;\mu}], \qquad \text{(C.1)}$$

where $U_{i,\mu}$ is the original thin link and the index ν in $\tilde{V}_{i,\mu;\nu}$ indicates that the fat link at location i and direction μ is not decorated with staples extending in direction ν.

The decorated links $\tilde{V}_{i,\mu;\nu}$ are constructed with a modified projected APE blocking from an other set of decorated links, $\bar{V}_{i,\mu;\rho\,\nu}$ as

$$\tilde{V}_{i,\mu;\nu} = Proj_{SU(3)}[(1-\alpha_2)U_{i,\mu} + \frac{\alpha_2}{4}\sum_{\pm\rho\neq\nu,\mu} \bar{V}_{i,\rho;\nu\,\mu}\bar{V}_{i+\hat{\rho},\mu;\rho\,\nu}\bar{V}^{\dagger}_{i+\hat{\mu},\rho;\nu\,\mu}]\,, \qquad \text{(C.2)}$$

where the indices $\rho\,\nu$ indicate that the fat link $\bar{V}_{i,\mu;\rho\,\nu}$ in direction μ is not decorated with staples extending in the ρ or ν directions. The decorated links $\bar{V}_{i,\mu;\rho\,\nu}$ are constructed from the original thin links with a modified projected APE blocking step

$$\bar{V}_{i,\mu;\nu\,\rho} = Proj_{SU(3)}[(1-\alpha_3)U_{i,\mu} + \frac{\alpha_3}{2}\sum_{\pm\eta\neq\rho,\nu,\mu} U_{i,\eta}U_{i+\hat{\eta},\mu}U^{\dagger}_{i+\hat{\mu},\eta}]\,. \qquad \text{(C.3)}$$

Here only the two staples orthogonal to μ, ν and ρ are used. With the construction eqs. (C.1)-(C.3) the fat link $V_{i,\mu}$ mixes thin links only from hypercubes attached to the original link. The hypercubic blocking is schematically represented in figure C.1. The parameters α_1, α_2 and α_3 can be optimized to achieve the smoothest blocked link configuration. The construction eqs. (C.1)-(C.3) can be iterated.

Bibliography

[1] M. Creutz, *Quarks, Gluons and Lattices.* Cambridge Monographs on Mathematical Physics. Cambridge University Press, 1983.

[2] M. Creutz, ed., *Quantum Fields on a Computer*, vol. 11 of *Advanced Series on Directions in High Energy Physics.* World Scientific, 1992.

[3] I. Montvay and G. Münster, *Quantum fields on a lattice.* Cambridge Monographs on Mathematical Physics. Cambridge University Press, 1994.

[4] H. J. Rothe, *Lattice Gauge Theories: An Introduction*, vol. 43 of *World Scientific Lecture Notes in Physics.* World Scientific, 1997.

[5] J. Smit, *Introduction to Quantum Fields on a Lattice: A Robust Mate*, vol. 15 of *Cambridge Lecture Notes in Physics.* Cambridge University Press, 2002.

[6] K. G. Wilson, *Confinement of quarks, Phys. Rev.* **D10** (1974) 2445–2459.

[7] H. Hamber and G. Parisi, *Numerical estimates of hadronic masses in a pure SU(3) gauge theory, Phys. Rev. Lett.* **47** (1981) 1792.

[8] E. Marinari, G. Parisi, and C. Rebbi, *Computer estimates of meson masses in SU(2) lattice gauge theory, Phys. Rev. Lett.* **47** (1981) 1795.

[9] D. Weingarten, *Monte Carlo evaluation of hadron masses*, . In *Coral Gables 1982, Proceedings, Field Theory In Elementary Particles*, 393-406 and Indiana Univ. Bloomington - IUHET-69 (81,REC.OCT.) 17p.

[10] N. Metropolis, A. W. Rosenbluth, M. N. Rosenbluth, A. H. Teller, and E. Teller, *Equation of state calculations by fast computing machines, J. Chem. Phys.* **21** (1953) 1087–1092.

[11] N. Cabibbo and E. Marinari, *A new method for updating su(n) matrices in computer simulations of gauge theories, Phys. Lett.* **B119** (1982) 387–390.

[12] S. Eisenstat and others., *Variational iterative methods for nonsymmetric systems of linear equations, SIAM J. Numer. Anal.* **20** (1983) 345.

[13] H. van der Vorst, *BiCGStab: A fast and smoothly converging variant of Bi-CG for the solution of nonsymmetric linear systems*, *SIAM J. Sc. Stat. Comp.* **13** (1992) 631–644.

[14] A. Frommer, V. Hannemann, B. Nockel, T. Lippert, and K. Schilling, *Accelerating Wilson fermion matrix inversions by means of the stabilized biconjugate gradient algorithm*, *Int. J. Mod. Phys.* **C5** (1994) 1073–1088, [hep-lat/9404013].

[15] K. G. Wilson, *Quarks and strings on a lattice*, . New Phenomena In Subnuclear Physics. Part A. Proceedings of the First Half of the 1975 International School of Subnuclear Physics, Erice, Sicily, July 11 - August 1, 1975, ed. A. Zichichi, Plenum Press, New York, 1977, p. 69, CLNS-321.

[16] B. Sheikholeslami and R. Wohlert, *Improved continuum limit lattice action for QCD with Wilson fermions*, *Nucl. Phys.* **B259** (1985) 572.

[17] M. Lüscher and P. Weisz, *O(a) improvement of the axial current in lattice QCD to one-loop order of perturbation theory*, *Nucl. Phys.* **B479** (1996) 429–458, [hep-lat/9606016].

[18] M. Lüscher, S. Sint, R. Sommer, P. Weisz, and U. Wolff, *Non-perturbative O(a) improvement of lattice QCD*, *Nucl. Phys.* **B491** (1997) 323–343, [hep-lat/9609035].

[19] **ALPHA** Collaboration, K. Jansen and R. Sommer, *O(alpha) improvement of lattice QCD with two flavors of Wilson quarks*, *Nucl. Phys.* **B530** (1998) 185–203, [hep-lat/9803017].

[20] **CP-PACS and JLQCD** Collaboration, N. Yamada *et al.*, *Non-perturbative O(a)-improvement of Wilson quark action in three-flavor QCD with plaquette gauge action*, hep-lat/0406028.

[21] M. Quenouille, *Approximate tests of correlation in time series*, *J. Royal Stat. Soc.* **B11** (1949) 18–84.

[22] J. Tukey, *Bias and confidence in not quite large samples*, *Ann. Math. Stat.* **29** (1958) 614.

[23] B. Efron, *Bootstrap methods: another look at the jackknife*, *Ann. Stat.* **29** (1979) 1–26.

[24] K. Levenberg, *A method for the solution of certain problems in least squares*, *Quart. Appl. Math.* **2** (1944) 164–168.

[25] D. Marquardt, *An algorithm for least-squares estimation of nonlinear parameters*, *SIAM J. Appl. Math.* **11** (1963) 431–441.

[26] **SELEX** Collaboration, M. Mattson *et al.*, *First observation of the doubly charmed baryon* Ξ_{cc}^{+}, *Phys. Rev. Lett.* **89** (2002) 112001, [hep-ex/0208014].

[27] **Particle Data Group** Collaboration, S. Eidelman *et al.*, *Review of particle physics*, *Phys. Lett. B* **592** (2004) 1.

[28] J.-M. Richard, *Double charm physics*, hep-ph/0212224.

[29] **SELEX** Collaboration, M. A. Moinester *et al.*, *First observation of doubly charmed baryons*, hep-ex/0212029.

[30] J. Russ, "High mass states in SELEX: Have doubly-charmed baryons been discovered?." Talk at Fermilab - Joint Experimental and Theoretical Physics Seminar - May 31, 2002, http://www-selex.fnal.gov/documentation/selex_wac.pdf.

[31] P. Cooper, "Heavy baryons - recent and very new results." Talk at BEACH 2002, Vancouver - June 25, 2002, http://beach2002.physics.ubc.ca/talks/Peter_Cooper.pdf.

[32] J. Russ, "The double charmed baryon family in SELEX - an update." Talk at Fermilab - Joint Experimental and Theoretical Physics Seminar - June 13, 2003, http://www-selex.fnal.gov/documentation/fnal.pdf.

[33] M. Moinester, "New horizons for charm baryon spectroscopy." Talk at Heavy Quark Physics at the Upgraded HERA Collider, 2003, Rehovot - October 19-22, 2003, http://www-zeus.desy.de/conferences/03/2003_Israel_Moinester.pdf.

[34] **SELEX** Collaboration, A. Ocherashvili *et al.*, *Confirmation of the double charm baryon* $\Xi_{cc}^{+}(3520)$ *via its decay to* $pD^{+}K^{-}$, hep-ex/0406033.

[35] V. V. Kiselev, A. K. Likhoded, and A. I. Onishchenko, *Lifetimes of doubly charmed baryons:* Ξ_{cc}^{+} *and* $\Xi_{cc}^{+}+$, *Phys. Atom. Nucl.* **62** (1999) 1940–1949.

[36] V. V. Kiselev and A. K. Likhoded, *Comment on 'First observation of doubly charmed baryon* Ξ_{cc}^{+}*'*, hep-ph/0208231.

[37] A. De Rujula, H. Georgi, and S. L. Glashow, *Hadron masses in a gauge theory*, *Phys. Rev.* **D12** (1975) 147–162.

[38] S. Fleck and J. M. Richard, *Baryons with double charm*, *Prog. Theor. Phys.* **82** (1989) 760–774.

[39] M. J. Savage and M. B. Wise, *Spectrum of baryons with two heavy quarks*, *Phys. Lett.* **B248** (1990) 177–180.

[40] E. Bagan, H. G. Dosch, P. Gosdzinsky, S. Narison, and J. M. Richard, *Hadrons with charm and beauty*, *Z. Phys.* **C64** (1994) 57–72, [hep-ph/9403208].

[41] R. Roncaglia, D. B. Lichtenberg, and E. Predazzi, *Predicting the masses of baryons containing one or two heavy quarks*, *Phys. Rev.* **D52** (1995) 1722–1725, [hep-ph/9502251].

[42] S. S. Gershtein, V. V. Kiselev, A. K. Likhoded, and A. I. Onishchenko, *Spectroscopy of doubly charmed baryons: Ξ_{cc}^{+} and Ξ_{cc}^{++}*, *Mod. Phys. Lett.* **A14** (1999) 135–146, [hep-ph/9807375].

[43] S.-P. Tong *et al.*, *Spectra of baryons containing two heavy quarks in potential model*, *Phys. Rev.* **D62** (2000) 054024, [hep-ph/9910259].

[44] D. Ebert, R. N. Faustov, V. O. Galkin, and A. P. Martynenko, *Mass spectra of doubly heavy baryons in the relativistic quark model*, *Phys. Rev.* **D66** (2002) 014008, [hep-ph/0201217].

[45] V. V. Kiselev and A. E. Kovalsky, *Doubly heavy baryons $\Omega(QQ')$ vs. $\Xi(QQ')$ in sum rules of NRQCD*, *Phys. Rev.* **D64** (2001) 014002, [hep-ph/0005019].

[46] I. M. Narodetskii and M. A. Trusov, *The doubly heavy baryons*, *Nucl. Phys. Proc. Suppl.* **115** (2003) 20–23, [hep-ph/0209044].

[47] I. M. Narodetskii, A. N. Plekhanov, and A. I. Veselov, *Spectroscopy of baryons containing two heavy quarks in nonperturbative quark dynamics*, *JETP Lett.* **77** (2003) 58–62, [hep-ph/0212358].

[48] M. A. Shifman and M. B. Voloshin, *Preasymptotic effects in inclusive weak decays of charmed particles*, *Sov. J. Nucl. Phys.* **41** (1985) 120.

[49] M. A. Shifman and M. B. Voloshin, *Hierarchy of lifetimes of charmed and beautiful hadrons*, *Sov. Phys. JETP* **64** (1986) 698.

[50] B. Guberina, B. Melic, and H. Stefancic, *Inclusive decays and lifetimes of doubly charmed baryons*, *Eur. Phys. J.* **C9** (1999) 213–219, [hep-ph/9901323]. Erratum: Eur. Phys. J. C13 (2001) 551.

[51] R. Lewis, N. Mathur, and R. M. Woloshyn, *Charmed baryons in lattice QCD*, *Phys. Rev.* **D64** (2001) 094509, [hep-ph/0107037].

[52] N. Mathur, R. Lewis, and R. M. Woloshyn, *Charmed and bottom baryons from lattice NRQCD*, *Phys. Rev.* **D66** (2002) 014502, [hep-ph/0203253].

[53] A. Ali Khan *et al.*, *Heavy-light mesons and baryons with b quarks*, *Phys. Rev.* **D62** (2000) 054505, [hep-lat/9912034].

[54] M. Di Pierro, *FermiQCD: A tool kit for parallel lattice QCD applications*, *Nucl. Phys. Proc. Suppl.* **106** (2002) 1034–1036, [hep-lat/0110116].

[55] M. Di Pierro, *Matrix distributed processing and FermiQCD*, hep-lat/0011083.

[56] D. Becirevic *et al.*, *Non-perturbatively improved heavy-light mesons: Masses and decay constants*, *Phys. Rev.* **D60** (1999) 074501, [hep-lat/9811003].

[57] **UKQCD** Collaboration, K. C. Bowler *et al.*, *Decay constants of B and D mesons from non-perturbatively improved lattice QCD*, *Nucl. Phys.* **B619** (2001) 507–537, [hep-lat/0007020].

[58] **UKQCD** Collaboration, C. R. Allton *et al.*, *The hyperfine splitting in charmonium: Lattice computations using the Wilson and Clover fermion actions*, *Phys. Lett.* **B292** (1992) 408–412, [hep-lat/9208018].

[59] **UKQCD** Collaboration, K. C. Bowler *et al.*, *Heavy baryon specroscopy from the lattice*, *Phys. Rev.* **D54** (1996) 3619–3633, [hep-lat/9601022].

[60] M. Ademollo, G. Veneziano, and S. Weinberg, *Quantization conditions for regge intercepts and hadron masses*, *Phys. Rev. Lett.* **22** (1969) 83–85.

[61] D. C. Lewellen, *Effective string amplitudes for hadronic physics*, *Nucl. Phys.* **B392** (1993) 137–161, [hep-th/9110026].

[62] S. R. Beane, *Chiral multiplets of large n(c) ground state baryons*, *Phys. Rev.* **D59** (1999) 031901, [hep-ph/9809328].

[63] M. Frank and P. J. O'Donnell, *Spin spin interactions in quarkonium*, *Phys. Lett.* **B159** (1985) 174. Addendum: Phys. Lett. B190 (1997) 235.

[64] H. J. Lipkin, *Relations between meson and baryon hyperfine splittings*, *Phys. Lett.* **B171** (1986) 293.

[65] H. J. Lipkin and P. J. O'Donnell, *Hyperfine interactions in charm and bottom systems*, *Phys. Lett.* **B409** (1997) 412–416, [hep-ph/9705363].

[66] **Particle Data Group** Collaboration, K. Hagiwara *et al.*, *Review of particle physics*, *Phys. Rev.* **D66** (2002) 010001.

[67] T. Bhattacharya, R. Gupta, G. Kilcup, and S. R. Sharpe, *Hadron spectrum with wilson fermions*, *Phys. Rev.* **D53** (1996) 6486–6508, [hep-lat/9512021].

[68] C. R. Allton, V. Gimenez, L. Giusti, and F. Rapuano, *Light quenched hadron spectrum and decay constants on different lattices*, *Nucl. Phys.* **B489** (1997) 427–452, [hep-lat/9611021].

[69] N. Cabibbo, *Unitary symmetry and leptonic decays*, *Phys. Rev. Lett.* **10** (1963) 531–532.

[70] M. Kobayashi and T. Maskawa, *CP violation in the renormalizable theory of weak interaction*, *Prog. Theor. Phys.* **49** (1973) 652–657.

[71] L. Wolfenstein, *Parametrization of the Kobayashi-Maskawa matrix*, *Phys. Rev. Lett.* **51** (1983) 1945.

[72] M. Schmidtler and K. R. Schubert, *Experimental constraints on the phase in the Cabibbo- Kobayashi-Maskawa matrix*, *Z. Phys.* **C53** (1992) 347–354.

[73] A. J. Buras, M. E. Lautenbacher, and G. Ostermaier, *Waiting for the top quark mass, $K^+ \to \pi^+ \nu\bar{\nu}$, $B_s^0 - \overline{B_s^0}$ mixing and CP asymmetries in B decays*, *Phys. Rev.* **D50** (1994) 3433–3446, [hep-ph/9403384].

[74] A. Stocchi, *Current status of the CKM matrix and the CP violation*, hep-ph/0405038.

[75] G. Buchalla, A. J. Buras, and M. E. Lautenbacher, *Weak decays beyond leading logarithms*, *Rev. Mod. Phys.* **68** (1996) 1125–1144, [hep-ph/9512380].

[76] D. Becirevic, D. Meloni, and A. Retico, *An estimate of the $K^0 - \overline{K^0}$ mixing amplitude*, *JHEP* **01** (2001) 012, [hep-lat/0012009].

[77] G. Kilcup, R. Gupta, and S. R. Sharpe, *Staggered fermion matrix elements using smeared operators*, *Phys. Rev.* **D57** (1998) 1654–1665, [hep-lat/9707006].

[78] **JLQCD** Collaboration, S. Aoki *et al.*, *Kaon B parameter from quenched lattice QCD*, *Phys. Rev. Lett.* **80** (1998) 5271–5274, [hep-lat/9710073].

[79] **SPQCDR** Collaboration, D. Becirevic *et al.*, *Kaon weak matrix elements with Wilson fermions*, *Nucl. Phys. Proc. Suppl.* **119** (2003) 359–361, [hep-lat/0209136].

[80] **JLQCD** Collaboration, S. Aoki *et al.*, *The kaon B-parameter with the Wilson quark action using chiral Ward identities*, *Phys. Rev.* **D60** (1999) 034511, [hep-lat/9901018].

[81] **CP-PACS** Collaboration, A. Ali Khan *et al.*, *Kaon B parameter from quenched domain-wall QCD*, *Phys. Rev.* **D64** (2001) 114506, [hep-lat/0105020].

[82] **RBC** Collaboration, T. Blum *et al.*, *Kaon matrix elements and CP-violation from quenched lattice QCD. I: The 3-flavor case*, *Phys. Rev.* **D68** (2003) 114506, [hep-lat/0110075].

[83] **MILC** Collaboration, T. DeGrand, *Kaon B parameter in quenched QCD*, *Phys. Rev.* **D69** (2004) 014504, [hep-lat/0309026].

[84] N. Garron, L. Giusti, C. Hoelbling, L. Lellouch, and C. Rebbi, *B_K from quenched QCD with exact chiral symmetry*, *Phys. Rev. Lett.* **92** (2004) 042001, [hep-ph/0306295].

[85] **ALPHA** Collaboration, P. Dimopoulos, J. Heitger, C. Pena, S. Sint, and A. Vladikas, *B_K from twisted mass QCD*, hep-lat/0309134.

[86] **RBC** Collaboration, T. Izubuchi, *B_K from two-flavor dynamical domain wall fermions*, hep-lat/0310058.

[87] M. Battaglia *et al.*, *The CKM matrix and the unitarity triangle*, hep-ph/0304132.

[88] R. Gupta, *Status of B_K from lattice QCD*, hep-lat/0303010.

[89] S. R. Sharpe, *Chiral perturbation theory and weak matrix elements*, *Nucl. Phys. Proc. Suppl.* **53** (1997) 181–198, [hep-lat/9609029].

[90] R. Gupta, D. Daniel, G. W. Kilcup, A. Patel, and S. R. Sharpe, *The Kaon B parameter with Wilson fermions*, *Phys. Rev.* **D47** (1993) 5113–5127, [hep-lat/9210018].

[91] G. Kilcup, D. Pekurovsky, and L. Venkataraman, *On the N_f and a dependence of B_K*, *Nucl. Phys. Proc. Suppl.* **53** (1997) 345–348, [hep-lat/9609006].

[92] N. Ishizuka *et al.*, *Viability of perturbative renormalization factors in lattice QCD calculation of the $K^0 - \overline{K^0}$ mixing matrix*, *Phys. Rev. Lett.* **71** (1993) 24–26.

[93] G. Kilcup, *Effect of quenching on the kaon B parameter*, *Phys. Rev. Lett.* **71** (1993) 1677–1679.

[94] W.-J. Lee and M. Klomfass, *Numerical study of $K^0 - \overline{K^0}$ mixing and B_K*, hep-lat/9608089.

[95] C. Bernard and A. Soni, "Cited as *'to be published'* in [96], but subsequently never published."

[96] A. Soni, *Weak matrix elements on the lattice - circa 1995*, *Nucl. Phys. Proc. Suppl.* **47** (1996) 43–58, [hep-lat/9510036].

[97] T. Inami and C. S. Lim, *Effects of superheavy quarks and leptons in low-energy weak processes $K_L \to \mu\bar{\mu}$, $K^+ \to \pi^+\nu\bar{\nu}$ and $K^0 \leftrightarrow \overline{K^0}$*, *Prog. Theor. Phys.* **65** (1981) 297.

[98] M. Ciuchini *et al.*, *Next-to-leading order QCD corrections to $\Delta F = 2$ effective Hamiltonians*, *Nucl. Phys.* **B523** (1998) 501–525, [hep-ph/9711402].

[99] D. Becirevic, *Lattice results relevant to the CKM matrix determination*, hep-ph/0211340.

[100] M. B. Gavela *et al.*, *The Kaon B parameter and K-π and K-$\pi\pi$ transition amplitudes on the lattice*, *Nucl. Phys.* **B306** (1988) 677.

[101] R. Gupta, T. Bhattacharya, and S. R. Sharpe, *Matrix elements of 4-fermion operators with quenched Wilson fermions*, *Phys. Rev.* **D55** (1997) 4036–4054, [hep-lat/9611023].

[102] S. Capitani *et al.*, *Perturbative renormalization of improved lattice operators*, *Nucl. Phys. Proc. Suppl.* **63** (1998) 874–876, [hep-lat/9709049].

[103] M. Crisafulli *et al.*, *Chiral behaviour of the lattice B_K-parameter with the Wilson and Clover Actions at $\beta = 6.0$*, *Phys. Lett.* **B369** (1996) 325–334, [hep-lat/9509029].

[104] **UKQCD** Collaboration, A. C. Irving, *Effects of non-perturbatively improved dynamical fermions in UKQCD simulations*, *Nucl. Phys. Proc. Suppl.* **94** (2001) 242–245, [hep-lat/0010012].

[105] **UKQCD** Collaboration, C. R. Allton *et al.*, *Effects of non-perturbatively improved dynamical fermions in QCD at fixed lattice spacing*, *Phys. Rev.* **D65** (2002) 054502, [hep-lat/0107021].

[106] **ALPHA, CP-PACS and JLQCD** Collaboration, R. Sommer *et al.*, *Large cutoff effects of dynamical Wilson fermions*, hep-lat/0309171.

[107] **ALPHA** Collaboration, M. Della Morte, R. Hoffmann, F. Knechtli, and U. Wolff, *Impact of large cutoff-effects on algorithms for improved Wilson fermions*, hep-lat/0405017.

[108] M. Hasenbusch. private communication.

[109] R. Sommer, *A New way to set the energy scale in lattice gauge theories and its applications to the static force and α_s in SU(2) Yang-Mills theory*, *Nucl. Phys.* **B411** (1994) 839–854, [hep-lat/9310022].

[110] D. Becirevic and G. Villadoro, *Impact of the finite volume effects on the chiral behavior of f_K and B_K*, *Phys. Rev.* **D69** (2004) 054010, [hep-lat/0311028].

[111] **JLQCD** Collaboration, S. Aoki *et al.*, *Light hadron spectroscopy with two flavors of O(a)-improved dynamical quarks*, *Phys. Rev.* **D68** (2003) 054502, [hep-lat/0212039].

[112] G. Martinelli, C. Pittori, C. T. Sachrajda, M. Testa, and A. Vladikas, *A general method for nonperturbative renormalization of lattice operators*, *Nucl. Phys.* **B445** (1995) 81–108, [hep-lat/9411010].

[113] A. Donini, V. Gimenez, G. Martinelli, M. Talevi, and A. Vladikas, *Non-perturbative renormalization of lattice four-fermion operators without power subtractions*, *Eur. Phys. J.* **C10** (1999) 121–142, [hep-lat/9902030].

[114] R. Frezzotti and G. C. Rossi, *Chirally improving Wilson fermions. I: O(a) improvement*, hep-lat/0306014.

[115] R. Frezzotti and G. C. Rossi, *Chirally improving Wilson fermions*, *Nucl. Phys. Proc. Suppl.* **129-130** (2004) 880–882, [hep-lat/0309157].

[116] M. Ciuchini *et al.*, *Unitarity triangle analysis in the standard model and sensitivity to new physics*, *ECONF* **C0304052** (2003) WG306, [hep-ph/0307195].

[117] **UTfit** Collaboration, M. Bona *et al.*, *CKM-triangle analysis: Updates and novelties for summer 2004*, hep-ph/0408079.

[118] A. Lenz, *Theoretical status of the lifetime predictions:* $(\Delta\Gamma/\Gamma)_{B_s}$, τ_{B^+}/τ_{B_d} *and* $\tau_{\Lambda_b}/\tau_{B_d}$, hep-ph/0107033.

[119] A. Lenz and S. Willocq, *Mixing and lifetimes summary*, *J. Phys.* **G27** (2001) 1207–1211.

[120] M. Neubert and C. T. Sachrajda, *Spectator effects in inclusive decays of beauty hadrons*, *Nucl. Phys.* **B483** (1997) 339–370, [hep-ph/9603202].

[121] LEP B Lifetime Working Group, "B lifetime averages." http://lepbosc.web.cern.ch/LEPBOSC/lifetimes/lepblife.html.

[122] **UKQCD** Collaboration, M. Di Pierro, C. T. Sachrajda, and C. Michael, *An exploratory lattice study of spectator effects in inclusive decays of the Lambda$_b$ baryon*, *Phys. Lett.* **B468** (1999) 143, [hep-lat/9906031].

[123] C.-S. Huang, C. Liu, and S.-L. Zhu, *Reanalysis of the four-quark operators relevant to Λ_b lifetime from QCD sum rule*, *Phys. Rev.* **D61** (2000) 054004, [hep-ph/9906300].

[124] **UKQCD** Collaboration, M. Di Pierro and C. T. Sachrajda, *A lattice study of spectator effects in inclusive decays of B mesons*, *Nucl. Phys.* **B534** (1998) 373–391, [hep-lat/9805028].

[125] E. Franco, V. Lubicz, F. Mescia, and C. Tarantino, *Lifetime ratios of beauty hadrons at the next-to-leading order in QCD*, *Nucl. Phys.* **B633** (2002) 212–236, [hep-ph/0203089].

[126] F. Gabbiani, A. I. Onishchenko, and A. A. Petrov, *Spectator effects and lifetimes of heavy hadrons*, hep-ph/0407004.

[127] C. Tarantino, *Beauty hadron lifetimes and B-meson CP-violation parameters from lattice QCD*, hep-ph/0310241.

[128] M. Ciuchini, E. Franco, V. Lubicz, and F. Mescia, *Next-to-leading order qcd corrections to spectator effects in lifetimes of beauty hadrons*, *Nucl. Phys.* **B625** (2002) 211–238, [hep-ph/0110375].

[129] **UKQCD** Collaboration, P. Lacock, A. McKerrell, C. Michael, I. M. Stopher, and P. W. Stephenson, *Efficient hadronic operators in lattice gauge theory*, *Phys. Rev.* **D51** (1995) 6403–6410, [hep-lat/9412079].

[130] E. Eichten and B. Hill, *An effective field theory for the calculation of matrix elements involving heavy quarks*, *Phys. Lett.* **B234** (1990) 511.

[131] **UKQCD** Collaboration, P. Boyle, *A novel gauge invariant multi-state smearing technique*, *J. Comput. Phys.* **179** (2002) 349–370, [hep-lat/9903033].

[132] **ALPHA** Collaboration, M. Della Morte *et al.*, *Lattice HQET with exponentially improved statistical precision*, *Phys. Lett.* **B581** (2004) 93–98, [hep-lat/0307021].

[133] **ALPHA** Collaboration, M. Della Morte *et al.*, *Static quarks with improved statistical precision*, *Nucl. Phys. Proc. Suppl.* **129** (2004) 346–348, [hep-lat/0309080].

[134] A. Hasenfratz and F. Knechtli, *Flavor symmetry and the static potential with hypercubic blocking*, *Phys. Rev.* **D64** (2001) 034504, [hep-lat/0103029].

[135] A. Hasenfratz, R. Hoffmann, and F. Knechtli, *The static potential with hypercubic blocking*, *Nucl. Phys. Proc. Suppl.* **106** (2002) 418–420, [hep-lat/0110168].

[136] T. Blum *et al.*, *Improving flavor symmetry in the kogut-susskind hadron spectrum*, *Phys. Rev.* **D55** (1997) 1133–1137, [hep-lat/9609036].

[137] **UKQCD** Collaboration, C. Michael and J. Peisa, *Maximal variance reduction for stochastic propagators with applications to the static quark spectrum*, *Phys. Rev.* **D58** (1998) 034506, [hep-lat/9802015].

[138] **APE** Collaboration, M. Albanese *et al.*, *Glueball masses and string tension in lattice qcd*, *Phys. Lett.* **B192** (1987) 163.